DEPARTAMENTO DE MOTOPROPULSION
Y TERMOFLUIDODINAMICA
ESCUELA TECNICA SUPERIOR DE INGENIEROS AERONAUTICOS
UNIVERSIDAD POLITECNICA DE MADRID
SPAIN

STUDY ON COMBUSTION PROCESSES IN REDUCED GRAVITY

VOLUME I

by
C. Sanchez Tarifa
A. Liñan Martinez
J.J.Salva Monfort
G.L. Juste
J.M. Tizon Pulido
J.M. Cura Velayos

It is acknowledge the valuable collaboration given to this work by Professor A.C. Fernandez-Pello University of California, Berkeley

LABORATORIO DE PROPULSION, E.T.S.I. AERONAUTICOS
Ciudad Universitaria, 28040 Madrid, SPAIN

DMT

March, 1990

CONTENTS

1. ABSTRACT OF THE WORK

1. ABSTRACT OF THE WORK

1.1. GENERAL CONSIDERATION ON THE WORKING PACKAGES

The following tasks have been carried out under the present Contract:

WP1. Continuation of the experiments on flame spreading in parabolic aircraft flights, conducted in one flight campaign.

These experiments have been, in part, a continuation of the preceeding research programmes and they were directed to the study of the influence of fuel thickness at reduced gravity on the flame spread velocity.

In addition, a few experiments were carried out in order to obtain some preliminary information on possible combustion experiments to be performed in a sounding rocket module.

WP2 and WP3. These works on the sounding rocket module and on the sounding rocket experiments were preceeded by a common study, which consisted in a review of the combustion experiments that could be carried out in a sounding rocket module. The requirements of the experiments were analised, with special emphasis on the essential factors of the time and space needed for each possible experiment.

It was definitively concluded that there is no practical way to keep constant the gaseous atmospheric composition in the module chamber throughout a stationary combustion process in a still atmosphere. This is due to the fact that there is not any practical feasible way to extract the combustion products and to feed into the module the oxygen or the reactant gases consumed without strongly disturbing the flow field. This occurs because under microgravity conditions gas velocities in combustion processes at constant pressure are essentially controlled by diffusion and they are usually very small.

As a consequence, the module has to contain a sufficient amount of oxidizer such that its variation during the combustion process should be permissible.

This requirement imposes limitations in the volume and combustion time, which are interdependent and in the size of the experiment.

In addition, the volume available has to be sufficiently large in order to avoid significant interference of the walls of the module on the combustion field. If the experiment is of a non-stationary nature and the flame size increases with time, as it occurs in many combustion processes, this imposes another limitation in the combustion time and in the size of the experiment.

The aforementioned review of the combustion processes is shown in this Final Report and from its conclusions the basic data for the study and specifications of the combustion module were obtained.

1.2. MULTIPLE EXPERIMENTS

From the aforementioned review it was concluded than in most combustion experiments times of the order of one minute would be sufficient.

Since there are six minutes at reduced gravity available, the problem of utilizing the module for several experiments has to be considered, specially taking into account the high cost of the launching of a sounding rockets.

Except for the experiments in which a little amount of oxidizer is consumed, such as in droplet combustion, reutilization of the module for multiple experiments require emptying the module and refilling it with the specified gaseous mixture. This process is mechanically simple but it presents the difficult problem of knowing the time required for the

oxygen or gaseous mixture introduced into the chamber to become at rest. The process is asymptotic, therefore it has to be specified the minimum value admitted for the gas fluctuation velocities (for example *<2 mm/s*).

The analytical solution of this problem is very difficult, and it is presently being studied by NASA.

Considering its importance, the problem has been studied experimentally under the present Contract. It has been concluded after a series of experiments with different tracers, that after elapsing times of the order of two minutes the fluctuation velocities were lower than *2 mm/s*, which were considered sufficiently small. This implies that two or three refills are possible in each flight.

A large amount of experiments would occupy the full available diameter of the module (*~40 cm*). Some experiments would need smaller diameters. This opens the possibility of utilizing several chambers inside the module, increasing the possibility of multiple experiments for each flight and reducing costs, and avoiding refilling in some cases.

A preliminary desing of this multiple combustion chamber solution has been carried out.

1.3. FORCED CONVECTION EFFECTS AT LOW REYNOLDS NUMBER

Forced Convection effects are currently considered of high interest in combustion processes at reduced gravity. This is due to two reasons: in the first place, forced convection effects at low Reynolds numbers cannot be experimentally studied at one *g* on the ground, because they are masked by free convection effects. On the other hand, if a fire takes place in a spacecraft or space laboratory it will be most likely take place in an environment of low velocity gas currents originated by the air conditioning equipment or even by the motion of people.

Forced convection effects can be studied in the sounding rocket module in two different ways: by moving the burning smaple along the module keeping the oxygen or oxidizers at rest, or by keeping the sample at rest and producing a continuous flow of gas at a given velocity.

Although their study was not specified in this Contract, both systems have been analysed.

The first system is relatively simple, requiring refilling of the module. Three or four experiments would be possible to carry out in each flight.

The second systems is mechanically very complicated requiring two valves controlled probably by a microcomputer. A specific system is proposed and studied. Its principal controlling laws are discussed, as well as the main problems and possible solutions.

In principle, this system offers the possibility of carrying out more experiments per flight than the first system. However, some important transient problems have to be thoroughly studied, requiring a test programme before concluding that the proposed system is a viable or better solution.

1.4. WP4. THEORETICAL STUDIES

The theoretical studied have been devoted to quiescent combustion and flame spreading utilizing numerical methods and an order of magnitude analysis.

Several important results have been obtained, as for example the influence of gravity on flame spreading depending on the fuel thickness, which have been experimentally verified during the parabolic flights.

In addition a study on the influence of forced convection on the flame spreading process has been carried out.

2. WP1. PARABOLIC AIRCRAFT FLIGHT

2. WP1. PARABOLIC AIRCRAFT FLIGHT

2.1. INTRODUCTION

An Experimental programme on flame spreading and quiescent heterogeneous combustion processes has been conducted on ground and at reduced gravity conditions in the SE 210 Caravell aircraft laboratory (Oct. 1989).

First, the interesting problem about the effect of gravity and solid fuel thickness on flame spreading processes, over PMMA samples, has been investigated.

To undertake some experimental work on this problem, it is necessary, at first, to select the shape of samples to be used and the appropiate thickness. Secondly, the more convenient operating conditions must be stablished.

So we have made some preliminary analytical estimations, leading to the conclusion that thin solid or hollow rods are the more interesting samples. Then we have developed an experimental ground work where manufacturing, ignition or structural samples problems are detected. Also the operating conditions are fixed and many data are adquired to be compared with those performed at microgravity conditions. Finally twelve successfully tests were performed at reduced gravity level $(10^{-2}g)$ on parabolic aircraft flight.

By other way, preliminary analysis of possible experiments for sounding rockets has revealed that quiescent combustion on cylindrical rods and pool fire on circular disks of PMMA are very interesting. Consequently the second objective of this experimental work has been directed to obtain preliminary information of the combustion processes and possible problems using these configurations.

2.2. THEORETICAL ANALYSIS AND ESTIMATIONS

In a previous ESA contract[1,2], a theoretical study was iniciated about the gravity influence on downward flame spreading process over solid rods. A scheme of the process is shown in figure 2.1.

Using an analysis of orders of magnitud the following relation was obtained for thermally thick rods:

$$U_F \sim \frac{\alpha_s}{\alpha_g}(\alpha_g g)^{1/3}(N_u N)^2 \qquad (1)$$

where

$$N = \frac{k_g}{k_s}\frac{(T_f - T_v)}{T_v - T_o} \qquad (2)$$

$$N_u = \frac{l_g (\partial T/\partial r)_a}{(T_f - T_v)} \qquad (3)$$

$$l_g \sim \alpha_g^{2/3}/g^{1/3} \qquad (4)$$

Whereas, for thermally thin rods, it results:

$$U_F \sim \frac{2\alpha_s}{a} N_u N \qquad (5)$$

It is interesting to extend this result to thermally thin hollow rods. So that following the same development, we get easily:

$$U_F \sim \frac{2a}{t(2a-t)}\,\alpha_s N_u N \qquad (6)$$

Note that t is the thickness of the tubular rod and that this last expression is a generalization of the expression *(5)*, since for a solid rod is $t=a$ simply.

In order to complete this study and analyze the influence of gravity it is necessary to determine the dependence of Nusselt number on gravity and geometry.

For this, we will suppose that the heat flux conducted from the gas to the solid is equal, in order of magnitud, to the heat flux conducted in a one dimensional conduction solution. In these conditions the temperature field solution is obtained from:

$$\frac{1}{r}\frac{\partial}{\partial r}\left(r\frac{\partial T}{\partial r}\right)=0$$

with,

$T=T_v$, for $r=a$

$T=T_f$, for $r=a+l_g$

so that, it results:

$$\left(\frac{\partial T}{\partial r}\right)_{a^+}=\frac{1}{a}\frac{(T_f-T_v)}{ln(1+l_g/a)} \qquad (7)$$

and taking into account the relations *(3)* and *(4)*, this leads to:

$$N_u=\frac{\alpha_g^{2/3}}{ag^{1/3}}\frac{1}{ln\left(1+\dfrac{\alpha_g^{2/3}}{ag^{1/3}}\right)} \qquad (8)$$

So that finally, we can write, for thermally thick rods:

$$U_F\sim\frac{\alpha_s\alpha_g^{2/3}}{ag^{1/3}}\left[\frac{N}{ln\left(1+\dfrac{\alpha_g^{2/3}}{ag^{1/3}}\right)}\right]^2 \qquad (9a)$$

and for thermally thin solid or hollow rods:

$$U_F \sim \frac{2}{t(2a-t)} \frac{\alpha_s \alpha_g^{2/3}}{g^{1/3}} \frac{N}{ln\left(1+\frac{\alpha_g^{2/3}}{ag^{1/3}}\right)} \qquad (9b)$$

Passing to the limit, when $a \to \infty$, we get the case of flame spreading over plates. Thus results for thermally thick plates:

$$U_F \sim \frac{N^2 \alpha_s}{\alpha_g^{2/3}} g^{1/3} \qquad (10a)$$

and for thermally thin plates

$$U_F \sim \frac{N\alpha_s}{t} \qquad (10b)$$

According to these two last relations, the variation of flame spreading velocity with gravity is qualitatively shown in figures 2.2 and 2.3. The interesting result is that flame spread velocity increases as gravity is reduced, for thermally thin rods. Note that, when $U_F \sim U_g \sim \sqrt{l_g g}$, there is no buoyancy effects, so that the effect of gravity disappears.

In figures 2.4 to 2.7, are shown some results of flame spreading velocity estimations, for both thermally thin hollow and solid rods.

2.3. EXPERIMENTAL WORK

2.3.1. Preliminiminary ground test

An experimental work was conducted on the ground, aimed at achieving the following objectives:

- Obtaining information about the samples structural behaviour (dripping or bending problems) that lastly would be tested in microgravity conditions.

- To verify that there is not combustion inside the tubular rods during the flame spreading process over tubular external surface.

- Obtaining spreading velocities data in function of thickness, diameter and the oxygen mass fraction to select the suitable dimensions of the samples and the mixture composition.

- Obtaining the values of the flame spreading velocities with the same samples, pressure and mixture composition and for the same range of thickness and radius that would later be obtained in flight during microgravity conditions.

Air was used for the inside part of the tubular rods as insulating material, because its conductivity is less than other typical insulating materials (see table I). Therefore it was necessary, to verify that there was not combustion inside the tubular rods, nor flame spreading. To perform this, the device shown in fig.2.8 was developed.

TABLE I

INSULATING MATERIAL	CONDUCTIVITY (KCAL/M.H°C)
Quartz glass	1.2
Ceramic (Gres)	0.9-1.4
Plaster	0.44
Concrete	0.21
PMMA	0.15
Asbestos	0.05
Wood (Balsa)	0.04
Air (50 C)	0.024
Silica gel	0.019

Downward-spreading velocities were measured, taking average values of several experiments for each case.

— Test equipment.

The experiments were performed in closed chambers. The chambers were the same as the ones utilized in previous campaignes in the Nasa KC-135 aircraft laboratory, with light modifications to improve safety and newly tested to verify ESA-CNES safety regulations.

It is necessary to point out that neither the gas composition nor the pressure inside the chamber changed substantially during the 20-22 s. of microgravity period, as it was seen in previous experiments [2] performed with samples greater than those used at present, and with flame spreading velocities higher than those expected in these experiments.

To measure flame spread velocity and the other characteristics of the flame, a photographic system was used. It consists of a photographic camera taking photos at 2 s time intervals and a video camera, recording continuosly, and taking 25 images by second.

Both systems allow the determination of flame front position, related to a fixed reference point, at known time intervals, so that the flame spread velocity can be calculated easily.

The video film is analyzed using a frame grabber and image processing software to calculate flame dimensions and spread rates, from the digitized data, more accuracy.

— Results

In the photo 2.9 is shown the combustion process, where it is possible to observe that there was not combustion inside the PMMA plates.

Photographs of the flames are shown in fig.2.10 and 2.11 and the results of the spreading velocities as a function of thickness for tubular rod and diameter for solid rod are shown in fig.2.12 and 2.13 for three oxygen mass fractions.

2.3.2. Experiments performed at microgravity conditions.

2.3.2.1. Downward flame spreading over rods

— Test Conditions and samples

The microgravity period has a duration of 20-22 s, of which only 10 s could be suitable to measure, because the first 5 s and the last one could be in the transition zones.

Considering this, and taking into account the theoretical velocity estimations, ground test data and the maximum length that can be obtained for the tubular and solid rods lead us the election of a 35% oxygen mass fraction and atmospheric pressure as the best solution for operating conditions.

The local pressure on the place where the parabolic fligth was performed (Bretigny-sur-Orge, Paris) was *P=756.8 mm Hg*, greater than that there was when the previous ground test were performed (*P=709.6 mm Hg*, Madrid).

Although the dependence of spread rate on pressure is slight, for thin samples[3], spread velocity increases with increasing pressure, due to the same test was repeated on ground at *P=756.8 mm Hg*, after the microgravity experiments, for comparison purposes.

Because the number of experiments was limited, three thicknesses were selected for tubular rods. The tests were run twice for each thickness to obtain more results and to prevent some possible failure.

The tests performed on tubular rods were the following:

Material : PMMA
Length : 60 mm
Diameter : 4 mm
Thickness t: 0.1, 0.15, 0.25 mm
Y_{O2} : 35%
Pressure : 756.8 mm Hg

The selection criterions for the test conditions for solid rods were similar to those used for tubular rods. Three diameters were selected and the tests were run twice for each diameter. Test carried out over solid rods were:

Material : PMMA
Length < 50 mm
Diameter : 1.5, 2.0, 2.5 mm
Y_{O2} : 35%
Pressure : 756.8 mm Hg

The test equipment was the same used on ground.

— Test Procedure

The ignition was carried out by means of an electric heated wire, coiled around the extremity of the sample. The ignition time was approximately 1-2 s.

The video camara was "switch on" before pull-up, and it was "switch off" after pull-out, while photographic camera was on at the same time that the ignition system. For the first flight experiments, ignition was performed at the beginning of microgravity period, being nearly simultaneous the ignition phase and transition one from 1 g to 10^{-2}g, as shown in gravity profiles. For the second and the third

flight, ignition was performed 4 s after injection point.

The maximum pressure inside the chamber was also recorded during the flame spreading processes for each experiment, being negligible the variation of pressure.

2.3.2.2. Quiescent combustion

The experiments carried-out were quiescent combustion on PMMA thick tubular rods and PMMA pool fires.

For quiescent combustion test, ignition began at both ends of the sample, as shown in Fig.2.14, where the used sample and sujection can be observed.

Pool-fire ignition was central, as shown in Fig.2.15. There is an initial flame spread process in both experiments. To have more time to observe the quiescent combustion phase of the experiment, it was selected the maximum possible oxygen mass fraction, Y_{O2}=88.9%, due to vacuum pump capacity.

In these experiments, the ignition system was started before and after the beginning of microgravity period to study possible ignition problems. The measuring equipment was the same used in the other test.

2.4. EXPERIMENTAL RESULTS AND ANALYSIS

2.4.1. Flame spreading process

In figures 16 and 17 are shown typical time evolution of the flame spreading process over a solid rod of 1.5 mm diameter, and over a tubular rod of 0.15 mm thickness respectively.

As we can observe, the flame presents sometimes a geometrical

configuration denoting free convection, but another times, the effect of convection is present in the vertical direction (up and down) as well as in the horizontal plane. This is because the process is very sensitive to gravity levels, and as the corresponding profiles of the parabolic flight show (see figures 2.18 and 2.19) there is fluctuations in gravity level, both in the vertical direction and in the horizontal plane. Observese que existen valores de g negativos, en algunos casos, segun el eje z (vertical) (eje x)

According to these operating conditions, the better we can do is measure simply the distance run by the flame between two instants, located into the microgravity operating conditions, with the additional requirement that the position of the flame front is clearly detected. In this way, a mean value of the flame spreading velocity can be calculated easily.

The results on flame spreading velocity, for all the experiments made in the campaign, are shown in figure 2.20 for solid rods, and in figure 2.21 for tubular rods, and compared with the results of the same experiments but at 1 g. As the figures show, the flame spreading velocity increases when the gravity is reduced, thus confirming theoretical trends.

As well, it can be seen that the flame spreading velocity increases as tubular rod thickness or solid rod diameter are reduced. We can say that this effect is the same in microgravity conditions as in 1 g.

By other way no ignition nor structural problems were observed at microgravity conditions.

2.4.2. Quiescent combustion on cylindrical rods.

Figure 2.22 shows the "ignition phase" of the quiescent combustion over a cylindrical rod. This is performed with two spreading flames proceding from both rod ends. The process is very fast and only

takes about 5-6 s. By other way, no ignition problems were detected at microgravity conditions.

Figure 2.23 is a typical record of the process, after the ignition phase was completed. As in the case of flame spreading, the effects of a fluctuating microgravity profile, see figures 24a-24b, are observed. Convection can be seen upwards sometimes and downwards another times.

Specially interesting are the pictures shown in Fig.2.25 obtained in the first parabola of the third flight. As these pictures show, there is a quite good flame symmetrie, denoting no convection and that is more important a one dimensional flame configuration at this condition.

Due to these non stationary operating conditions, it is imposible to prove the interesting theoretical result concerning the travel of the flame front far away of the rod axis.

Also it appears that the period of microgravity is too small for this purpose.

2.4.3. Disk pool fire

Only one test of the three prepared run succesfully. For the two failed test, ignitor started at microgravity conditions. In one case the ignition was got to late in the microgravity period, and in the other there was no ignition. As ignition was got at microgravity condition for this sample and for the other used, the ignition fail was atrributed to bad perfomance of the ignitor, due to a defect of manufacturing, in spite of care taken to reproduce the prototype used in ground tests. This should be taken into account for future experiments.

Figure 2.26 shows the time evolution of the sucessfull test. In this case ignition started at *1 g*, before "Injection", so that the

effect of variable gravity conditions on the combustion process can be observed. As the gravity is reduced, the height of the flame disminishes and its shape gets more and more rounded. Also it is observed how the horizontal acelerations deform the axial symmetrie of the flame.

2.5. CONCLUSIONS

- The experimental results show that the flame spreading velocity on thin tubular or thin solid rod samples is greater at microgravity conditions ($\sim 10^{-2} g$) than at *1 g*, thus confirming analytic theoretical estimations.

- The flame spreading velocity increases as tubular rod thickness or solid rod diameter are reduce, the influence of thickness or diameter in microgravity conditions is the same that at *1 g*.

- For the quiescent combustion process on cylindrical rods, the treatment given to the ends, has proved to be satisfactory to get a one dimensional combustion process. However, to test correctly this process, more observation time and constant microgravity level are needed.

- Pool fire experiment shows that the process is greatly influenced by the gravity level. Flame height decreases with gravity and takes a round shape.

- For all samples used, no especial ignition or structural problems were detected. Hovewer the flame front position and shape are very sensitive to gravity fluctuations.

REFERENCES

1. C. Sánchez Tarifa et al. *"Preparatory Study on Heterogeneous Combustion Processes Under Microgravity Conditions"* ESA-CR n°6284/85/F/FL, Oct. 1986.

2. C. Sánchez Tarifa et al. *"on Heterogeneous Combustion Processes Under Microgravity Conditions"* ESA-CR n°6934/86/F/FL, Feb. 1988.

3. R.A. Altenkirch, R. Eichhorn and P.C. Shang, *"Buoyancy Effects on Flames Spreading Down Thermally Thin Fuels"* Comb & Flame, 37 71-83 (1980).

Acknowlendgment

This experimental work has been sponsored by the Microgravity Departament of ESA. The excellent assistant of its directive personnel, as well as that of ESTEC, CNES-CEV and Orbitics personnel is acknowledged and appreciated.

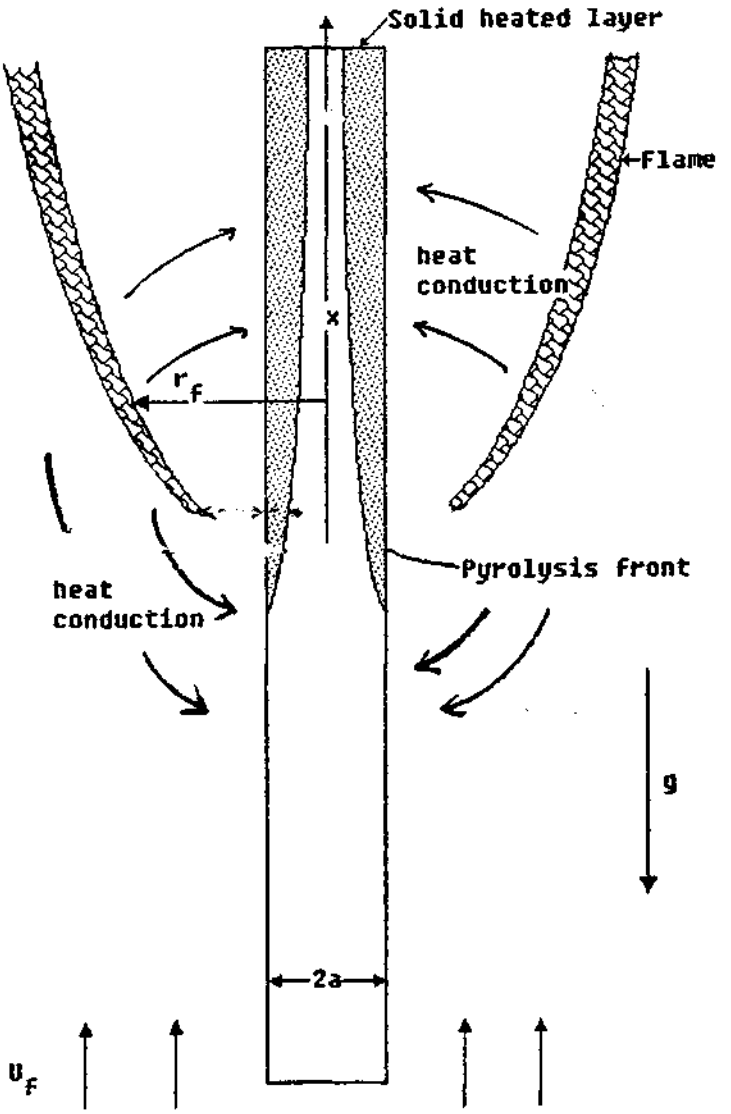

Fig. 2.1. Schematic of the flame spread region

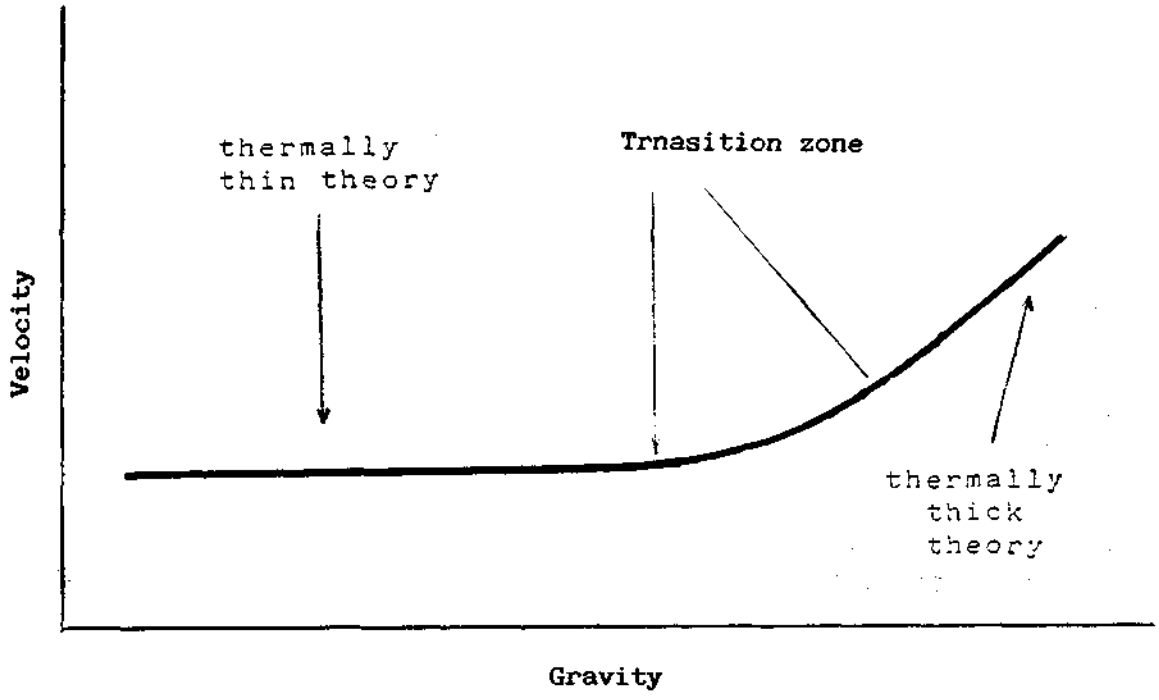

Fig. 2.1 Influence of gravity for flat plates

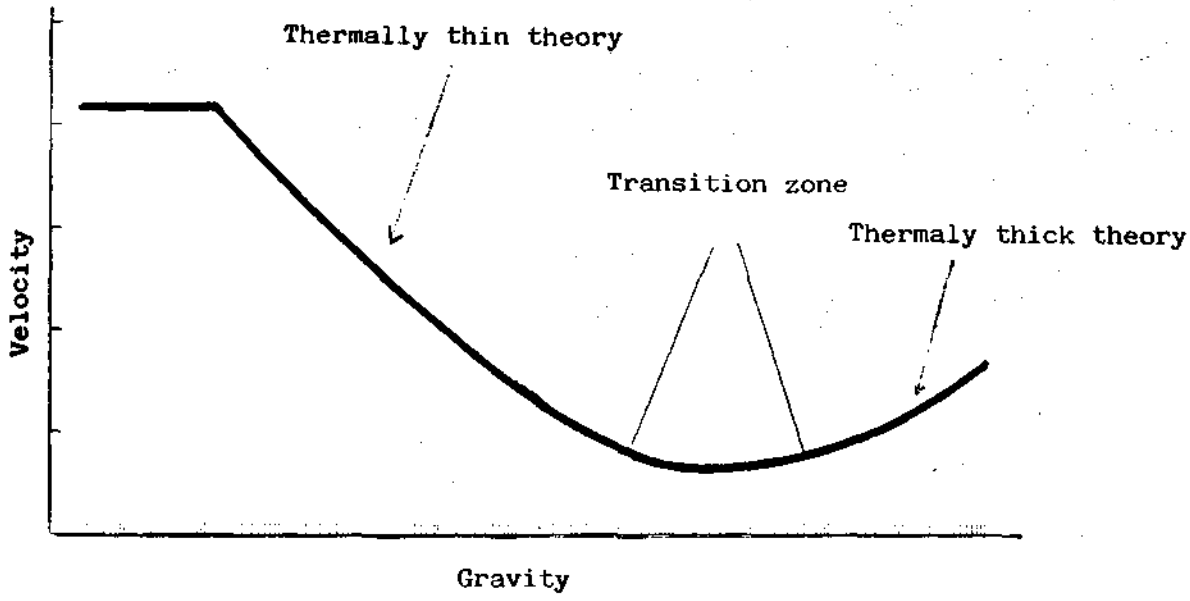

Fig. 2.3 Influence of gravity for solid rod

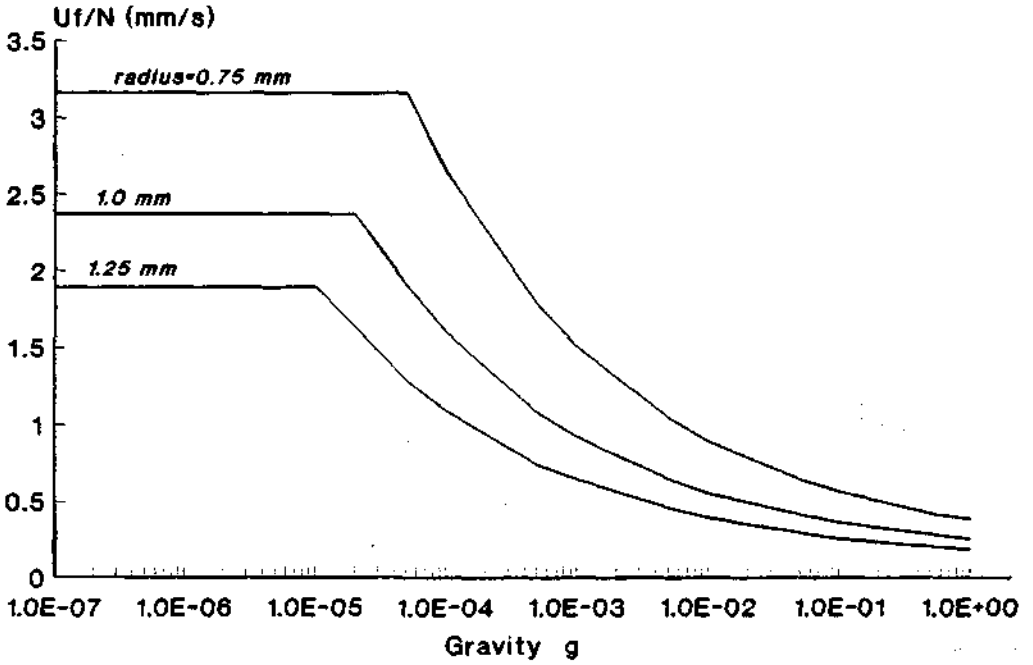

Fig. 2.4 Influence of gravity for thermally thin solid rods

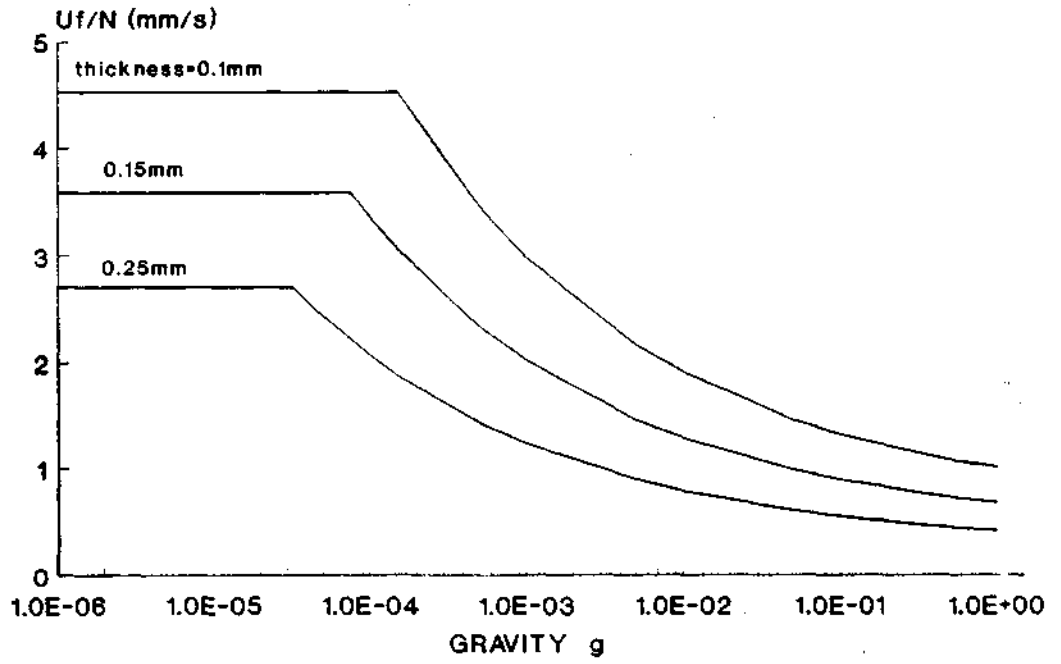

Fig. 2.5 Influence of gravity for thermaly thin solids
(Tubular rod, Ø = 4 mm)

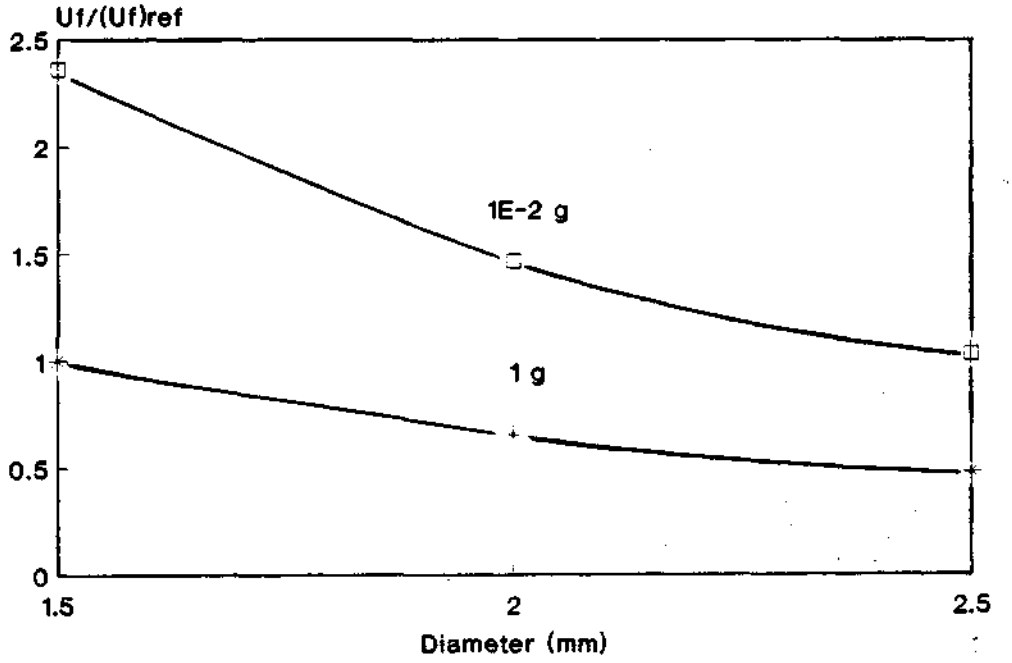

Fig. 2.6 Estimated flame spreading velocity vs. diameter
Solid rod. Y_{02} =35 % , P = 1 atm.

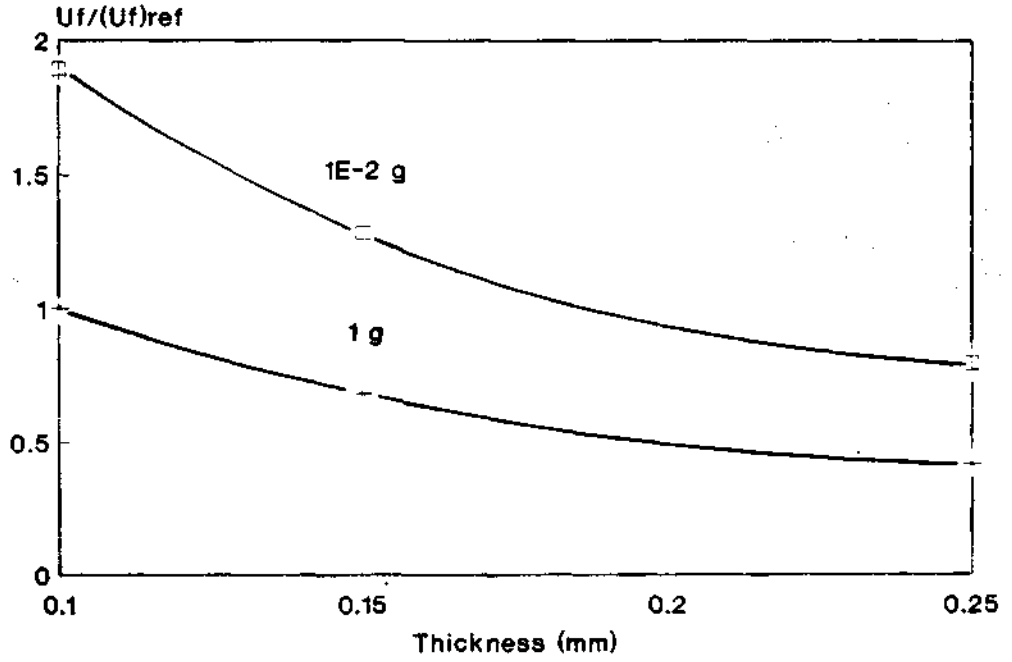

Fig. 2.7 Estimated flame spreading velocity vs. thickness
Tubularrod. Y_{02} = 35 % , P = 1 atm, Ø = 4 mm.

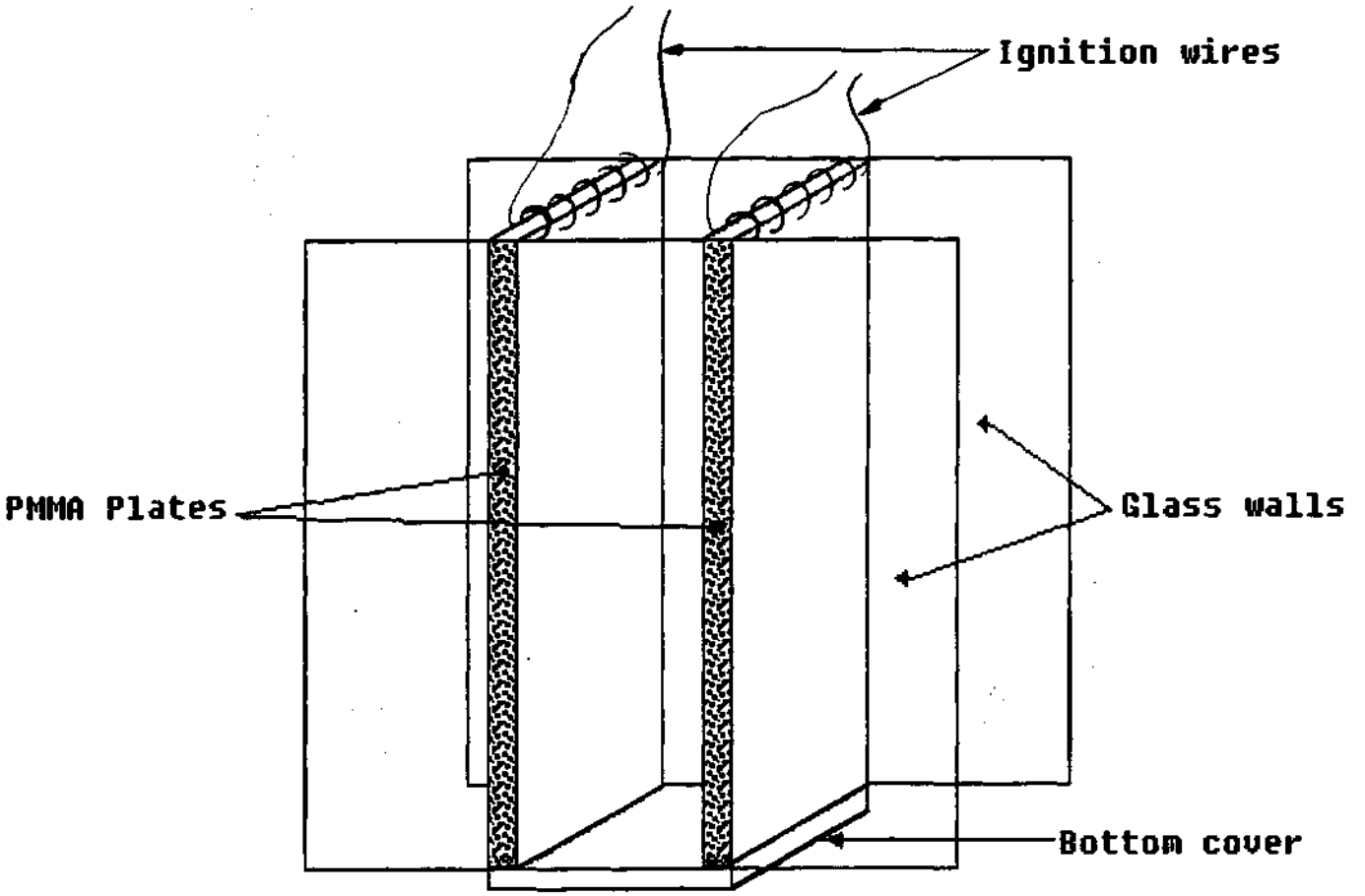

Fig. 2.8 Demostrating device for combustion inside tubular rods.

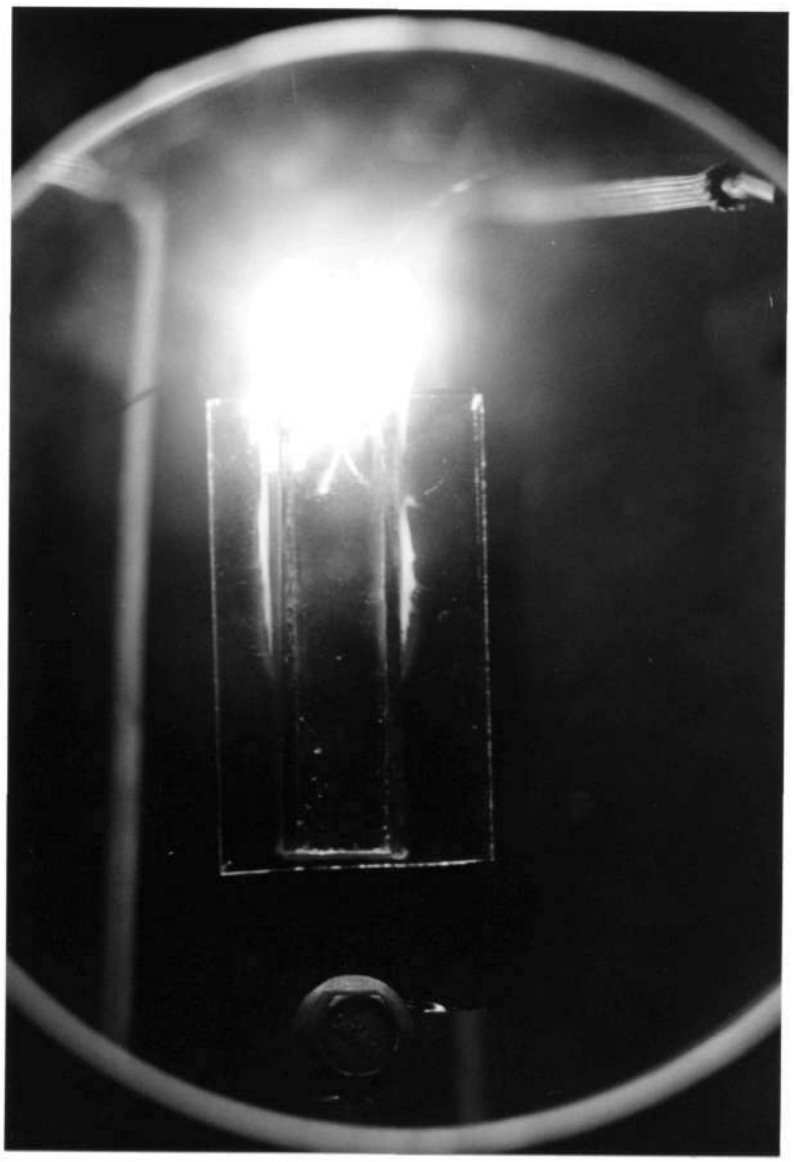

Fig. 2.9 Combustion process over PMMA plates

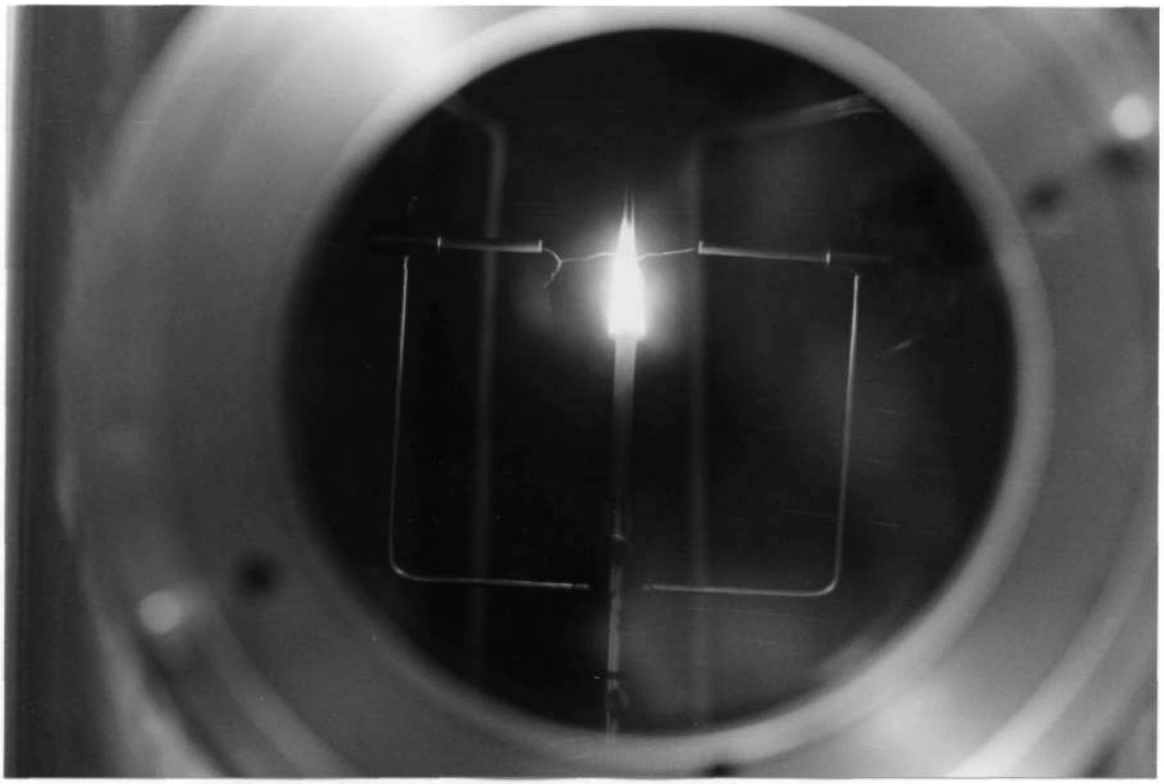

Fig. 2.10 Downward flame spreading over tubular rod at 1g.
Y_{O2} = 35 % ; P = 1 atm ; Ø = 4 mm ; t = 0.1 mm

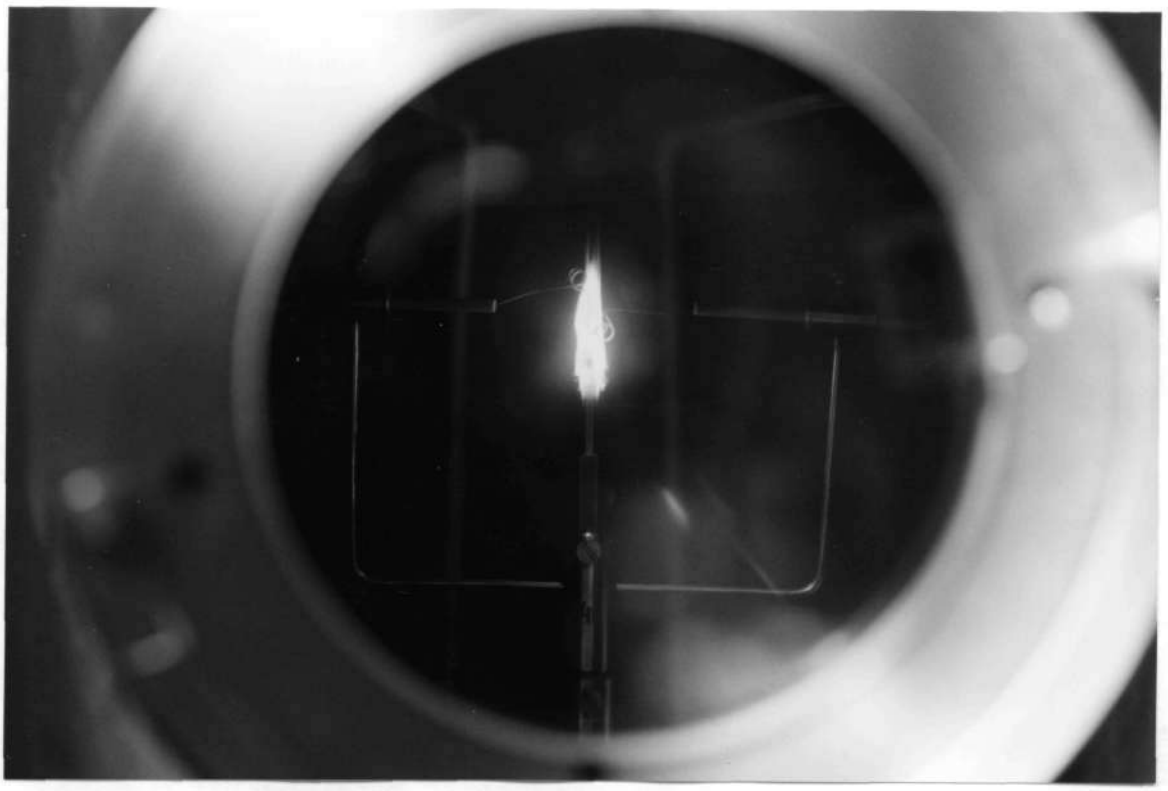

Fig. 2.11 Downward flame spreading over solid rod at 1 g
Y_{O2} = 35 % ; P = 1 atm ; Ø = 1.5 mm

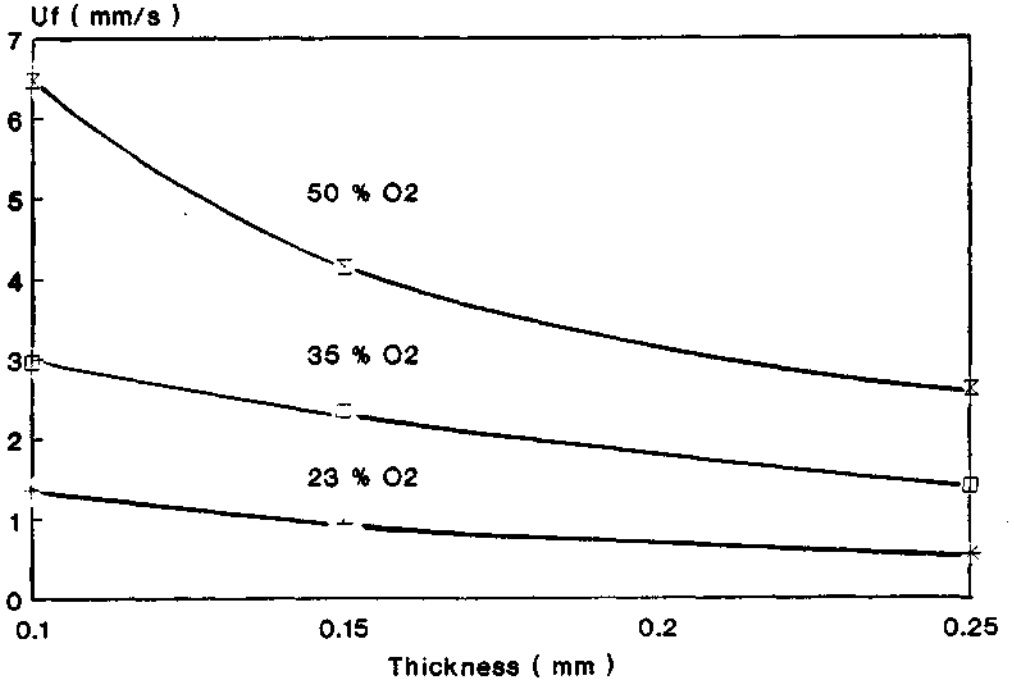

Fig. 2.12 Experimental downward flame spreading velocity vs. thickness. Effect of oxygen mass fraction. Tubular rod, Ø ≈ 4 mm, P = 756 mm Hg, 1 g

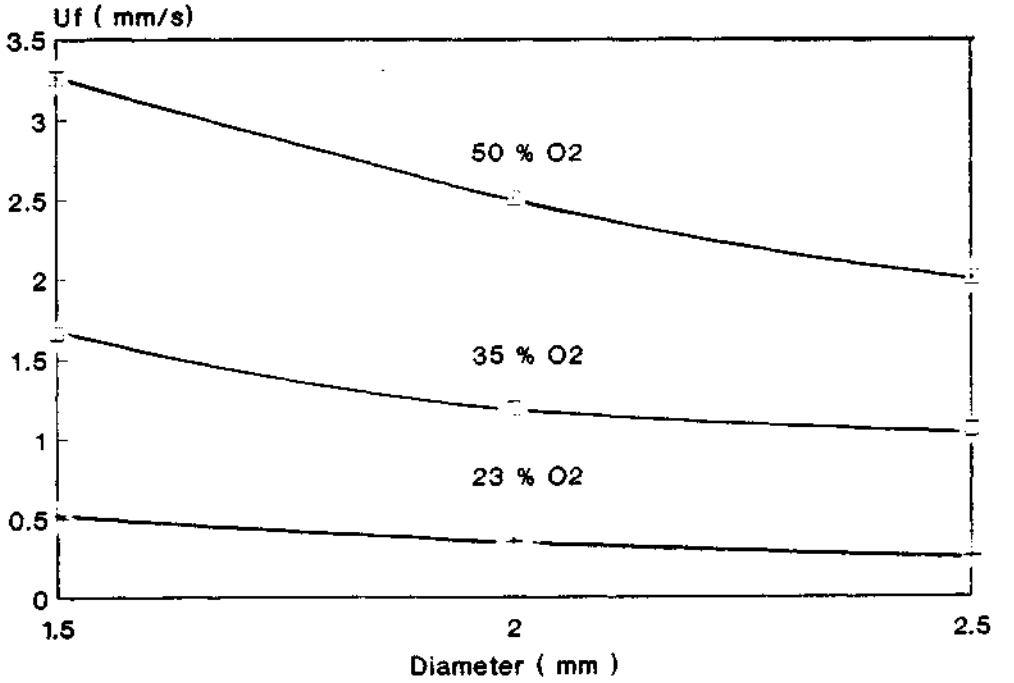

Fig. 2.13 Experimental downward flame spreading velocity vs. diameter. Effect of oxygen mass fraction. Solid rod, P = 756 mm Hg, 1 g

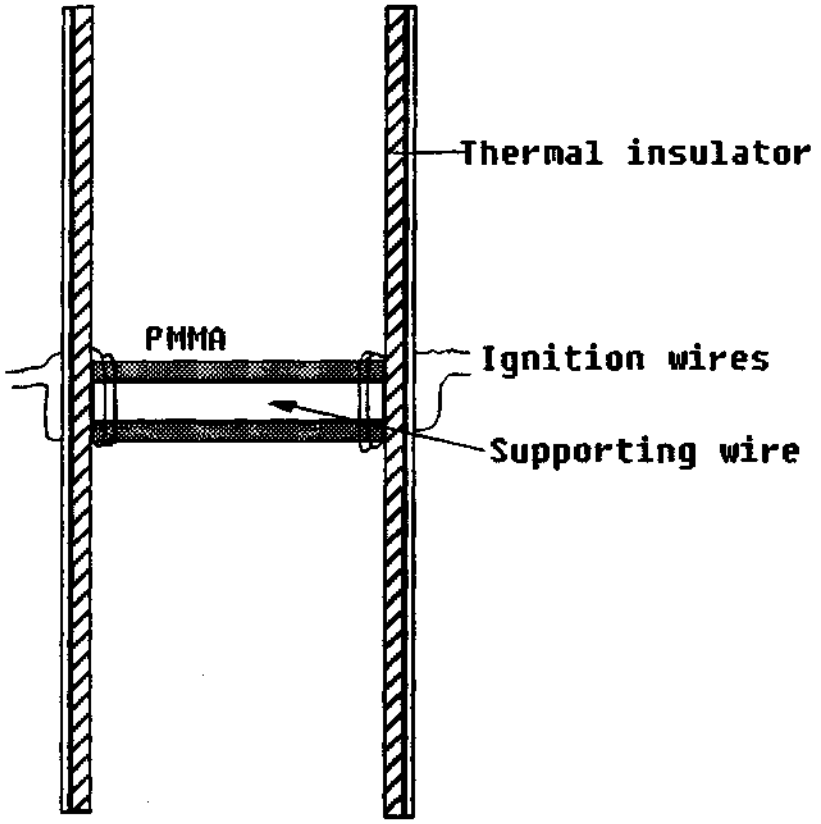

Fig. 2.14 Sample for cylindrical evolving flame

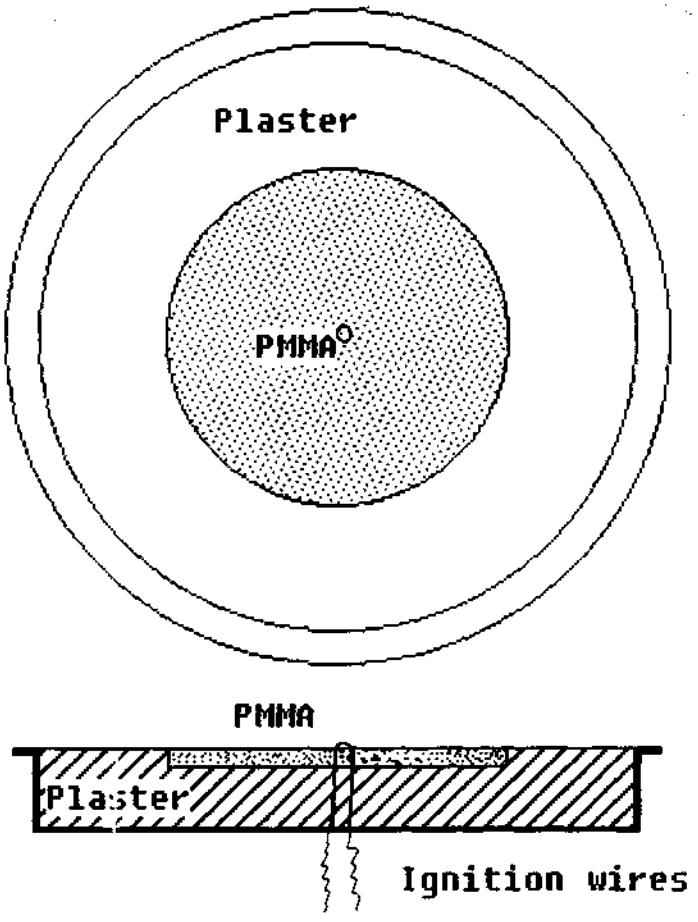

Fig. 2.15 Sample for Disk Pool Fire

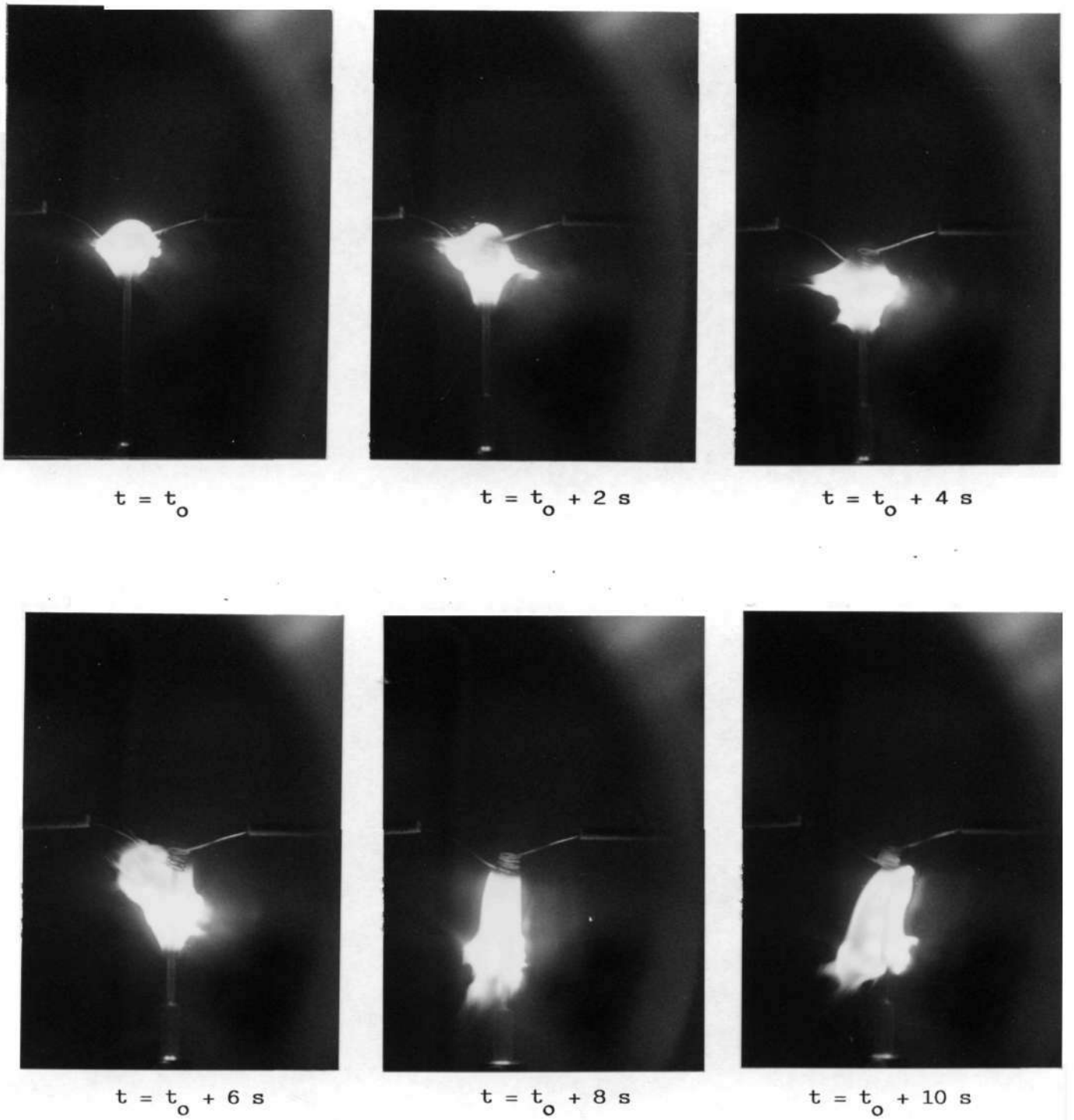

Fig. 2.16 Flame spreading process over solid rod at microgravity conditions in the CEV Caravelle Aircraft Laboratory. Y_{02} = 35 % ; Ø = 1.5 mm P = 756 mm Hg ;

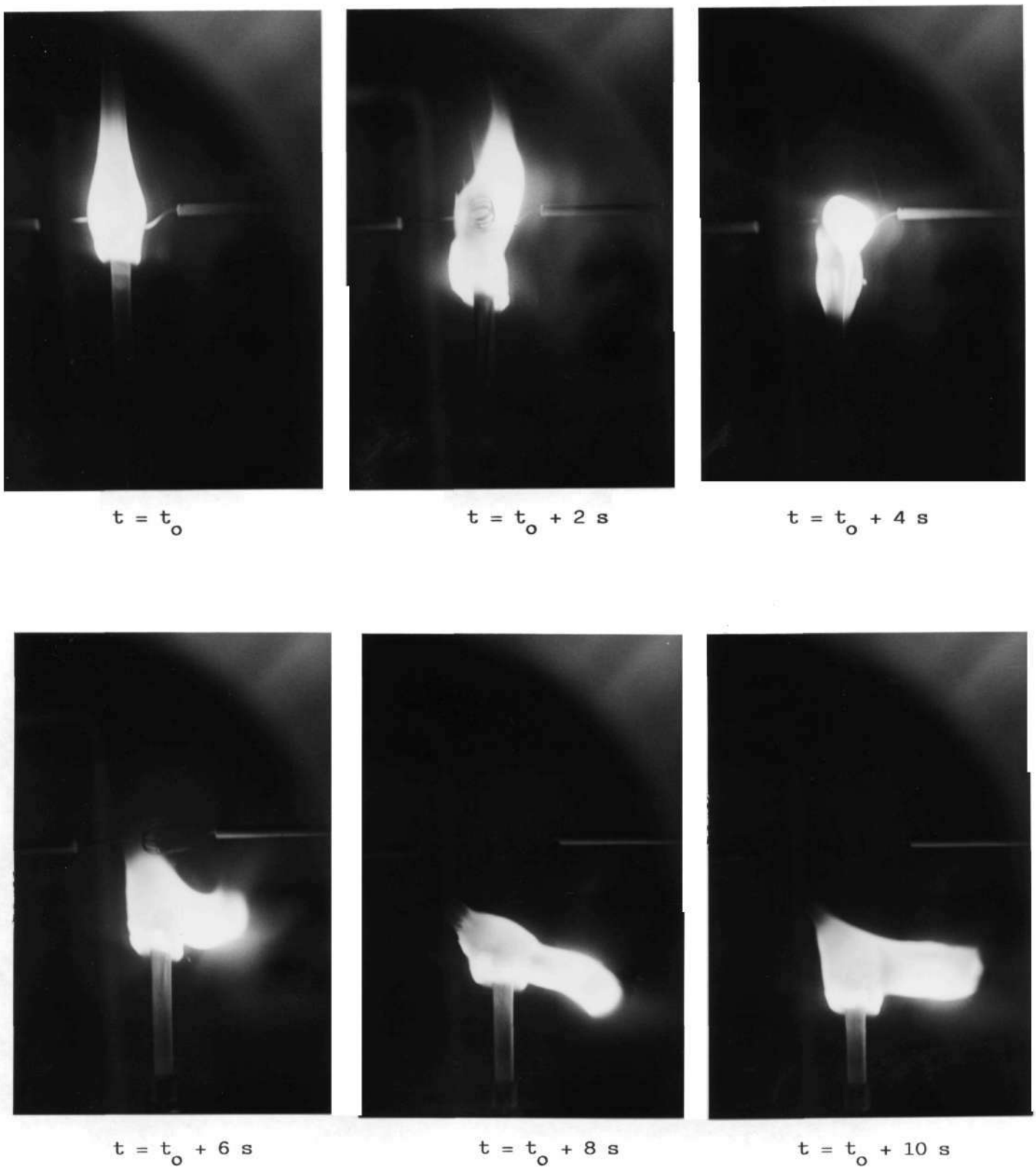

Fig. 2.17 Flame spreading process over tubular rod at microgravity conditions in the CEV Caravelle Aircraft Laboratory. Y_{02} = 35 % ; Ø = 4 mm
t = 0.15 mm ; P = 756 mm Hg

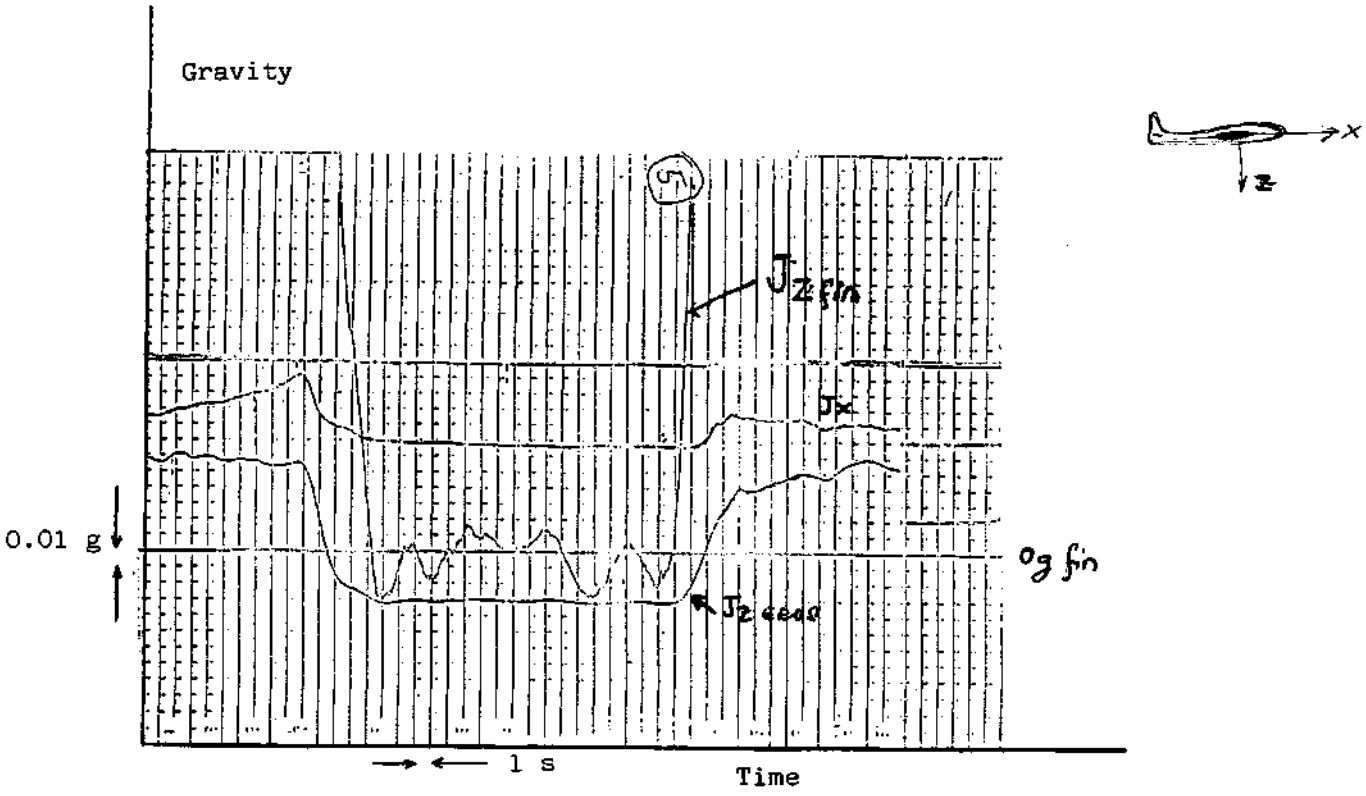

Fig. 2.18 Profile of Gravity for Parabola 5, third flight

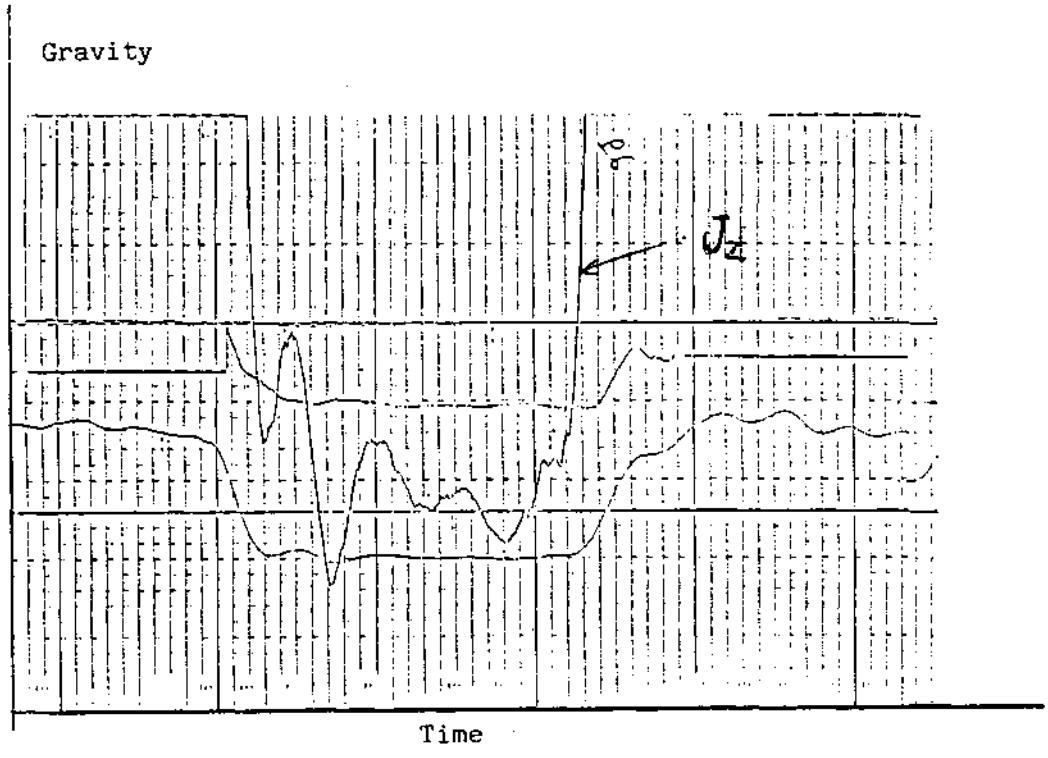

Fig. 2.19 Profiles of Gravity for Parabola 6, second fligth

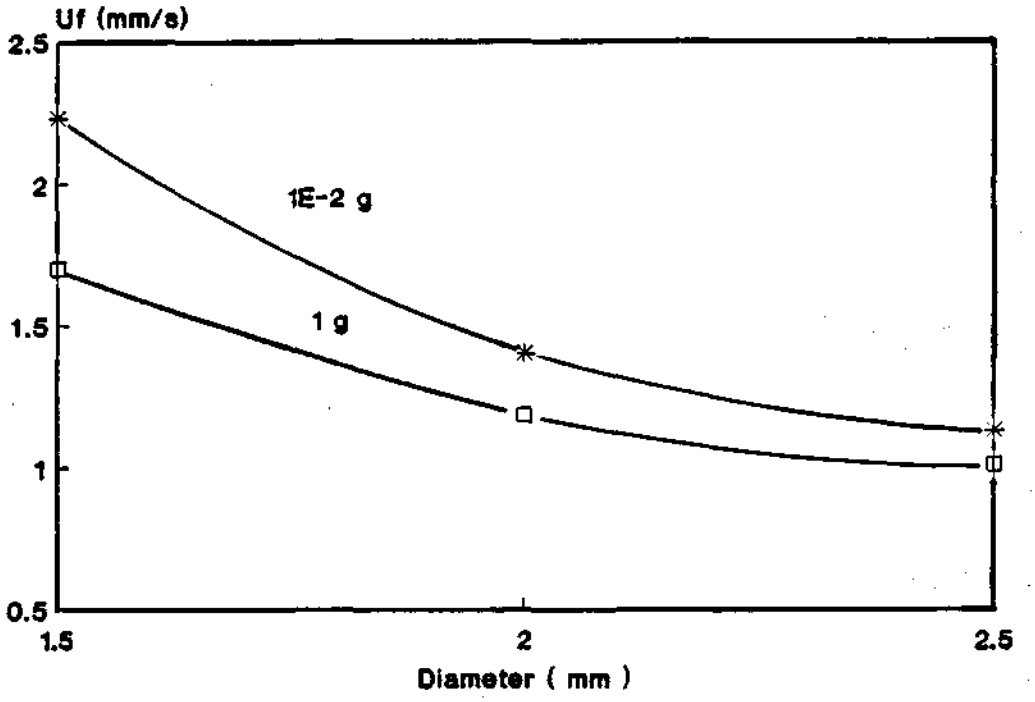

Fig. 2.20 Experimental downward flame spreading velocity vs. diameter. Solid rod. Y_{02} = 35 %. P = 756 mm Hg

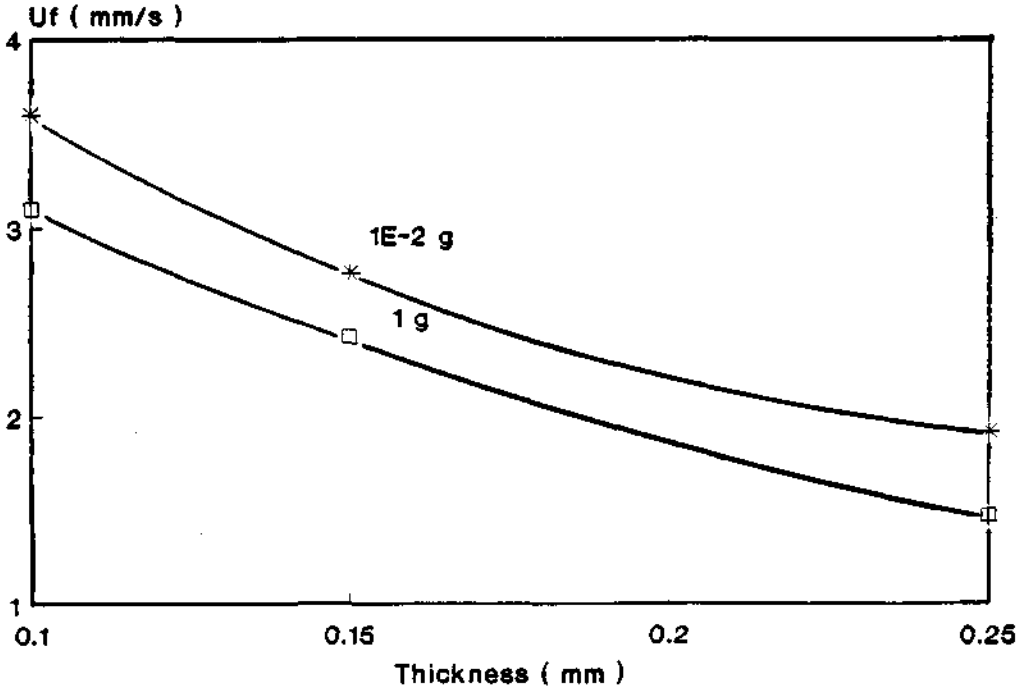

Fig. 2.21 Experimental downward flame spreading velocity vs. thickness. Tubular rod. Y_{02} = 35 % P = 756 mm Hg. Ø = 4 mm

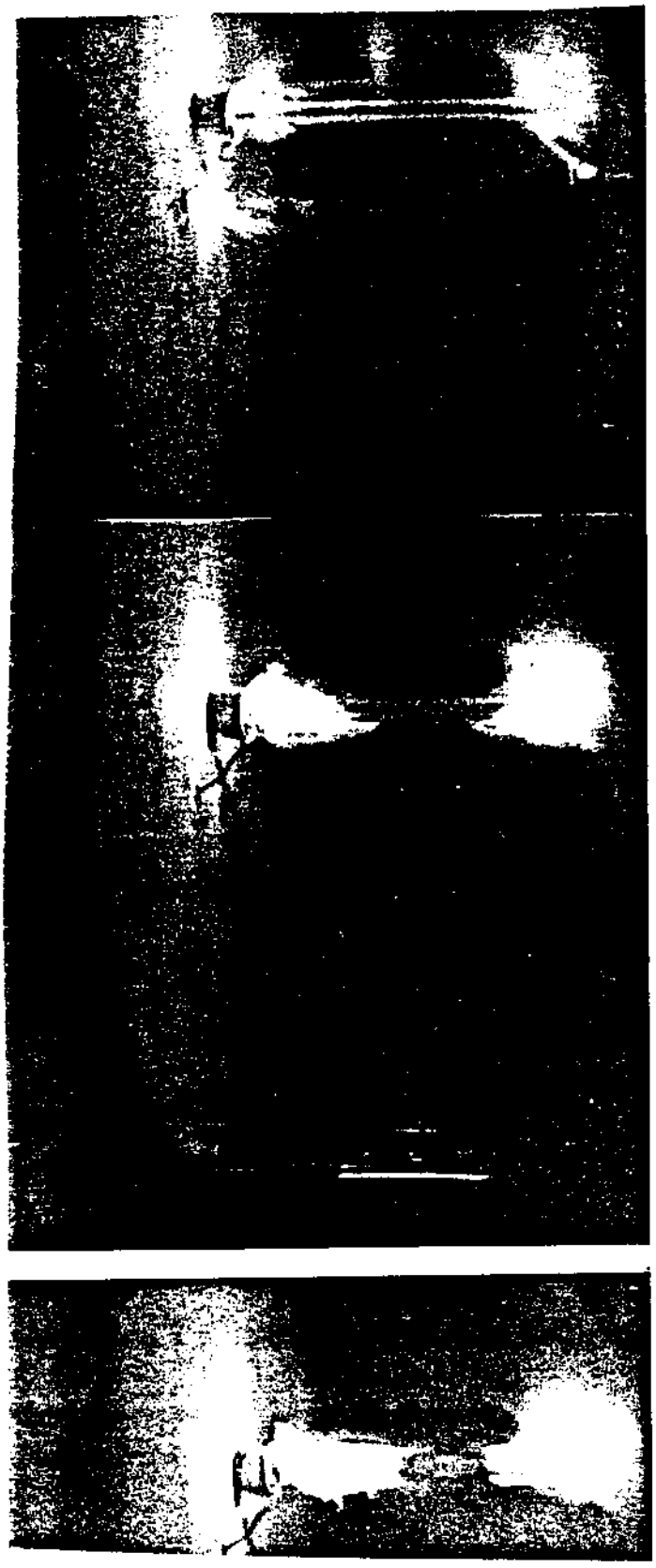

Fig. 2.22 Ignition Process for Quiescent Combustion Experiment at Microgravity Conditions in the CEV Caravelle Aircraft Laboratory.

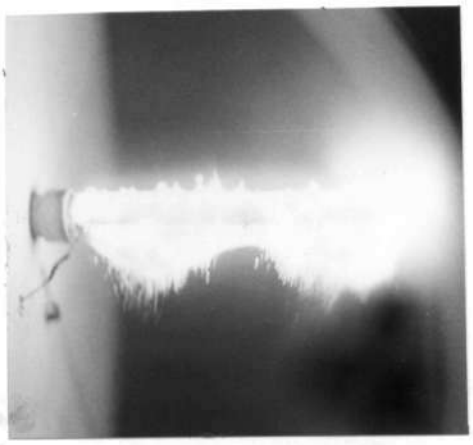

$t = t_o$

$t = t_o + 2$ s

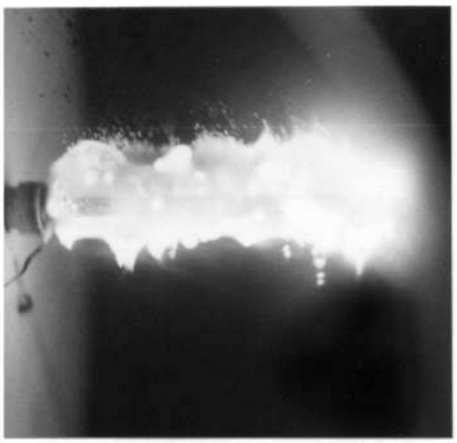

$t = t_o + 4$ s

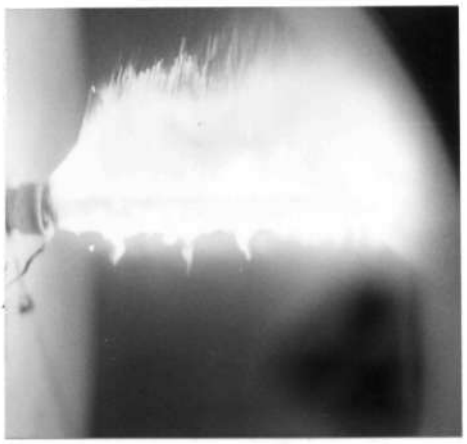

$t = t_o + 6$ s

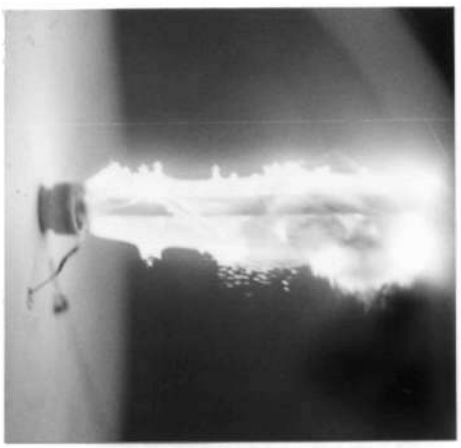

$t = t_o + 8$ s

Fig. 2.23 Quiescent Combustion on cylindrical rod at Microgravity conditions in the CEV Caravelle Aircraft Laboratory.
Y_{02} = 89 % ; P = 756 mm Hg ; Ø = 4 mm

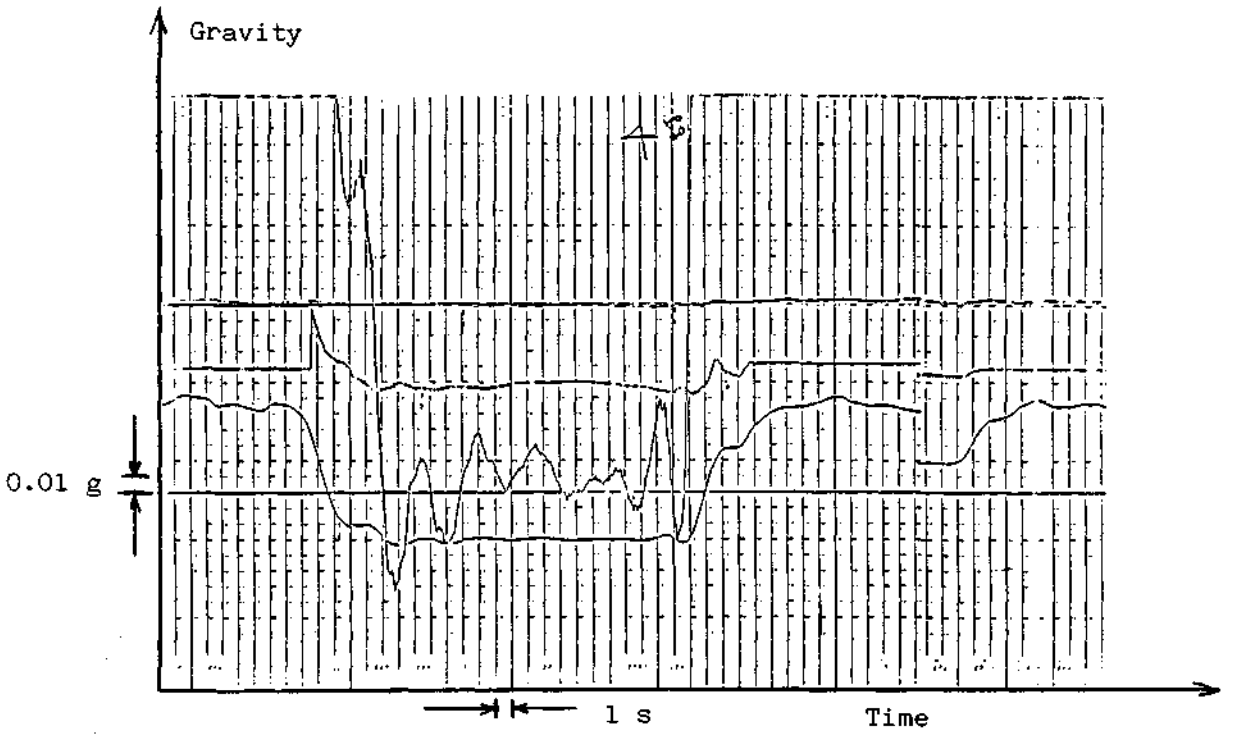

Fig. 2.24 a Profile of Gravity for Parabola 8, second flight

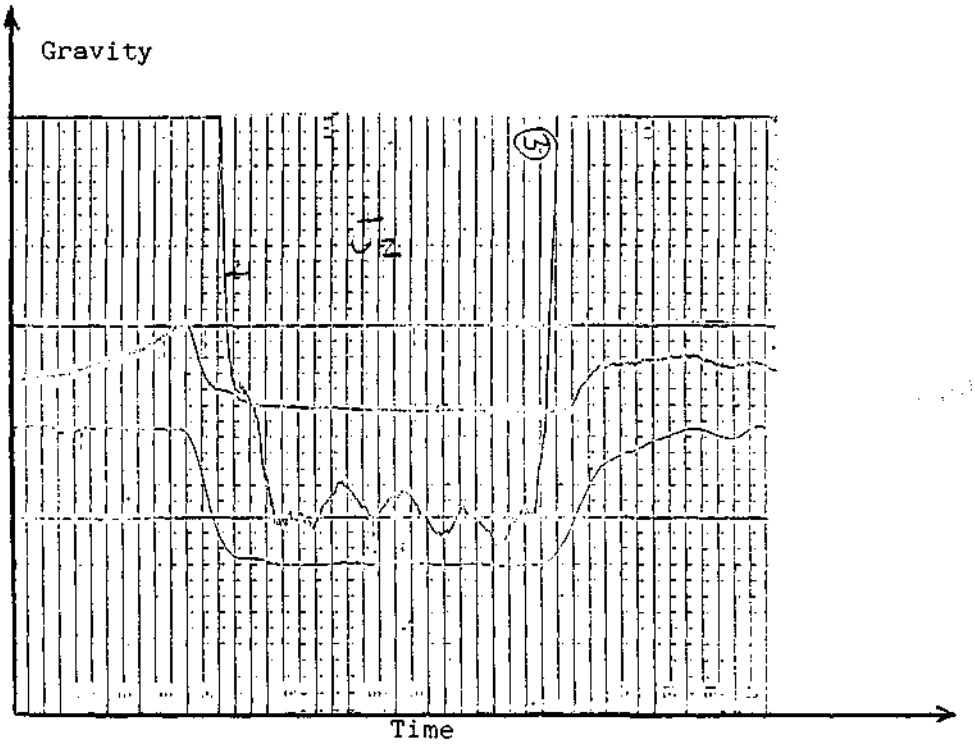

Fig. 2.24 b Profile of Gravity for Parabola 3, Third Flight

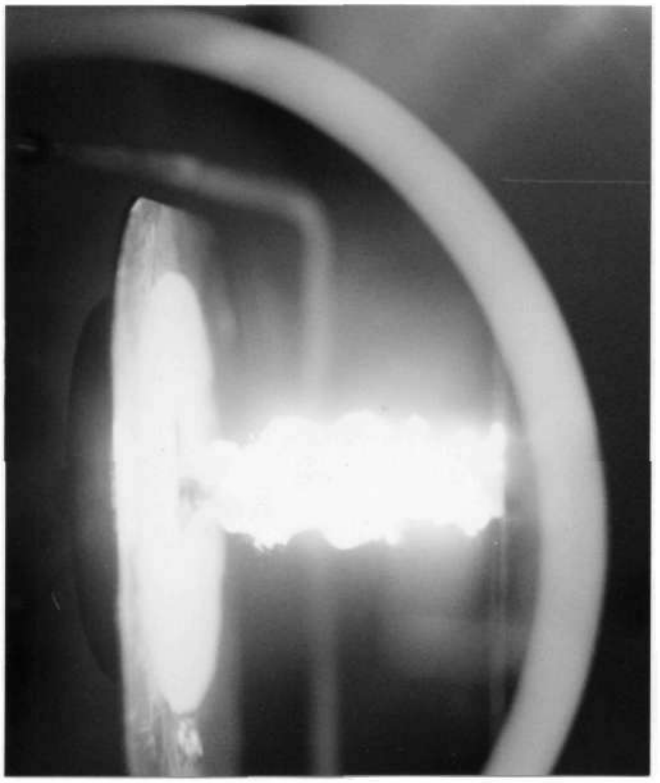

$t = t_o$

$t = t_o + 4$ s

Fig. 2.25 Quiescent combustion on cylindrical rod at microgravity conditions in the CEV Caravelle Aircraft Laboratory.
Y_{02} = 89 % ; P 756 mm Hg ; Ø = 4 mm

$t = t_o$

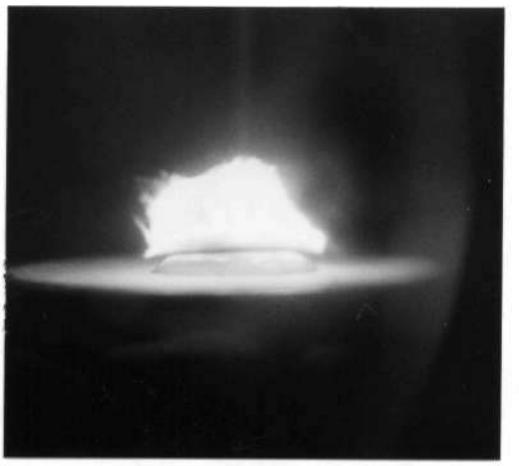

$t = t_o + 2$ s

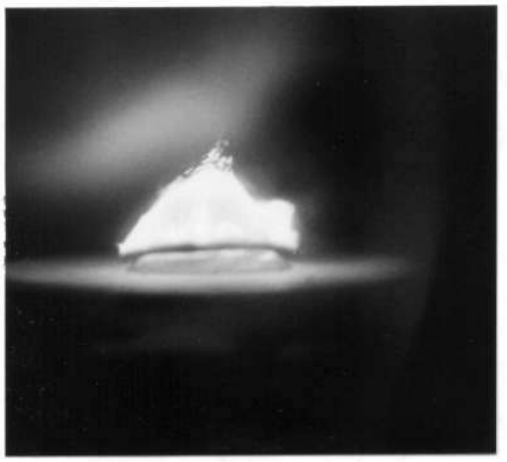

$t = t_o + 4$ s

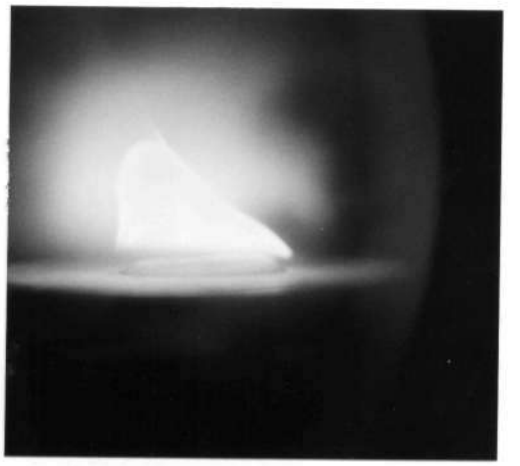

$t = t_o + 6$ s

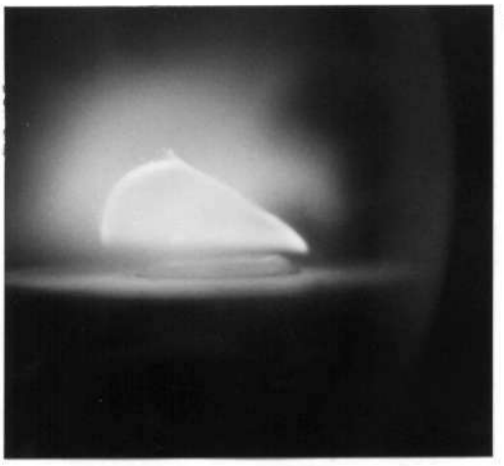

$t = t_o + 8$ s

$t = t_o + 10$ s

Fig. 2.26 Pool fire combustion at microgravity conditions in the CEV Caravelle Aircraft Laboratory.
$Y_{02} = 89$ % ; P = 756 mm Hg

3. WP2 AND WP3. SOUNDING ROCKET MODULE AND SOUNDING ROCKET EXPERIMENT

3. WP2 AND WP3. SOUNDING ROCKET MODULE AND SOUNDING ROCKET EXPERIMENT

These two Work Packages will have in common the following studies:

3.1. Review of Possible Experiments
3.2. Refilling of the Module
3.3. Forced Convection Problems

3.1. REVIEW OF POSSIBLE EXPERIMENTS

3.1.1. Introduction.

A review of the possible combustion problems which might be investigated in a sounding rocket module is carried out.

Taking into account the pressing problems and limitations that exist in the environment conditions in a sounding rocket module, the following parameters were considered:

- Characteristic length of the experiment.
- Characteristic time.
- Possibility of carriyng out multiple experiments in each launching.
- Number of experiments.
- Interest of forced convection effects.
- Possibility of utilizing multiple chambers within the module.
- Remarks.

The results are presented in the following Tables.

ANALYSIS OF COMBUSTION PROCESSES AT REDUCED GRAVITY

IN A SOUNDING ROCKET MODULE

FLAME SPREADING

EXPERIMENT	CHARACT. LENGHT	CHARACT. TIME	MULTIPLE EXPERIMENT	NUMBER OF EXPERIMENTS	FORCED CONV. EFFECTS	POSSIBILITY OF MULT. CHAMBERS	REMARKS
SOLID (PMMA)	10-30 cm	30-60 s	YES (WITH REFILL OR FORCED CONV.)	3-4 OR MORE	HIGH INTEREST	POSSIBLE	VERY SUITABLE
LIQUID	10-20 cm	30-40 s	YES (WITH REFILL OR FORCED CONV.)	3-4 OR MORE	HIGH INTEREST	POSSIBLE	INITIAL SHAPE & SAFETY PROBLEMS VERY SUITABLE
THIN SHEETS	10-20 cm	15-20 s	YES	SEVERAL	HIGH INTEREST	POSSIBLE	SUITABLE
SOLID&LIQUID ABOVE FLASH POINT	10-30 cm	0.01-0.1 s	YES	SEVERAL	HIGH INTEREST	POSSIBLE	SAFETY PROBLEM VERY SUITABLE

ANALYSIS OF COMBUSTION PROCESSES AT REDUCED GRAVITY

IN A SOUNDING ROCKET MODULE

POOL BURNING

EXPERIMENT	CHARACT. LENGHT	CHARACT. TIME	MULTIPLE EXPERIMENT	NUMBER OF EXPERIMENTS	FORCED CONV. EFFECTS	POSSIBILITY OF MULTIPLE CHAMBERS	REMARKS
LIQUID FUEL (HYDROCARBONS)	5-10 cm	0.5-1 min	YES (WITH REFILL OR FORCED CONV.)	2 - 3	HIGH INTEREST	NO	INITIAL SHAPE & SAFETY PROBLEM VERY SUITABLE
SOLID FUEL (PMMA)	5-10 cm	1-2 min	YES (WITH REFILL OR FORCED CONV.	2 - 3	HIGH INTEREST	NO	VERY SUITABLE

ANALYSIS OF COMBUSTION PROCESSES AT REDUCED GRAVITY

IN A SOUNDING ROCKET MODULE

SMOLDERING COMBUSTION

EXPERIMENT	CHARACT. LENGHT	CHARACT. TIME	MULTIPLE EXPERIMENT	NUMBER OF EXPERIMENTS	FORCED CONV. EFFECTS	POSSIBILITY OF MULTIPLE CHAMBERS	REMARKS
CELLULOSIC MATERIALS	1 cm	4 min	YES (WITH MULT. CHAMB.)	3 OR MORE	HIGH INTEREST	YES	VERY SUITABLE
FOAMS POL.	5 cm	3 min	YES (WITH MULT. CHAMB.)	3 OR MORE	HIGH INTEREST	YES	VERY SUITABLE

ANALYSIS OF COMBUSTION PROCESSES AT REDUCED GRAVITY

IN A SOUNDING ROCKET MODULE

DROPLETS AND SOLID PARTICLES

EXPERIMENT	CHARACT. LENGHT	CHARACT. TIME	MULTIPLE EXPERIMENT	NUMBER OF EXPERIMENTS	FORCED CONV. EFFECTS	POSSIBILITY OF MULTIPLE CHAMBERS	REMARKS
LIQUID DROPLETS (HYDROCARBONS)	1 mm	1 s	YES	SEVERAL	HIGH INTEREST	YES	DROP TOWERS RESULTS AVAIL.
SOLID PARTICLES (ALUMINIUM, COAL)	1 mm	1 s	YES	SEVERAL	HIGH INTEREST	YES	-
SLURRIES	1 mm	1-2 s	YES	SEVERAL	HIGH INTEREST	YES	-
SUPERCRITICAL DROPLETS	1 mm	0.5 s	YES	SEVERAL	HIGH INTEREST (DIFFICULT)	YES	REQUIRES SPECIAL CHAMBER

ANALYSIS OF COMBUSTION PROCESSES AT REDUCED GRAVITY

IN A SOUNDING ROCKET MODULE

GASEOUS FUELS INJECTED IN THE CHAMBER

EXPERIMENT	CHARACT. LENGHT	CHARACT. TIME	MULTIPLE EXPERIMENT	NUMBER OF EXPERIMENTS	FORCED CONV. EFFECTS	POSSIBILITY OF MULTIPLE CHAMBERS	REMARKS
POROUS BURNER	~10 cm (DIAMETER)	8-15 s	YES (WITH REFILL OR FORCED CONV.)	3-4 POSSIBLE MORE	HIGH INTEREST	POSSIBLE	-
GASEOUS JET	~1 cm (DIAMETER) 5-10 cm (FLAME LENGHT)	5-10 s	YES	SEVERAL	-	POSSIBLE	-
FLAME INSTABILITIES IN POROUS BURNERS AND JETS	~1 cm 5-10 cm	0.2 s	YES	SEVERAL	-	POSSIBLE	-

ANALISYS OF COMBUSTION PROCESSES AT REDUCED GRAVITY

IN A SOUNDING ROCKET MODULE

PREMIXED FLAMES

EXPERIMENT	CHARACT. LENGHT	CHARACT. TIME	MULTIPLE EXPERIMENT	NUMBER OF EXPERIMENTS	FORCED CONV. EFFECTS	POSSIBILITY OF MULTIPLE CHAMBERS	REMARKS
ONE DIMENSIONAL PROPAGATION	100 cm (LENGTH) 10 cm (DIAMETER)	0.5 s	YES (WITH MULTIPLE CHAMBERS)	3 OR MORE	-	YES (3 OR MORE)	-
SPHERICAL PROPAGATION	20-30 cm	0.5 s	YES(3 OR MORE SPHERES)	-	-	YES (3 OR MORE SPHERES)	-
PREMIXED JETS	1 cm (DIAMETER) 10 cm (FLAME)	0.2 s	YES	-	-	YES	-

ANALYSIS OF COMBUSTION PROCESSES AT REDUCED GRAVITY

IN A SOUNDING ROCKET MODULE

IGNITION

EXPERIMENT	CHARACT. LENGHT	CHARACT. TIME	MULTIPLE EXPERIMENT	NUMBER OF EXPERIMENTS	FORCED CONV. EFFECTS	POSSIBILITY OF MULTIPLE CHAMBERS	REMARKS
CONDENSED FUELS (PILOTED IGNITION)	5-10 cm	1 min	YES (REFILL. REQUIRED)	2-3	DIFFICULT	POSSIBLE	SUITABLE
SPONTANEOUS IGNITION	5-10 cm	1 min	YES (REFILL. REQUIRED)	2-3	DIFFICULT	POSSIBLE	SUITABLE
IGNITION BY RADIATION	5-10 cm	2 min	YES (REFILL. REQUIRED)	2	DIFFICULT	POSSIBLE	SUITABLE

3.1.2. Conclusions

The following principles conclusions may be derived from the preceeding Tables:

- A large variety of combustion experiments are suitable to be conducted in a sounding rocket module.

- Most experiments require combustion times smaller than 1 minute.

- Since there are six minutes at reduced gravity available, there exists the possibility of carrying out multiple experiments in each launching.

- If the amount of oxygen consumed in each experiment is small (droplet combustion, for example), to carry out multiple experiments is relatively simple.

- In most cases, emptying and refilling of the chamber will be required.

- This process, which is mechanically simple, presents the problem of the time required to become the oxygen or gases in introduced into the chamber below a minimun permissible level of the fluctuation velocities.

- This problem, including venting, will be specially studied.

- Forced convocation effects are very interesting in many experiments. A special study will be devoted to the problem of generating forced convection effects.

- Some combustion experiments require small space. Therefore, there exists the possibility of utilizing several chambers within the module.

3.2. REFILLING OF THE MODULE

3.2.1. Introduction.

The objetive of this experimental programme is to study the time needed to reduce the fluctuation velocities of the oxygen (or other reactant mixture) in the combustion module once it is refilled down to a minimum prescribed value.

3.2.2. Methods for velocity measuring.

In the first stage, some techniques were analyzed for consideration to measure the velocity in the chamber. These techniques were:

- Hot wire anemometry *(HW)*
- Laser anemometry *(LDV)*
- Visualitation methods.
  - Particle Image Velocimetry.
  - Speckle Velocimetry.
  - LIF.

In the first place, the use of hot wire anemometry has the inconvenience of giving us a punctual measure of the velocity in function of the time. Considering the flow field in the chamber after the refilling, it is interesting to obtain a measure of the velocity in as much flow as possible in function of the time.

Secondly, the order of the velocities to measure is about 2-10 *mm/s*, and so the calibration of the *HW* must be done very carefully because the velocities are very low.

Thirdly, the free convection generate by the heated sensor at such low velocities makes it necessary to work with a sensor of low

temperature, and this convection can not be include in the calibration because the measure is made in a closed chamber. Lastly the hot wire anemometry is an intrusive method and disturbes the flow.

The laser anemometry does not present the problem of calibration and is a non-intrusive technique, but it has the inconvenience of giving us the velocity only at one point in function of the time. Due to this, it is necessary to repeat the test many times with the same conditions in order to obtain a representative sample of the velocities field inside the chamber, which is required in order to affirm that the flow field inside the chamber is repetitive (of course from the macroscopic point of view it is expected to be repetitive).

To have a temporal observation, partial or complete, of the flow field it is necessary to use flow visualization techniques, especially particle image velocimetry.

In these techniques, foreign particles are added to the flowing fluid and, if they are small enough, one may assume that the motion of these particles is the same as that of the fluid in direction and magnitude.

Although these methods can produce errors for unsteady flows due to the finite size of the particles, they can serve to determine the order of the maximum velocities in the chamber and its temporal evolutions for long times.

Other techniques, like laser induced fluorescence (LIF), to measure velocity have not been considered due to their complexity and the necessity of disposing high power laser with determined wave lengths.

3.2.3. Experimental work.

The procedure has been measuring the velocity through seeding small particles. In this method, foreign particles are added to the flow, it is illuminated and several photos are taken at known intervals of time and with controlled exposure time.

— Test equipment.

The test have been realized in a modified test chamber utilized in parabolic flights whose shape and dimensions are showed in fig.3.2.1 in which the windows for illumination and observation of the flow, the valves and the two kinds of devices utilized to fill the chamber, are shown.

The illumination has been made using a 4 watt laser Ar-Ion (Ar^{-}), and expanding the laser beam in a light sheet using cylindrical lenses as is shown in fig.3.2.2 so that only a thin plane of the flow is lighted. The photographic camera axis is perpendicular to the observation plane. In the fig.3.2.3 a general vision of the instalation used to carry out the test can be observed.

— Particle selection.

The general requirements for tracer particles are, usually:

- being neutrally buoyant,
- Being non-toxic and non-corrosive,
- having low mixing rates with the main fluid and
- high degree of light reflectivity.

A general rule is that the particle should be as small as possible, at least one order of magnitude smaller than the fine structure of the studied flow.

Therefore the required particle diameter is inversely proportional to the observation time, which is the function of the expected velocities in the flow.

Tracer particles for gaseous flows are solids or liquids. In the table I are shown several kinds of tracers usually used in air.

TABLE I

PARTICLE	DIAMETER
Lycopodium	30 μm
Oil drops	1 μm
Cigarette smoke	0.2 μm
Metaldehyde	1 mm
Atomized DOP	1 μm
Glass spheres	20 μm
Marble dust	1 μm
Aluminium oxide	2-3 μm
Magnesium oxide	2-3 μm

The tracers particles used were:

- Smoke generated by oil
- Lypocopodium
- Aluminium oxide
- Magnesium oxide

Smoke was eliminated due to the convection generated by the device for generating smoke in the chamber. The smoke must be produced before the refilling, because if it is made during it the streaklines can not be identified over a suitable distance due to the diffusion of the smoke in the air.

The diameter of Lycopodium particles is larger than that of magnesium or aluminium oxide. Finally, magnesium particles were selected

because they were more visible than the aluminium oxide ones for the laser power available in the laboratory.

— Test procedure.

In the first stage, a pressure of around 100 *mm Hg* was established and subsequently the chamber was refilled until atmospheric pressure was reached, introducing the tracer particles at the same time. At 15 *s* after the valve was opened, the first photo was taken, taking the others at intervals of 30 *s* in some test and of 15 *s* in the others. Two kinds of filling were made. The first, directly through the valve and the other through a damping system as is shown in fig.3.2.1.

The exposure time used was 2 *s*, because the expected velocities inside the chamber after 30 *s* were of the order of 2-10 *mm/s*, producing traces large enough to measure the velocity with correct accuracy. So it can be assumed that the largest traces detected corresponded to particles that were in the light sheet and not to particles that were passing through it.

In spite of all these reasons and due to the flow field existing in the chamber, some photos were not suitable because there were not enough traces in the observation plane.

The illumination was continuos during the first test, but it was observed that this method generated convection in the chamber due to the heating of the chamber walls, so during the final test, the test section was only lighted during exposure time.

To measure the velocity, the photograps were digitized and analyzed using a frame grabber and image processing software.

3.2.4. Experimental results.

In fig. 3.2.5 the maximun velocities in the chamber are shown in

fuction of the time for both kinds of filling. This figure gives us an order of the maximum velocities that is expected in the chamber after the filling in function of the time.

In the first place, it can be observed that, after the first 15 *s*, there is a low difference between both kinds of filling, this means that the invluence of the filter is only appreciable in the first seconds, about 4-5 *s*. Secondly, there is a quick decline of the velocities in the chamber, reaching velocities less than 10 *mm/s* at 15 *s* and of the order of 2 *mm/s* at 120 seconds after the moment at which the valve was opened.

It is pointed that this experimental programme has been carried out in a combustion chamber of 25 *cm* in diameter, and the combustion module will have a diameter of about 40 *cm*. Due to the predominant local nature of the fluctuation velocities attenuation phenomenon it is expected that this difference in dimensions will have a negligible influence on the results.

Utmost care must be taken in order of not generating forces during the venting process, which might disturb other simultaneous experiments.

The exhaust valve could discharge into a ring which will have venting holes distributed regularly along the periphery of the module. The jets will discharge radially, and if this radial discharge would not be permissible circular caps might be placed at each outlet to prevent the production of axial forces.

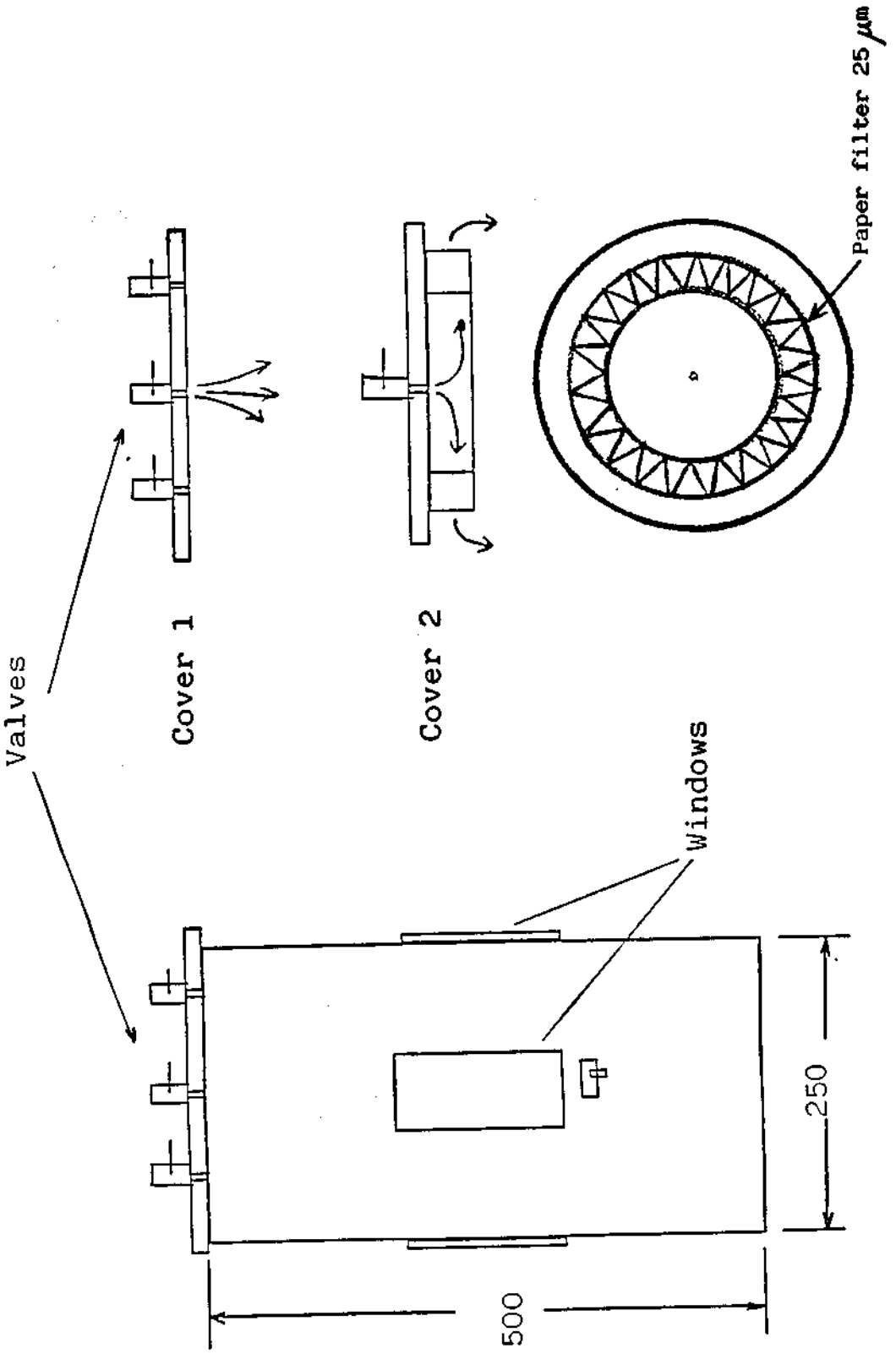

Fig. 3.2.1 Schematic diagram of test chamber

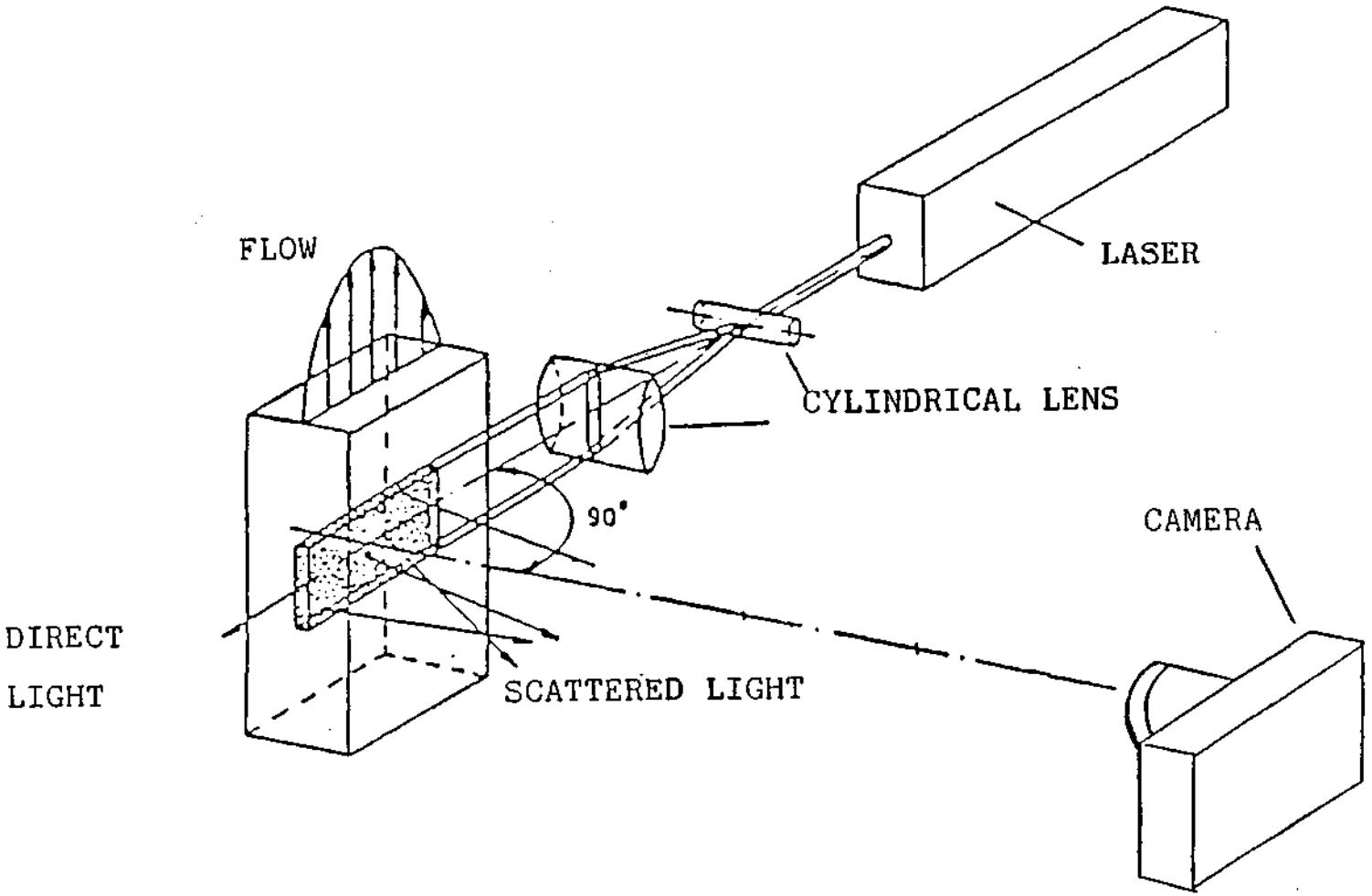

Fig. 3.2.2 Illumination and recording system for the observation of tracer particles

Fig. 3.2.3 Experimental installation

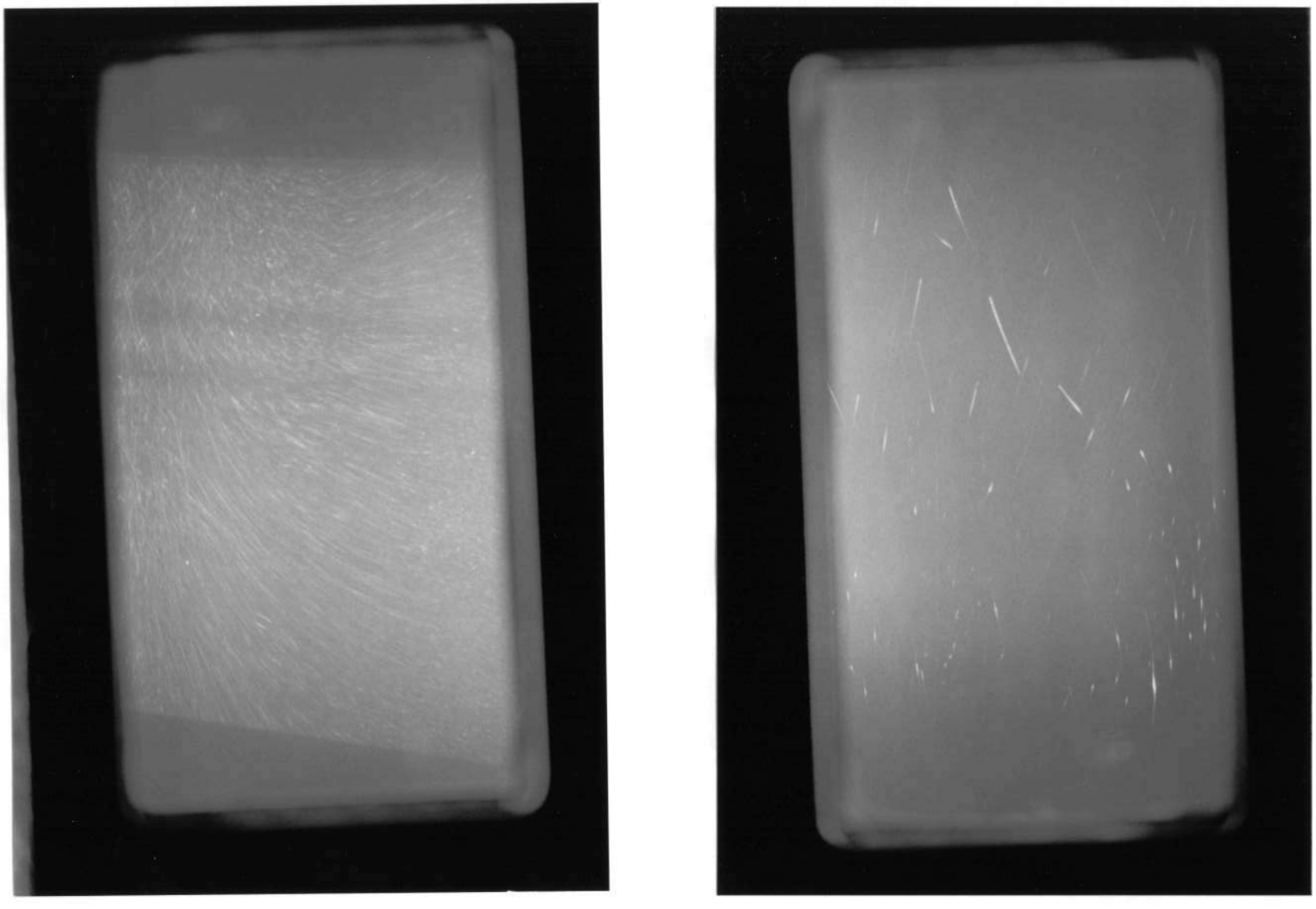

(a) (b)

Fig. 3.2.4 Flow field inside the chamber. (a) High density of particles ; (b) low density of particles

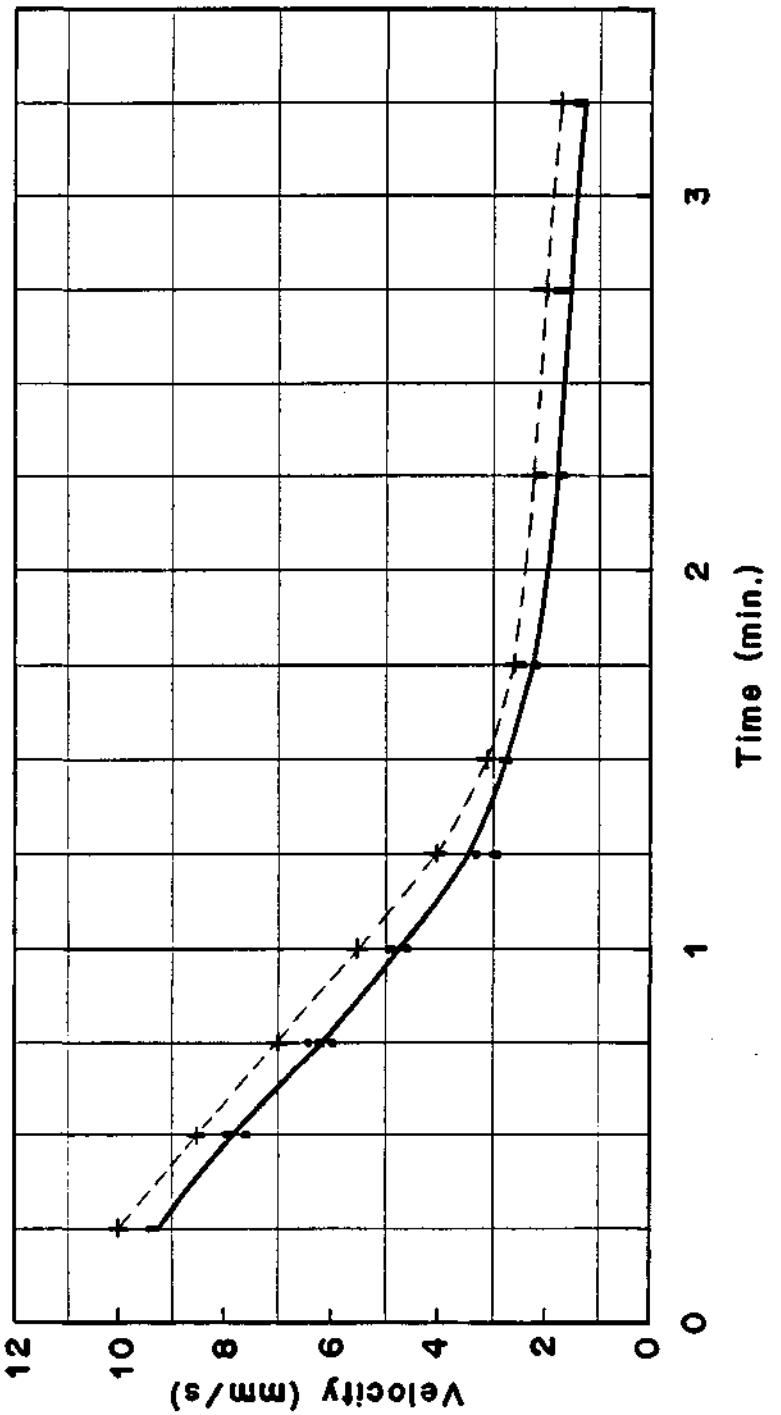

Fig. 3.2.5 Maximum Velocities inside the chamber vs. time

3.3. FORCED CONVECTION EFFECTS

3.3.1. Introduction

It was mentioned in the Introduction of this Report that the study of forced convection at low Reynolds Numbers in combustion processes at reduced gravity it is actually considered of high interest. This is primarily due to the fact that a fire in a space laboratory or spacecraft would take place in an environment of low gas velocities originated by the air or oxygen conditioning system and even by the motion of people.

On the other hand, it is not possible to study forced convection effects at low Reynolds Number on the ground at 1 *g*, because of the strong interference of free convection effects even at low Grashof Numbers, as for example, in droplets combustion.

In a sounding rocket module forced convection effects can be produced is two ways; by moving the burning sample along the module keeping the atmosphere at rest, or conversely, keeping the combustion experiment at rest and by generating a flow of the oxygen or reactant gases at a controllable velocity.

3.3.2. Motion of the Sample

This system is mechanically simple. With a variable speed electric DC micromotor it is possible to generate the motion of the sample at a easily controllable velocity. Since forced convection velocities are small, from 0.5 up to 6 or 8 *cm/s* with, a module of 120-140 *cm* in length there will a wide range of combustion times available.

There is the inconvenient that after each run it would have to be allowed a sufficient time for the atmosphere to become at rest. We have

shown that these times are long and the sample will kept burning in the meantime. Therefore, it is required to refill the chamber between experiments. This emptying and refilling process would also extinguish the flame of the first sample.

Depending of the type of the experiments, and according to the times require to damp the fluctuations velocities after each refilling, it looks feasible to run three and even four experiments in each launching.

A sketch of this type of module is shown in fig.3.3.1.

3.3.3. Forced Convection Flow Generation

The problem of generating a one-dimensional convective flow at constant velocity which could be changed after each experiment will be briefly discussed, and a preliminary analysis of a specific system will be carried out.

The oxygen or reactant gases will have to be carried out in a high pressure bottle and dicharged through a controllable valve.

Means would have to be provided to damp the kinetic energy and to assure one-dimensional flow in the combustion chamber. A thick porous wall appear suitable.

Two means look possible to extract the gases out of the combustion chamber: to use a small compressor to fill a bottle in the module, or to vent off the gases to the exterior of the module.

This second system looks much simpler. The venting would have to be carried out through a controllable valve and according to the general conditions for venting gases in the sounding rocket, specially avoiding the introduction of forces.

Another porous wall would have to be placed at the end of the combustion chamber in order to assure that the one-dimensional flow would not disturbed by the venting process.

This porous wall will also act as a heat sink and if its heat capacity is sufficiently large it will reduce the variation of gas temperature at the exhaust valve. This problem will be discussed in the following paragraphs.

3.3.4. Analysis of the System[1]

3.3.4.1. Stationary isothermal solution at the outlet.

The aim of the design proposed is to produce a uniform, steady, low speed gas flow in a chamber or combustion module where a sample is to be burned under reduced gravity conditions.

The velocity range must be controlled and kept constant at any value within the range 5-100 *mm/s* during one minute approximately, although a non steady combustion process takes place in the chamber.

The possibility of an stationary flow in the chamber with the configuration proposed is explored for an isothermal condition at the outlet as a preliminary step to the combustion process.

A sketch of the configuration proposed is shown in the adjoined figure. The test chamber is separated from the pre-chamber and post-chamber by the two abovementioned porous walls that assure one dimensional and uniform conditions within the chamber. The flow is controlled by two valves with variable areas.

The pressure difference between the pre-chamber and between the

[1] This study has been carried out by Sener.

post-chamber and the exterior is supposed to be always over the critical value, so that the value are considered permanently choked.

3.3.4.1. Set of equations.

The complete equation set that provides the system behaviour with the symbols listed in the Appendix I is:

$$VO \frac{d\rho_o}{dt} = -GO \qquad (1)$$

$$PO/PO(0) = [\rho O/\rho O(0)]^{\gamma} \qquad (2)$$

$$GO = \left[\frac{2}{\gamma+1}\right]^{\frac{\gamma+1}{2(\gamma-1)}} \sqrt{\gamma PO\rho O}\ AO \qquad (3)$$

$$V1 \frac{d\rho_1}{dt} = GO-G1 \qquad (4)$$

$$V1 \frac{dP_1}{dt} = \gamma[GO\ PO/\rho O - G1\ P1/\rho 1] \qquad (5)$$

$$G1 = \frac{K1\ A\ (P1^2-P2^2)}{2\mu\ e1\ Rg\ Tp1} \qquad (6)$$

$$V2 \frac{d\rho_2}{dt} = GO-G2 \qquad (7)$$

$$V2 \frac{dP_2}{dt} = (\gamma-1)\ G1\ Cp\ Tp1 - \gamma G2\ P2/\rho 2 \qquad (8)$$

$$G2 = \frac{K2\ A\ (P1^2-P2^2)}{2\mu\ e2\ Rg\ Tp2} \qquad (9)$$

$$V3 \frac{d\rho_3}{dt} = G2 - G3 \qquad (10)$$

$$V3 \frac{dP_3}{dt} = (\gamma-1)\ G2\ Cp\ Tp2 - \gamma G3\ P3/\rho 3 \qquad (11)$$

$$G3 = \left[\frac{2}{\gamma+1}\right]^{\frac{\gamma+1}{2(\gamma-1)}} \sqrt{\gamma P3 \rho 3}\ A3 \qquad (12)$$

If *Ao*, *A3*, *Tp1*, *Tp2* and the initial conditions for pressure and densities are known, the twelve previous equations can solve *P0*, $\rho 0$, *G0*, *P1*, $\rho 1$, *G1*, *P2*, $\rho 2$, *G2*, *P3*, $\rho 3$, *G3* as function of time.

— Steady conditions in test chamber

The objetive is to mantain steady defined condition in test chamber *G2*, *p2* and $\rho 2$. To avoid transition effects we assume that test pressure and density are the same that initial condition. Therefore porous wall temperature *Tp1* and *Tp2* are also equal to initial temperature *T2(0)*.

With the paramenter values supposed in annex II, a preliminary estimation can be obtained

$$G2 = \rho 2\ U2\ A = 7.2\ 1\text{-}3\ Kg/s$$

From *(7)*, as $\rho 2$ is to be constant, *G1* = *G2*. And from *(6)* an estimation of pressure difference across porous wall can be obtained

$$P1 - P2 = 36\ Pa$$

From *(9)*, *P3* must be also constant and the pressure diference is

$$P2 - P3 = 9\ Pa$$

From *(10)-(12)* is easy to obtain that the other variables of the postchamber must be constant *G3* = *G2*, and $\rho 3 = P3/p2 \cdot \rho 2$

This also allows to assure that the value *A3* must be kept at constant value during the test

$$A3 = \frac{G3}{\left[\frac{2}{\gamma+1}\right]^{\frac{\gamma+1}{2(\gamma-1)}} \sqrt{\gamma P3 \rho 3}} = 27\ mm^2$$

— Tank output valve regulation

Once obtained $P1$ from (6), the system (1)-(5) allows to study how must be controlled the area $AO(t)$ to keep $P1$ constant, and how the density and pressure inside the tank decrease.

It is convenient to obtain a set of nondimensional equations for this process. The characteristic values are taken from test chamber conditions.

$XO = \rho O/\rho 2$
$X1 = \rho 1/\rho 2$
$\varphi O = PO/P2$
$\varphi 1 = P1/P2$
$gO = GO/G2$
$g1 = G1/G2$
$WO = VO/V2$
$W1 = V1/V2$
$\alpha = AO/AOmax$
$\tau = t/tc$

with $tc = V2\rho 2/G2 = L2/U2 = 15\ s.$

This nondimensional systems so defined is

$$WO \frac{dXO}{d\tau} = -gO \qquad (13)$$

$$\varphi O/\varphi O(O) = [XO/XO(O)]^{\gamma} \qquad (14)$$

$$W1 \frac{dX1}{d\tau} = gO-g1 \qquad (15)$$

$$g0\ \varphi 0/\ X0 = g1\ \varphi 1/\ X1 \qquad (16)$$

$$g0 = B\sqrt{\varphi 0\ X0}\ \alpha 0(\tau) \qquad (17)$$

where $B = \dfrac{\left[\frac{2}{\gamma+1}\right]^{\frac{\gamma+1}{2(\gamma-1)}}\ \sqrt{\gamma P2\rho 2}\ A0\ max}{G2}$

From the system *(13)-(17)* and the initial conditions *X0(0)*, *X2(0)* = *1*, the evolution with time of *X0*, *X1*, $\varphi 1$ and *g0* can be obtained and then from *(17)* the law for the regulation of the tank output valve $\alpha_o(\tau)$.

Example

With the parameters and initials conditions assumed in Appendix II, the system *(13)-(17)* has been integrated to obtain the *A0* law. The non dimensional results are given in table 1. With an initial tank pressure of 20 bars, and a test duration of 60 *s.*, the output area *A0* is increased from 1.4 mm^2 to 3 mm^2. The tank reduce its density to half the initial value.

Conclusion

The desing allow a constant mass flow in the test chamber and the valve regulation law can be obtained easily as has been showed. But this preliminary modelization show some points and lacks were further study must be performed:

- The output area of the tank is quite small, and problably mechanical problems must be resolved to control it accurately.
- The transitional effects, specially if the experiment is to be repeated with changes in test conditions, must be also considered.

TABLE 1. EXAMPLE OF TANK VALVE AREA LAW WITH TIME

τ	X_o	X_1	α_o
0.0000000E+00	20.00000	1.000000	0.3500000
0.1000000	19.77431	1.000617	0.3543507
0.2000000	19.54785	1.002265	0.3603483
0.3000000	19.32080	1.004696	0.3662594
0.4000000	19.09331	1.007725	0.3721447
0.5000000	18.86546	1.011217	0.3780519
0.6000000	18.63734	1.015072	0.3840186
0.7000000	18.40901	1.019217	0.3900750
0.8000000	18.18050	1.023599	0.3962457
0.9000000	17.95184	1.028179	0.4025508
1.000000	17.72305	1.032928	0.4090080
1.100000	17.49415	1.037829	0.4156324
1.200000	17.26515	1.042865	0.4224379
1.300000	17.03605	1.048029	0.4294376
1.400000	16.80686	1.053313	0.4366439
1.500000	16.57759	1.058715	0.4440690
1.600000	16.34822	1.064232	0.4517254
1.700000	16.11877	1.069863	0.4596254
1.800000	15.88924	1.075611	0.4677821
1.900000	15.65961	1.081475	0.4762088
2.000000	15.42990	1.087458	0.4849197
2.100000	15.20010	1.093564	0.4939297
2.200000	14.97020	1.099795	0.5032546
2.300000	14.74020	1.106155	0.5129111
2.400000	14.51011	1.112648	0.5229171
2.500000	14.27991	1.119278	0.5332917
2.600000	14.04961	1.126050	0.5440554
2.700000	13.81919	1.132970	0.5552299
2.800000	13.58866	1.140143	0.5668390
2.900000	13.35801	1.147274	0.5789080
3.000000	13.12724	1.154669	0.5914641
3.100000	12.89634	1.162236	0.6045370
3.200000	12.66531	1.169980	0.6181584
3.300000	12.43413	1.177910	0.6323629
3.400000	12.20282	1.186033	0.6471881
3.500000	11.97135	1.194358	0.6626745
3.600000	11.73972	1.202892	0.6788665
3.700000	11.50793	1.211646	0.6958125
3.800000	11.27597	1.220629	0.7135652
3.900000	11.04383	1.229852	0.7321825
4.000000	10.81150	1.239326	0.7517277

3.3.4.2. Variable temperature at the outlet.

Introduction

With a combustion process on the probe, the cold flow model previously discussed is not longer applicable without a detailed analysis of the modifications that the combustion produces.

The combustion is intended to be performed at constant pressure. The hot gases form a hot wake downstream the probe, changing the uniformity of temperature and density at the cross section. Without entering in detail in this combustion dynamic, some aspects of its influence in the desing of the module can be considered.

Porous wall thermal behaviour

The hot gases that flow into the porous wall have a temperature much higher (up to 1000 K), than the initial temperature of the porous solid material (around 300 K). It is necessary to estimate two important characteristic times.

The first is the time required for the gas to be cooled and acquire the solid temperature. This is controlled by a heat conducting process at porous scale. The time *tc1* compared with the residence time in the porous wall is much shorter:

$$\frac{tc1}{tr} = \frac{\rho\ Cp\ \delta^2 U}{K\ \ e} = \frac{\mu\ Cp}{K}\ \frac{\rho U \delta}{\mu}\ \frac{\delta}{e}\ Pr\ Re\ \frac{\delta}{e} = 10^{-4}$$

The second characteristic time is due to the time required for the solid to increase the temperature with the heat received from the flow *tc2*.

$$tc2 = \frac{\rho m\ Cm\ e}{\rho\ CpU} = 10^3 s$$

During the six minutes of the total test duration the maximum increase in temperature is $\Delta Tm = (Tg-Tm)\ to/tc2 = (Tg-Tm)\ 0.36 = 200\ K$.

So, although the porous wall does not reach the gas temperature, the increase and the non uniformity across the section, means that this thermal behaviour must be study in detail and can be critical for the desing of this wall.

Exit mass flow regulation

The post-chamber receives the gas coming out of the second porous wall. If due to the previous estimation this gas does not have a uniform and stationary temperature, the regulation of the output valve is not a simple as in the cold flow condition.

The temperature or pressure must be controlled in significant points and this information will serve for the control of the output valve with the aim of having the stationary and desired flow characteristics in the combustion chamber.

Transients flows

The module must be designed to allow change in the test condition, in order to allow several flow values in the same flight. The change in velocity implies transient flows which behaviour must be study.

The best test conditions order, the time needed for the test in the chamber flow conditions with the uniformity and low level of turbulence specified, are problems to be study in detail.

This change in test conditions also means a change in the areas of the control valves.

Conclusions

These comentaries show that a detailed desing analysis must be taken to be solve the thermal, fluid dynamics and control problems. This information will be essential to the selection and desing of materials, dimensions, control transducers and other technical solutions.

The relation between the variables and test conditions should be controlled by a microprocessor to monitor the process, and adjust the variables of control (valve areas) to the desired and scheduled conditions.

APPENDIX I

A = *chamber section area.*

AO, A3 = *valve areas.*

B = *non-dimensional constan.*

Cm = *porous wall solid density.*

Cp = *gas specific heat.*

e = *porous wall thickness.*

G = *mass flow.*

g = *non-dimensional gas flow.*

K = *Darcy constant.*

P = *pressure.*

Rg = *gas constant.*

t = *time.*

Tp = *porous wall temperature.*

U = *gas velocity.*

V = *volume.*

W = *non-dimensional volume.*

X = *non-dimensional density.*

α = *non-dimensional valve area.*

δ = *porous typical dimension*

φ = *non-dimensional pressure.*

μ = *gas dynamic viscosity.*

γ = *gas specific heat relation.*

ρ = *gas density.*

ρm = *porous wall solid density.*

τ = *non-dimensional time.*

APPENDIX II

A = 0.1256 m.

$AOmax$ = 4 mm.

Cm = Cp

$e1$ = 40 mm

$e2$ = 10 mm

$K1$ = $K2$ = 10^{-10}m

$P2$ = 100.000 pa

Rg = 260 Jul/Kg/K

Tp = 300 k

$U2$ = 4 cm/s

$W1$ = 0.333

WO = 0.444

$XO(O)$ = 20

$\varphi O(O)$ = 20

δ = 10^{-5}m

μ = 2 10^{-6}Kg/m/s

γ = 1.4

$\rho 2$ = 1.43 kg/m

ρm = 1000 $\rho 2$

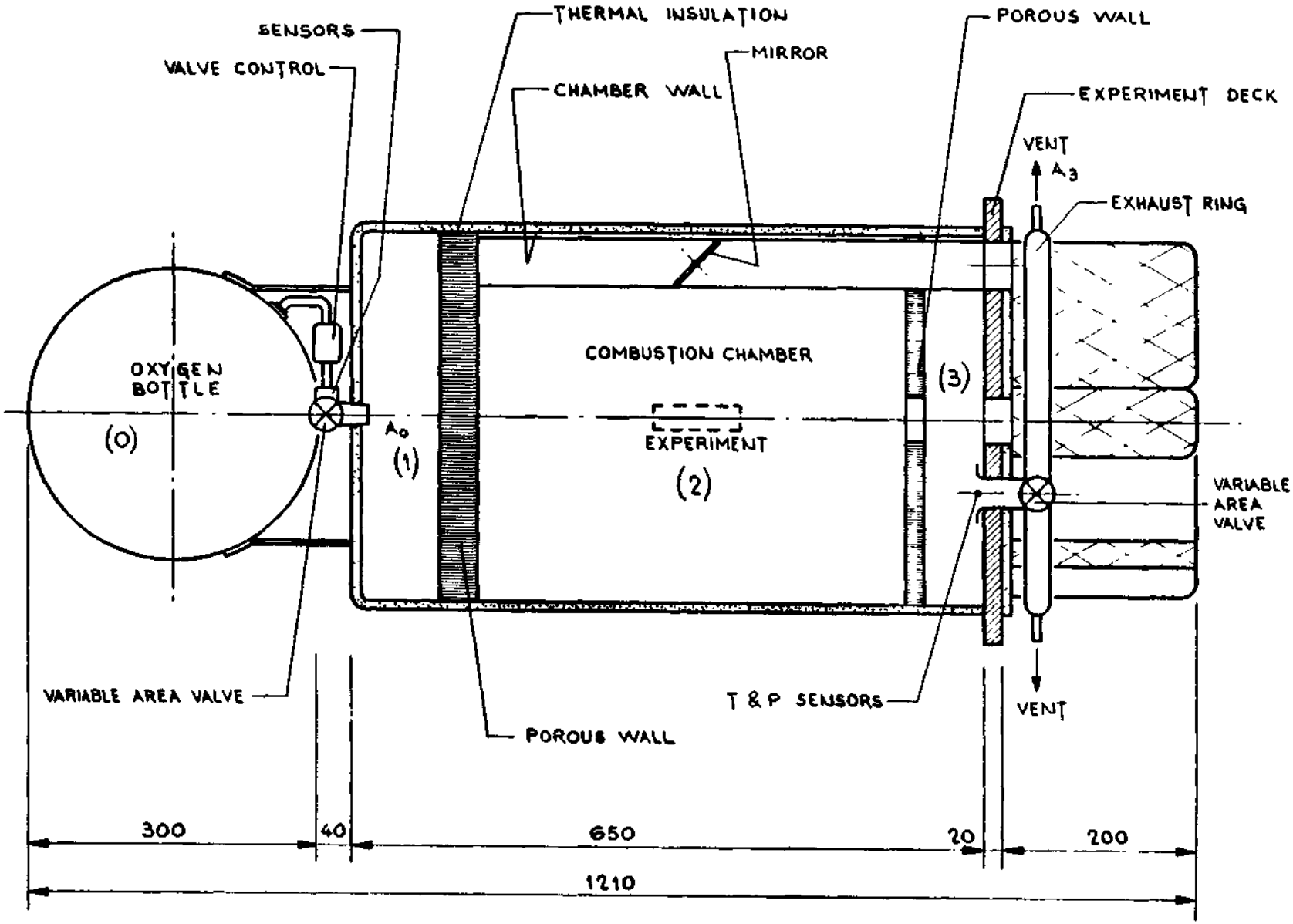

LONGITUDINAL SECTION

Fig. 3.3.1

COMBUSTION MODULE

FORCED CONVECTION BY GAS MOTION.

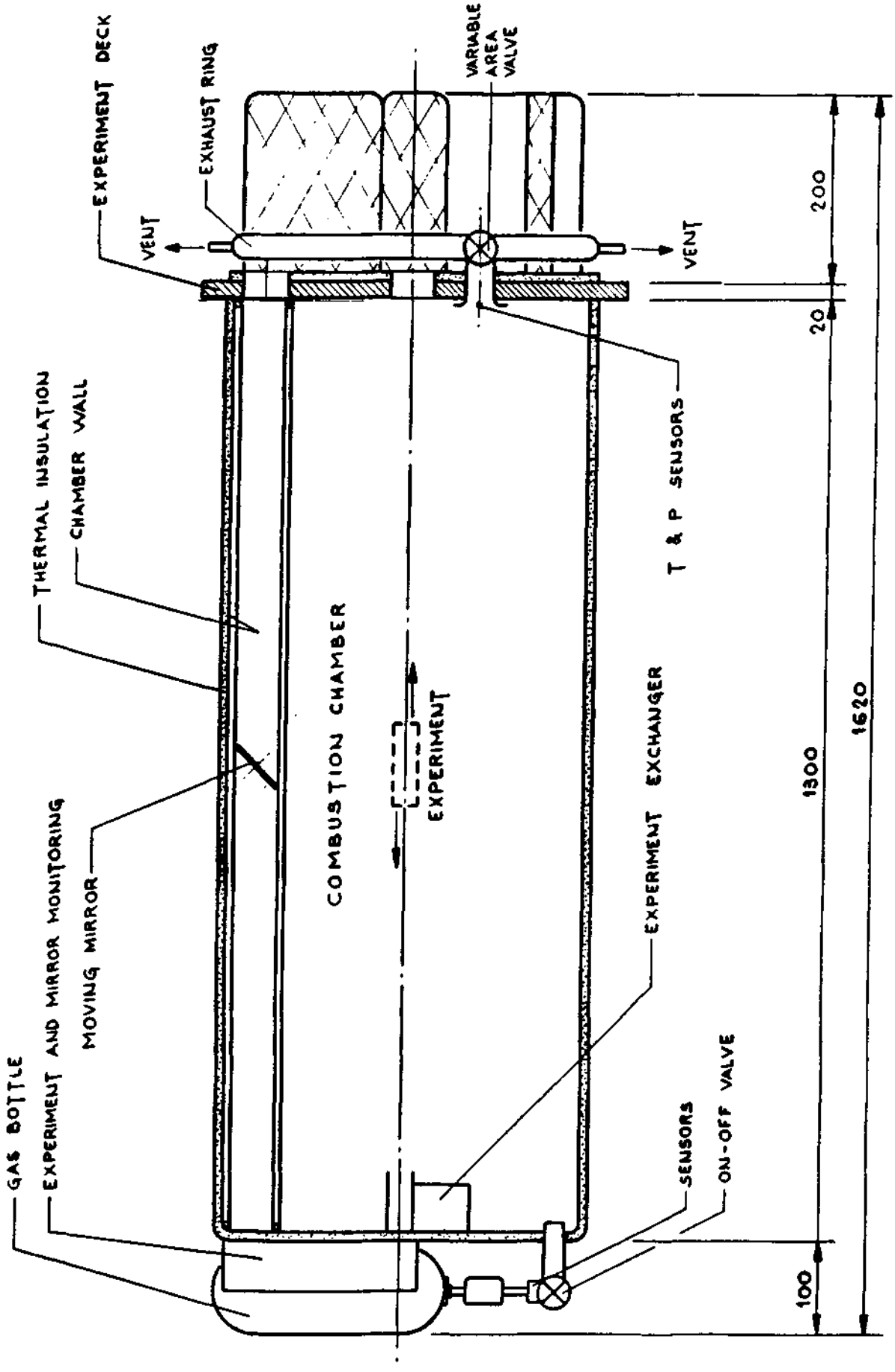

LONGITUDINAL SECTION

Fig. 3.3.2

COMBUSTION MODULE

FORCED CONVECTION BY EXPERIMENT'S MOTION.

4. WP4 THEORETICAL ASPECTS OF FLAME SPREAD ALONG SOLID FUEL RODS OR SLABS

4. WP4 THEORETICAL ASPECTS OF FLAME SPREAD ALONG SOLID FUEL RODS OR SLABS

4.1. INTRODUCTION

The combustion of solid fuels occurs only after mixing, in the gas phase, of the oxygen with the fuel generated by an endothermic gasification process. Heat must be transferred from the gas phase reaction zone to the surface of the solid, to provide for the energy required for heating the condensed fuel to the temperature of vaporization and for the heat of vaporization.

The heat transfer mechanism, from the gas phase reaction zone to the solid, may be radiation or conduction, counteracting the convective flow in the gas generated by the gasification process.

The gasification and the gas phase reactions can be triggered, over a region of the solid, by local ignition, and then the reaction will extend to other regions of the solid by means of a flame spread process.

The flame spread velocity is influenced by the gas phase convective flow that may exist in the front region of the flame; this flow may be the result of the effect of a forced flow or due to the effects of gravity forces. The flame spread velocity is also influenced by the finite value of the reaction rates. This is so because, due to the large sensitivity of the reaction rates with temperature, the flame front does not generally reach the surface of the solid, where the temperature is equal or lower than the vaporization temperature T_v; the finite rate effects influence the flame spread velocity when the thickness of the quench layer is comparable to the characteristic length of the flame front region δ_g, and may lead to limits in the flame spread process when the gas velocity in the flame front region is large enough.

The reader may find good reviews in Reference 1-3 of the large

literature that exists describing, experimentally and theoretically, the process of flame spread over solid fuels.

Experiments of flame spread in microgravity conditions have been carried out at Nasa-Lewis, using drop-tower techniques to study the flame spread along very thin fuel sheets, see for example Reference 4. The flame spread velocity along these thin sheets varies inversely with their thickness, being large enough so that the spread process can be observed during the short microgravity period of the experiment.

Experiments of flame spread along thicker slabs and fuel rods were also carried out by our Group in parabolic flights of the NASA KC-135 airplane and in a ESA Caravelle, where the gravity level is of the order of 10^{-2} of the normal gravity during 20 seconds.

The theoretical analysis given, in Ref. 5, the Final Report of our previous Contract with ESA, showed that the parabolic flight experiments correspond to the transition from a regime with the flame spread velocity dominated by gravity to a regime where the flame velocity levels toward the gravity free value. In this report we extend the order of magnitude analysis of the flame spread process of Ref.5 to clarify the geometrical effects on the flame spread process and to describe the effects of convection in a direction opposite to that of the flame spread direction.

We shall leave aside the effects of radiation losses from the flame, because they do not play a significant role in the flame spread process along thin fuel samples. On the other hand, the radiant losses from the fuel surface may result in flame extinction, as it has been shown by T'ien and coworkers, see Ref.4 and 6.

In the analysis that will be presented in the following we shall begin by considering the gas phase reaction rates to be infinitely fast, and neglect also the radiant losses from the solid surface. We shall

indicate afterwards when and how their effects may be important.

In Section II we shall summarise the order of magnitude analysis of Ref. 5 to describe the flame spread process in the absence of forced convection along a fuel slab, of thickness $2a$, in a direction opposite to that of the gravity forces.

In Section III the analysis will be extended to the description, under the same conditions, of the flame spread process along fuel rods of radius a.

In Section IV and V we leave aside gravity effects but retain the effects of forced convection, with velocity U_B in a direction opposite to that of flame spread. Section IV is devoted to the case of fuel slabs and Section V to the case of fuel rods.

In Section VI we discuss the effects of finite rate chemistry and of radiant losses from the fuel surface.

4.2. GRAVITY EFFECTS ON FLAME SPREAD ALONG FUEL SLABS

If the length of the burning slabs is L_b we may expect velocities of the order of $\sqrt{gL_b}$ due to buoyancy effects in the hot flame region. If the Grashoff number, or square of the Peclet number $\sqrt{gL_b}\, L_b/\alpha_g$, based on the typical gas phase thermal diffusivity α_g, is large compared with one, we will encounter a thin thermal boundary layer over the pyrolising fuel where the gas phase chemical reaction takes place; the heat conducted from the flame to the solid sustains the gasification process. The analysis of the vaporization process in most of the surface can be carried out using the boundary layer approximation, implying the neglect of upstream heat conduction in the gas and solid. See Ref. 7.

However the flame spread process requires heating of the solid from its initial temperature T_∞ until the surface temperature reache the

indicate afterwards when and how their effects may be important.

In Section II we shall summarise the order of magnitude analysis of Ref. 5 to describe the flame spread process in the absence of forced convection along a fuel slab, of thickness $2a$, in a direction opposite to that of the gravity forces.

In Section III the analysis will be extended to the description, under the same conditions, of the flame spread process along fuel rods of radius a.

In Section IV and V we leave aside gravity effects but retain the effects of forced convection, with velocity U_B in a direction opposite to that of flame spread. Section IV is devoted to the case of fuel slabs and Section V to the case of fuel rods.

In Section VI we discuss the effects of finite rate chemistry and of radiant losses from the fuel surface.

4.2. GRAVITY EFFECTS ON FLAME SPREAD ALONG FUEL SLABS

If the length of the burning slabs is L_b we may expect velocities of the order of $\sqrt{gL_b}$ due to buoyancy effects in the hot flame region. If the Grashoff number, or square of the Peclet number $\sqrt{gL_b}\, L_b/\alpha_g$, based on the typical gas phase thermal diffusivity α_g, is large compared with one, we will encounter a thin thermal boundary layer over the pyrolising fuel where the gas phase chemical reaction takes place; the heat conducted from the flame to the solid sustains the gasification process. The analysis of the vaporization process in most of the surface can be carried out using the boundary layer approximation, implying the neglect of upstream heat conduction in the gas and solid. See Ref. 7.

However the flame spread process requires heating of the solid from its initial temperature T_∞ until the surface temperature reache the

vaporization value T_v. This heating, in the absence of radiation, requires upstream heat conduction through the solid or through the gas phase. We shall in our analysis show that for many solid fuels, of the type of PMMA, both mechanisms play a significant role. The effects of radiation on flame spread over plastic fuels were analysed by Tarifa et al in Ref.8.

We must therefore encounter a flame front region, see Fig. 1, serving as the leading edge of the flame, which when examined with a reference frame attached to the front will have a steady structure. Let δ_g be the typical size of this front region and U_g the typical gas phase velocity in the region; U_g will be equal to the front propagation velocity U_p in the absence of forced flow or buoyancy effects, but U_g may be large compared with U_p in the presence of these effects.

If upstream gas phase heat conduction from the flame toward the solid is a dominant mechanism for flame spread, the corresponding Peclet number must be of order unity

$$U_g \delta_g / \alpha_g = 1 \qquad (1)$$

The chemical reaction between the pyrolising fuel and the oxygen must take place in this region with a heat release that causes the gas phase temperature to rise up to values close to T_f, the adiabatic flame temperature between the unit mass of fuel and the required mass of air for stoichiometric combustion; $T_f - T_\infty$ is proportional to the oxygen mass fraction in the air.

The typical velocity induced in the flame front region by gravity forces is given in order of magnitude, by

$$U_g = \sqrt{g \delta_g} \quad , \qquad (2)$$

where a factor of order $\sqrt{(T_f - T_\infty)/T}$ has been left out, because it is of

order unity.

When Eqs. *(1)* and *(2)* are used, we obtain the relations

$$U_g=(g\alpha_g)^{1/3} \quad , \quad \delta_g=\alpha_g^{2/3}g^{-1/3} \tag{3}$$

We anticipate here that the flame spread process will not be possible if the size δ_g of this region is smaller than the thickness of the premixed flame of a stoichiometric mixture of the fuel and air.

In order to calculate the flame spread velocity we need to describe the heating of the solid from its initial temperature T_∞ to the vaporization temperature T_v. Let k_s be the heat conductivity of the solid and δ_s the transverse thickness of the heated layer in the solid; by requiring the continuity of the heat fluxes at the solid-air interface, just upstream of the vaporization front, we obtain, in order of magnitude,

$$k_g(T_f-T_\infty)/\delta_g = k_s(T_v-T_\infty)/\delta_s \tag{4}$$

or

$$\delta_g/\delta_s = N = k_g(T_f-T_\infty)/k_s(T_v-T_\infty) \tag{5}$$

The parameter N measures the relative importance, for thick fuel slabs, of the upstream heat conduction along the solid and along the gas. If $N \gg 1$, upstream heat conduction along the solid can be neglected; then, the thickness δ_s of the heated layer in the solid under the flame front region is $\delta_s \ll \delta_g$, small compared with its longitudinal extent.

In this case, the balance of convection, with the velocity U_p, and transverse heat conduction in the solid leads to the relation

$$\delta_s = \sqrt{\alpha_s \delta_g / U_p} \qquad (6)$$

From Eqs. *(1)*, *(5)* and *(6)* we obtain

$$\frac{U_p \delta_g}{\alpha_s} = \left(\frac{\delta_g}{\delta_s}\right)^2 = N^2 \qquad (7)$$

and, for thermally thick solids :

$$U_p / U_g = N^2 \alpha_s / \alpha_g \qquad (8)$$

a result first derived by de Ris, Ref. 9.

Relation (8) is valid as long as the solid behaves as thermally thick (that is for $\delta_s < a$), even for values of N of order *1*. In the cases $N \ll 1$, upstream heat conduction through the solid is the dominant mechanism, and the gas phase boundary layer is thin in the flame front region.

In the absence of forced convection, with gravity dominated flow in the flame front region, the value of U_g entering Eq*(8)*, is given by Eq*(3)*; so that

$$U_p = N^2 g^{1/3} \alpha_s \alpha_g^{-2/3} \qquad (9)$$

a relation for the flame spread velocity valid as long as

$$\delta_s = \delta_g / N = \alpha_g^{2/3} g^{-1/3} N^{-1} < a \qquad (10)$$

If g is lowered below the value g_1 defined by

$$g_1^{-1/3} \alpha_g^{2/3} = Na \qquad (11)$$

The solid will no longer behave as thermally thick, and the

dependence of U_p on g will no longer follow Eq *(9)*.

For values of $g < g_1$ the heat conduction in the solid transverse to the slab is fast enough that the temperature variations across the slab can be neglected. By using an overall energy balance for the region of the slab ahead of the vaporization region, we obtain, for thermally thin slabs, in order of magnitude

$$\rho_s c_s (T_v - T_\infty) a U_p = \delta_g k_g (T_f - T_\infty)/\delta_g \qquad (12)$$

or equivalently,

$$U_p = U_o = \alpha_s N/a \qquad (13)$$

where $\alpha_s = k_s/\rho_s c_s$ is the thermal diffusivity of the solid; a result also obtained by de Ris, valid for values of g smaller than the transition value g_1 given by *(11)*.

Thus U_p is found to decrease with g, following Eq*(9)*, when $g > g_1$ and then levels to the value $U_p = U_o$ given by Eq. *(13)*. The size δ_g of the flame front region and the gas velocities there are still determined by Eq *(3)*, that is, by gravity effects, if the values of g is larger than a second critical value g_2, defined by

$$U_g = U_o = (g_2 \alpha_g)^{1/3} = \alpha_s N/a \qquad (14)$$

For smaller values of g, $g < g_2$, the convective effects due to buoyancy are negligible in the flame front region, and the thickness of this region will take its zero gravity value δ_o, given by

$$\delta_o = \alpha_g / U_o = a\alpha_g / \alpha_s N \qquad (15)$$

For values of g in the interval (g_2, g_1) we may expect a weak but non-negligible effect of gravity on the heat transfer to the solid from

the gas phase; the Nusselt number, of order unity, which should appear as a factor in the right hand side of *(13)*, and thereby in *(13)*, will change when g becomes of order g_2 and the buoyancy forces stop playing a role in the gas phase.

Notice that

$$(g_2/g_1) = (N^2\alpha_s/\alpha_g)^3 \qquad (16)$$

a extremely small value so that even though gravity forces do not significantly influence the flame spread velocity, they really influence the structure of the front region.

4.3. GRAVITY EFFECTS ON FLAME SPREAD ALONG FUEL RODS

When flame spread takes place in a direction opposite to gravity, along a fuel rod of radius a, the structure of the flame front region is locally planar for large values of g when $\delta_g = \alpha_g^{2/3} g^{-1/3}$ is small compared with a. The order of magnitude of the results will not change as long as δ_g does not rise to values large compared with a.

In particular, the thickness δ_s of the heated layer in the solid will still be given by Eq*(5)*, and therefore the rod will behave as thermally thick as long as $\delta_g/N < a$. If N is of order unity, as in the case of flame spread along PMMA rods, we find that the transition, with decreasing values of g, from thermally thick to thermally thin takes place roughly at the same value of g as the transition in the gas phase from a planar front structure to one dominated by geometrical effects. See Fig. 2 for an shematic picture of the flow in this case.

If $\delta_g \gg a$, then in the gas phase we encounter two regions: An outer region where convection and radial and axial heat conduction and diffusion are balanced, so that U_g and δ_g are related by *(1)*, and an interior region close to the rod $r \sim a$, where only radial heat conduction and diffusion

are important, including perhaps the effects of the radial convection due to vaporization. The analysis of this inner region can be carried out using the approach of Ref. 10, and leads to the introduction of a large Nusselt number

$$N_u = (\delta_g/a)/ln(1+\delta_g/a) \qquad (17)$$

in the right hand side of Eq *(12)* when writing the energy balance for the fuel rod upstream of the vaporization region. In this case we obtain

$$\rho_s c_s (T_v - T_\infty)\pi a^2 U_p = 2\pi a\, k_g (T_f - T_\infty)\, N_u \qquad (18)$$

Then the front velocity U_p is given by

$$U_p = 2\alpha_s N(\delta_g/a^2)/ln\,(1+\delta_g/a) \qquad (19)$$

where $\delta_g = \alpha_g^{2/3} g^{-1/3}$, as long as $U_g = (g\alpha_g)^{1/3}$ is larger than U_p.

Notice that, according to Eq.(9), for $g>g_1$ the resulting value of U_p decreases with decreasing values of g, with g_1 given by the condition

$$\alpha_g^{2/3} g_1^{-1/3}/N = a, \qquad (20)$$

U_p goes through a minimum, when $g \sim g_1$, and then begins to grow, according to Eq *(19)*, as $g^{-1/3}$.

When at a second critical value g_2 of g, U_p has grown to a value U_a such that

$$U_a = 2\alpha_s N(\delta_2/a^2)/ln(1+\delta_2/a) = (g_2\alpha_g)^{1/3} \qquad (21)$$

where $\delta_2 = = \alpha_g^{2/3} g_2^{-1/3} = \alpha_g/U_a$, the apparent flow effect due to flame spread becomes dominant. For values of $g<g_2$, and for zero gravity, the

flame spread velocity U_a is given by

$$\left(\frac{U_a a}{\alpha_g}\right)^2 = 2\,\frac{\alpha_s}{\alpha_g}\,N \,/\, ln\left(1+\frac{\alpha_g}{U_a a}\right) \qquad (22)$$

reflecting a dependence of the flame front velocity on a^{-1}.

4.4. FLAME SPREAD ALONG FUEL SLABS AGAINST CONVECTION

We shall describe in this Section the process of flame spread in the boundary layer generated by a flow with velocity U_b parallel to the surface of the fuel slab. The Reynolds, or the Peclet number $U_B L_f/\alpha_g$, based on the distance L_f from the fuel plate leading edge to the flame front, will be considered large compared with unity, for the flow to be of the boundary layer type, but not so large that the flow becomes turbulent.

The description of the structure of the flame front region must be carried out using a reference system moving with the front, but we shall find out that the front velocities are small compared with the forced flow velocities, except for very small values of U_B.

The flow structure over the fuel plate shows, when seen with the length scale L_f, see Fig.3, a thin boundary layer, with no surface gasification upstream of the flame front, followed by a thicker boundary layer, over the pyrolizing region of the slab. A thin diffusion flame, embedded in the boundary layer, separates the oxygen free region close to the fuel surface from the fuel free region outside.

The displacement effect of the boundary layer on the outside flow changes drastically on the flame front region, or leading edge of the diffusion flame. The flow displacement is strong downstream of the flame front, due to the thermal expansion effects, associated with the chemical heat release, and also due to the transverse gas flow due to

gasification. The sudden jump in displacement effects introduces a triple-deck region in the flow past the fuel slab, centered in the flame front region.

In this triple deck region, the sudden increase in flow displacement causes the pressure to rise locally over the ambient pressure in a region of extent $L_f(U_B L_f/\alpha_g)^{-3/8}$, moderarately large compared with the boundary layer thickness, $\delta_B = L_f(U_B L_f/\alpha_g)^{-1/2}$; see for example the review article, Ref.11, of Smith. The rising pressure felt by the flow upstream of the flame front causes the velocities to decrease and an outer displacement of the streamlines; just downstream of the flame front the pressure gradients effects accelerate the flow. The response of the flow is inviscid in the upper irrotational deck, outside the boundary layer and in the midle, main boundary layer, deck where the flow is rotational. Viscous diffusion and heat conduction effects are confined to the thin lower deck, the viscous sublyer of thicknes $L_F \cdot (U_B L_f/\alpha_g)^{-5/8}$. Upstream heat conduction or diffusion play a negligible effect in the viscous sublayer, and can be neglected when describing the triple-deck structure, which includes a diffusion flame sheet in the viscous sublayer downstream of the flame front.

It is important to notice that the overpressures generated in the triple-deck region may cause, if the displacement effects are strong enough, separation of the flow just ahead of the flame front; in this case, the flow structure and rate of flame spread will change dramatically. In any case, the displacement effects will decrease the wall velocity gradient, maintaining its order of magnitude, from its value just upstream of the triple-deck region.

Embedded in the lower deck of the triple-deck region there is a Navier-Stokes region, of size $\delta_g = L_f(U_B L_f/\alpha_g)^{-3/4}$, where upstream heat conduction and diffusion are important. This is the flame front region, which determines the spreading velocity, and where the diffusion flame is anchored. This region is bounded, above and upstream, by the constant

shear flow that the lower deck has close to the wall when it reaches the flame front.

The velocity gradient, of the order of U_B/δ_B, together with the conditions.

$$U_g/\delta_g = U_B/\delta_B \qquad \text{and } U_g\delta_g/\alpha_g = 1 \tag{23}$$

determines the length and velocity scales of this region

$$U_g = U_B(\alpha_g/L_f U_B)^{1/4} \quad , \quad \delta_g = L_f(\alpha_g/U_B L_f)^{3/4} \tag{24}$$

We can now use the analysis of the heat transfer process to the solid of Section II, leading to the relation *(7)*, for the thickness of the heated layer in the solid, and *(8)* for the flame spread velocities, when U_B is large enough so that $\delta_s < a$, and the solid behaves as thermally thick. When we use Eqs. *(24)* with Eqs. *(6)* and *(8)*, we obtain

$$U_p = U_B N^2(\alpha_s/\alpha_g)(\alpha_g/L_f U_B)^{1/4} \tag{25}$$

$$\delta_s = L_f(\alpha_g/U_B L_f)^{3/4}/N \tag{26}$$

For values of U_B smaller than a trasition value U_1 defined by

$$U_1 L_f/\alpha_g = (L_f/Na)^{4/3} \tag{27}$$

the slab behaves as thermally thin. The overall heat balance equation *(12)* leads again to the flame spread velocity given by Eq. *(13)*, apparently independent of the mode of heat transfer in the gas phase. A Nusselt factor, of order unity, not written in the right hand side of Eq. *(13)*, will be different for the flows due to natural convection and for those due to forced flow.

When U_B decreases to a new value U_2, a new transition will occur,

with only a minor change in the flame spread velocity, when the forced velocity in the flame front region, becomes equal to $U_o = U_2$ is given by

$$U_2 L_f/\alpha_g = \{(\alpha_s N/\alpha_g)(L_f/a)\}^{4/3} \qquad (28)$$

typically, very small compared with U_1. For values of $U_B < U_1$, only the convective effects due to the motion of the front, with velocity $U_o = \alpha_s N/a$, which remain at zero gravity, are important in the flame front region, of size $\delta_g = \alpha_g/U_o$.

4.5. FLAME SPREAD ALONG FUEL RODS AGAINST CONVECTION

If flame spread is taking place against the flow of velocity U_B parallel to the rod, the flame front region will be located again in the bondary layer of thickness $\delta_B = \sqrt{\alpha_g L_f/U_B}$. If δ_B is small or comparable with the radius a, the flame front structure will be planar-like, because $\delta_g \ll \delta_b$.

Significant geometrical effects will appear at lower Reynolds numbers, resulting in a thickness of the viscous boundary layer

$$\delta_B/a = (L_f/a)\sqrt{\alpha_g/U_B L_f} \qquad (29)$$

large compared with a.

For these values of the Peclet number $U_B L_f/\alpha_g$, resulting in $\delta_B/a \gg 1$, the velocity distribution will be given in an inner region $r \ll \delta_B$ by the logarithmic law

$$u = U_B \frac{\ln (r/a)}{\ln (\delta_B/a)} \qquad (30)$$

For values of $r-a \sim \delta_g$, corresponding to the flame front region, $u \sim U_g$ is given, according to (30), in order of magnitude, by

$$U_g/U_B = \frac{ln\ (1+\delta_g/a)}{ln\ (1+\delta_B/a)} \qquad (31)$$

where we have changed the factor $ln\ (\delta_B/a)$ to $ln(1+\delta_B/a)$, in order to extend the order of magnitude estimate *(31)* to cases where $\delta_B/a \ll 1$.

In the flame front region $\delta_g U_g/\alpha_g = 1$, so that

$$\frac{\alpha_g}{\delta_B U_B} = \sqrt{\frac{\alpha_g}{L_f U_B}} = \frac{(\delta_g/a)\ ln\ (1+\delta_g/a)}{(\delta_B/a)\ ln\ (1+\delta_B/a)} \qquad (32)$$

indicating that the Peclet number $L_f U_B/\alpha_g$ must be of order $(L_f/a)^2$, if we want δ_B/a to be of order unity. In this case $\delta_g/a \ll 1$, and then

$$\delta_g/a = \{(\alpha_g/U_B a)\ ln(1+\delta_B/a)\}^{1/2} \qquad (33)$$

When this is taken into Eq.*(31)* we obtain

$$U_g/U_B = \{(\alpha_g/U_B a)/ln(1+\delta_B/a)\}^{1/2} \qquad (34)$$

to be used with Eq*(29)* to give U_g as a function of U_B.

For very large values of the Peclet number we obtain the planar results; while for values of $U_B L_f/\alpha_g \ll (L_f/a)^2$, the dependence of U_g on U_B changes from the planar dependence $U_B^{3/4}$ to the approximate dependence $U_B^{1/2}$, shown by *(34)* when $\delta_B \gg 1$.

The result *(34)* when used with the relation

$$U_p/U_g = N^2 \alpha_s/\alpha_g \qquad (35)$$

valid as long as the solid behaves as thermally thick and δ_g/a, given by *(33)*, is small compared with 1, leads to the following expression

$$U_g/U_B = N^2(\alpha_s/\alpha_g)\{(\alpha_g/U_B a)/\ln(1+\delta_B/a)\}^{1/2} \qquad (36)$$

for the flame spread velocity.

For values N of order unity, the transtion from thermally thick to thermally thin, occurring when $\delta_s=\delta_g/N = a$, will take place when $\delta_g=a$ or, roughly, according to Eq.(33), when $U_B a/\alpha_g$ becomes of order unity:

Namely, for $N \sim 1$, when U_B decreases below the value U_1 given by

$$U_1 a/\alpha_g = 1 \qquad (37)$$

For values of $U_B a/\alpha_g \ll 1$, we can still use the relation (32), but the resulting value of δ_g/a given by

$$(\delta_g/a)\ln(1+\delta_g/a) = (\alpha_g/U_B a)\ \ln(1+\delta_B/a) \qquad (38)$$

will be large compared with 1.

In this case, and also in cases when δ_g/a is of order 1, we must account for geometrical effects when calculating the heat transfer to the rod. This is given, per unit rod length, in order of magnitude, by

$$2\pi a k_g(\partial T/\partial r)_a = 2\pi a k_g\{(T_f-T_\infty)/a\}/\ln(1+\delta_g/a) \qquad (39)$$

if we take into account that in the inner region, $r \sim a$, the radial heat conduction is dominant giving a logarithmic profile to T.

When, with $N \sim 1$, $\delta_g \gg 1$, heat conduction transverse to the rod makes the radial temperature variations negligible; the rod behaves as thermally thin. An overall heat conduction balance applied to the rod upstream of the vaporization region, gives the relation

$$U_p = 2N\alpha_S\delta_g a^{-2}/\ln(1+\delta_g/a) \qquad (40)$$

and when using *(32)*

$$U_p = \frac{2N\alpha_s}{a}\,\frac{\alpha_s}{U_B a}\,\ln(1+\delta_B/a)\{\ln(1+\delta_g/a)\}^{-2} \qquad (41)$$

where the factor $\alpha_g/U_B a$ is large compared with 1 in the thermally thin limit.

Notice the approximate dependence a^{-2} and U_B^{-1} of U_p on a and U_B, in contrast with the planar case when U_p in the thermally thin limit is given by $\alpha_s N/a$. The difference is due to effect of geometrical enhancement of the heat flux.

The resulting value of U_p ceases to be valid when it becomes equal to the value of U_g given by Eq.*(31)*. For lower values of U_B the convective effects in the flame front region will be determined by the front motion with velocity U_o, and not by the forced convective flow.

In the flame front region

$$U_o \delta_o/\alpha_g = 1 \qquad (42)$$

and the overall energy balance, see Eq.*(40)* for comparison, gives

$$(U_o a/\alpha_s \alpha_g)^2 = 2N/\ln(1+\alpha_g/U_o a) \qquad (43)$$

the value that we may expect to encounter in zero gravity. This is to be compared with the result $U_o a/\alpha_s = N$, of the planar case. The main effect of the cylindrical geometry is to replace α_s by $\sqrt{\alpha_s \alpha_g}$, so that the value of U_o is significantly larger.

4.6. EFFECTS OF FINITE REACTION RATES AND RADIATION LOSSES

We shall simply indicate here how these effects may influence the

flame propagation process.

The influence of finite reaction rates will be described using an Arrhenius model for the reaction, and Fick's law for the fuel diffusivity. The quasi-steady conservation equation for the fuel mass fraction Y_F in the flame front region takes the form

$$\vec{V}\cdot\nabla Y_F - \frac{1}{\rho}\nabla\cdot(\rho D_F \nabla Y_F) = -B\, e^{-E/RT} Y_o Y_F \qquad (44)$$

where Y_o is the mass fraction of the oxygen, B the frequency factor of the reaction and E its activation energy; D_F is the fuel diffusivity, of the order of the gas phase thermal diffusivity, α_g.

The mass fractions in the flame front region are of order unity, and have spatial variations of order unity: so that the order of magnitude of the three terms in Eq.(44) are equal, respectivelu, to the inverse of the residence time, δ_F/U_g, the diffusion time δ_g^2/α_g, and the chemical time, $t_{ch} \sim B^{-1} e^{E/RT}$.

The diffusion and residence times are of the same order in the flame front region. The ratio of the residence time to the chemical time is the Damköhler number of the flow

$$D_a = (\delta_g/U_g) \cdot B\, e^{-E/RT} \qquad (45)$$

If the Damköhler number were small, (compared with one) everywhere in the flame front region, flame propagation would not be possible.

Due to the strong dependence of the reaction rates with temperature, the value of the Damköhler number will change in the flame front region from $(\delta_g/U_g)B\, e^{-E/RT_v}$ to $(\delta_g/U_g)B\, e^{-E/RT_e}$.

If

$$(\delta_g/U_g)B\, e^{-E/RT_v} \gg 1 \qquad (46)$$

the reaction will take place in a diffusion controlled way at a flame sheet, where the temperature rises from T_v to the adiabatic flame temperature value, T_g, away from the plate. On the other limit

$$(\delta_g/U_g)B\ e^{-E/RT_f} \gg 1 \qquad (47)$$

the reaction would be frozen in the flame front region and the flame spread process would not be possible.

In order of magnitude, the condition

$$(RT_f/E)^2(\delta_g/U_g)B\ e^{-E/RTf} \gg 1\ , \qquad (48)$$

where the factor $(RT_f/E)^2$ comes from rough order of magnitude estimates of the concentrations in the reaction zone, coincides approximately with the condition that the size of the region equals the thickness of the transport zone of the premixed flame in a stoichiometric mixture of the fuel and air.

For values of the Damköhler number intermediate between the two we find in the flame front region a quenched zone, where the reactant mix without chemical reaction effects, separated from two chemical equilibrium regions, one with $Y_F = 0$ and the other with $Y_o = 0$, by a premixed reaction zone with two branches(one lean and the other rich). The two equilibrium regions are separated by a diffusion flame sheet.

The temperature T_c in the premixed flame is determined roughly, by the condition

$$(RT_f/E)^2(\delta_g/U_g)B\ e^{-E/RTc} \gg 1 \qquad (49)$$

The flow is frozen in the region where $T<T_c$, and we have equilibrium

with $Y_F Y_o = 0$ in the region where $T > T_c$.

Notice that in the estimates given above the gas phase the residence time, (δ_g / U_g), in the flame front region enters, and this is determined by the analysis of the previous sections.

In order to discuss the influence of the heat losses by radiation from the surface, considered in Ref.6, we shall model them with $\varepsilon\sigma T^4$ as the energy emitted per unit surface and time. Its peak value, $\varepsilon\sigma T_v^4$, must be compared with the heat arriving to the interface from the gas phase, $k_g (T_f - T_\infty)/\delta_g$, where δ_g is determined by the analysis of the previous sections. If

$$\varepsilon\sigma T_v^4 > k_g (T_f - T_\infty)/\delta_g \qquad (50)$$

we may expect extinction due to surface radiation effects. This will be the case when the size of the flame front region increases above a critical value.

REFERENCES

1. Williams, F.A. *"Mechanisms of fire spread"* 16th. Int.Symp. on Combustion. The Combustion Institute, pp 1281-1294, (1969).

2. Fernández Pello, A.C. and Hirano, T. *"Controlling mechanisms of flame spread"*. Comb. Sci. Tech. 32, pp.1-31 (1983).

3. Williams, F.A. *"Combustion Theory"*. Benjamin Cummings (1985)

4. Olson, S. Ferkul, P.V. and T'ien, J.S. *"Near-limit flame spread over a thin solid fuel in microgravity"*. 22th. Int. Symp. on Combustion. The Combustion Institute (1988).

5. Tarifa, C S., Liñán, A., Salvá, J.J. Corchero, G. y Juste, G.L. *"Heterogeneous combustion processes under microgravity"* Final Report LPTR 88-01 for la ESA. Dpto. de Motopropulsión y Termofluidodinámica. U.P.M. Febrero 1988.

6. Foutch, D.W. and T'ien, J.S. *"Exctinction of a stagnation point diffusion flame at reduced gravity"* AIAA J. 25, pp.972-976 (1987).

7. Vedha-Nayagam, M. and Altenkirch, R.A. *"Gravitational effects on flame spreading over thick solid surfaces"*. Acta Astronáutica 12, pp.565-576, (1985).

8. Tarifa, C.S., Pérez del Notario, P. y Muñoz Torralbo, A., *"On the process of flame spreading over the surface of plastic fuel in an oxidizing atmosphere*, 12 th. Int. Symp. on Combustion, pp.229-240. The Combustion Institute 1969.

9. De Ris, J.N. *"Spread of a laminar diffusion flame"*. 12th. Int. Symp. on Combustion. The Combustion Institute, pp, 241-252, 1969.

10. Tarifa, CS., Liñán, A., Salvá, J.J., Montañés, J.L., Corchero, G.y Juste, G.L. *"Preparatory study on heterogeneous combustion processes under microgravity"* Final Report for ESA. Contract U.P.Madrid (1986).

11. Smith, F.T. *"On the high Reynolds number theory of laminar flows"* IMA J. Appl. Math. 28, pp. 207-281 (1982).

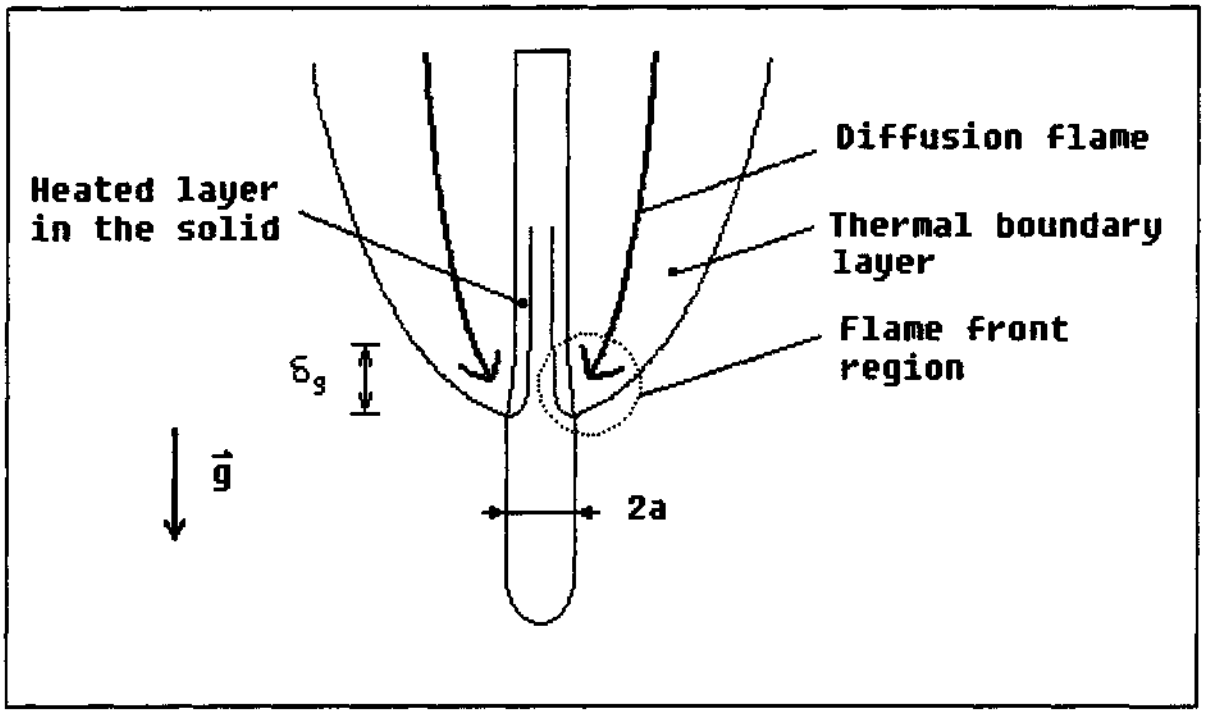

Fig.1.- Schematic of the flame spread process on a fuel slab, with gravity.

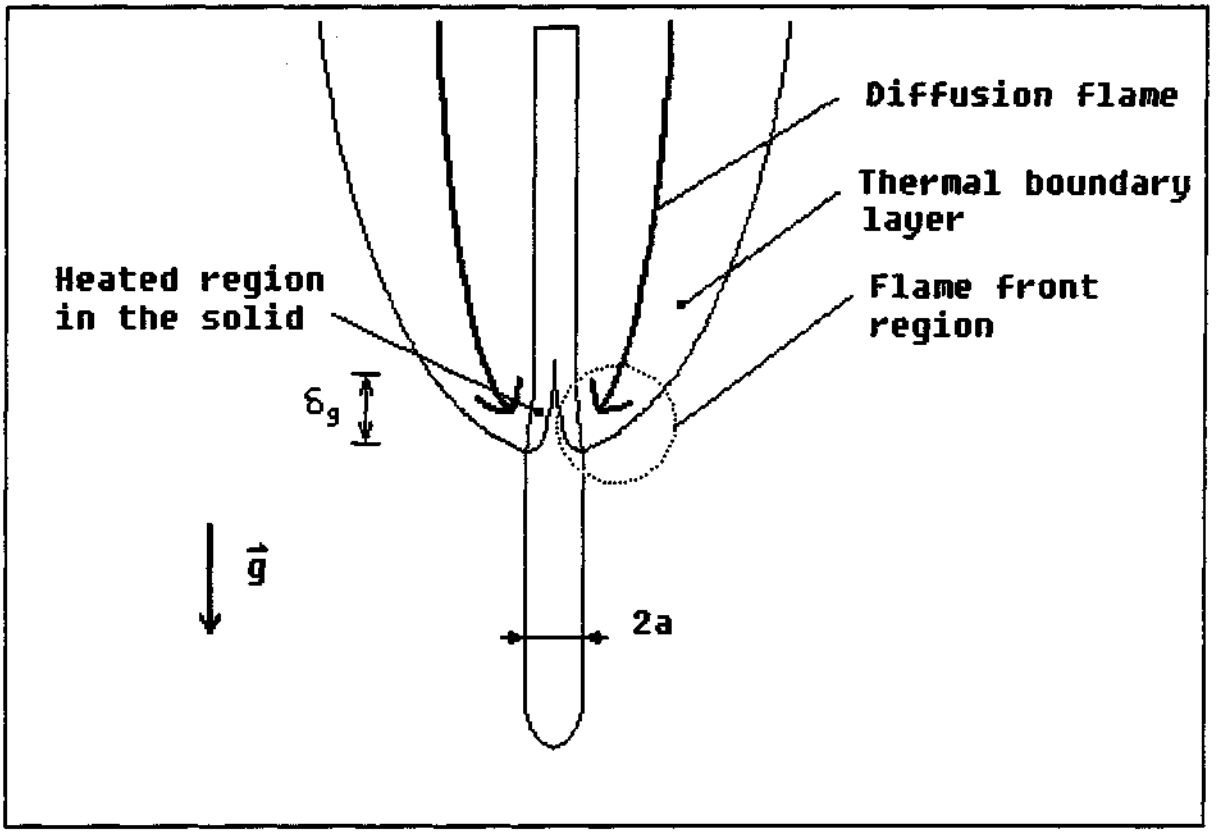

Fig.2.- Schematic flow structure for flame spread, against gravity, along fuel rods.

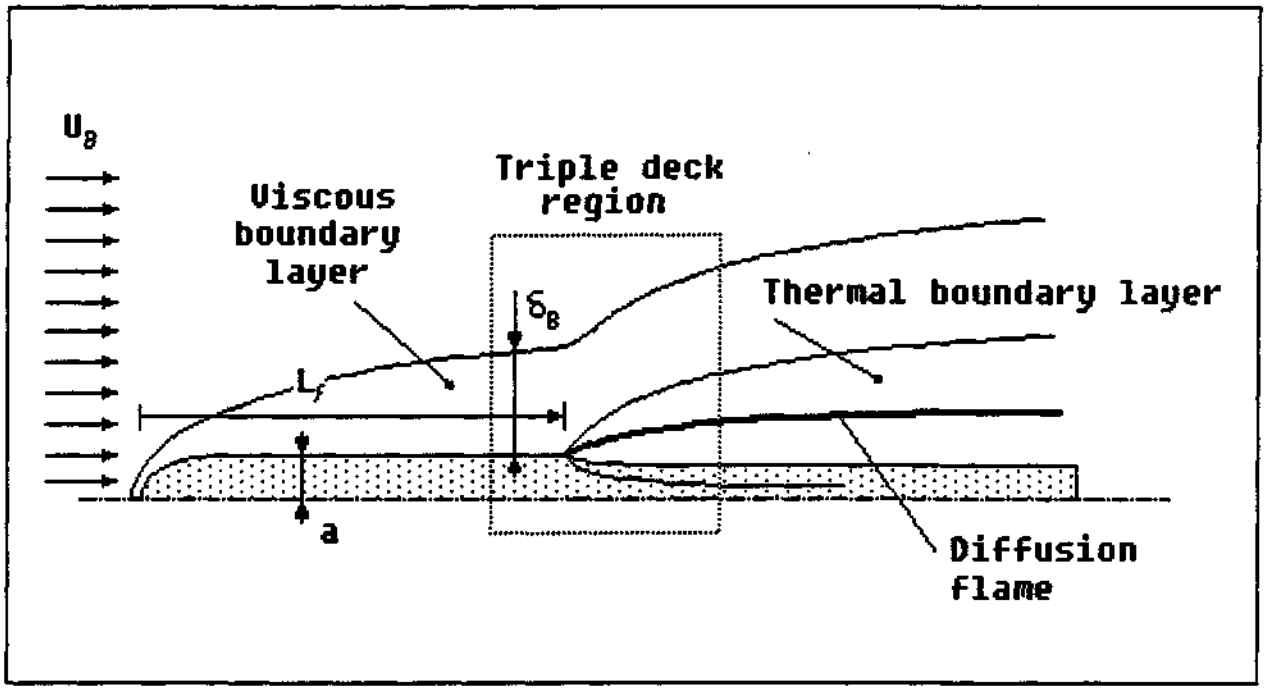

Fig. 3(a).- Schematic of the flow structure with flame spread over a slab against a convective flow.

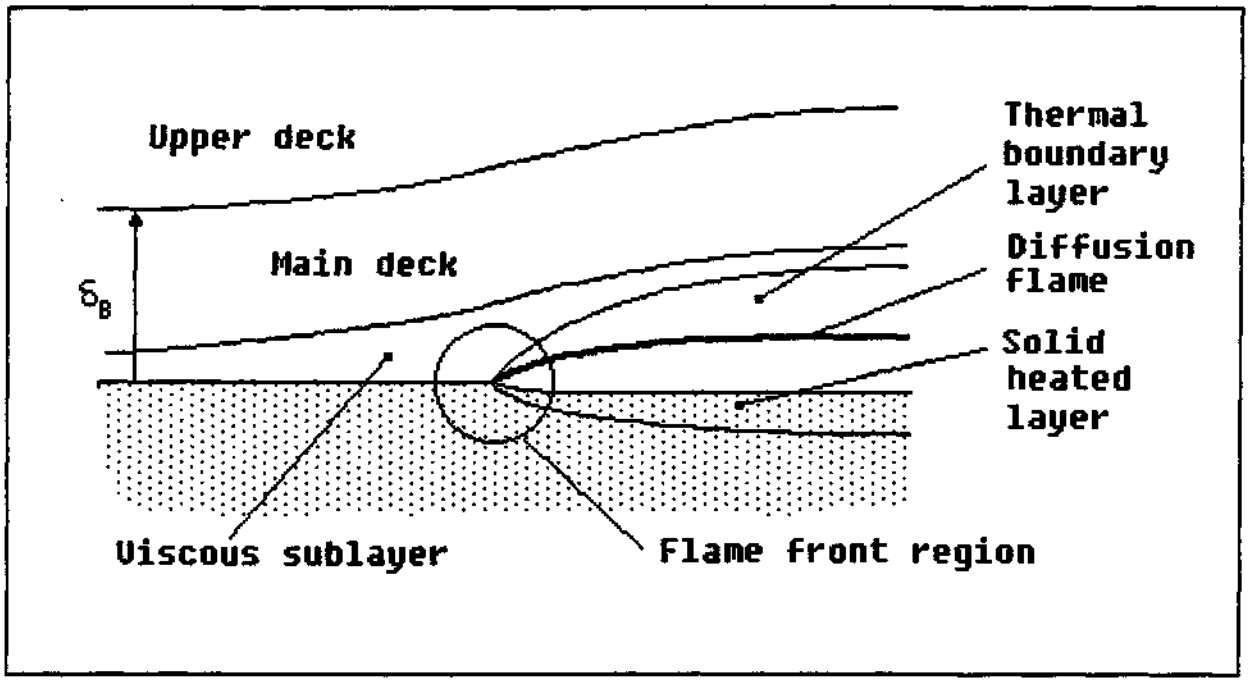

Fig. 3(b).- Triple deck region.

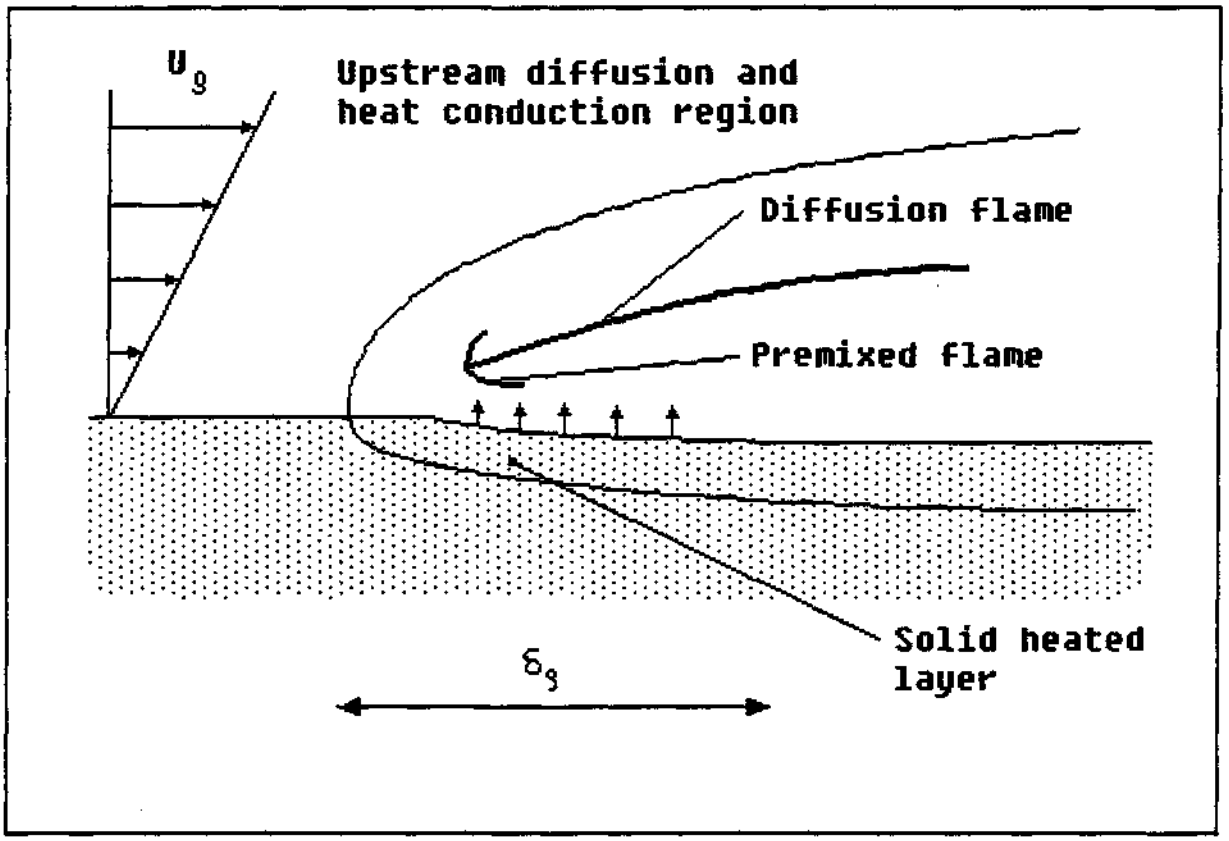

Fig. 3(c).- Flame front region.

5. WP4 - NUMERICAL STUDY ON QUIESCENT COMBUSTION

LIST OF SYMBOLS

a - *Rod radius.*

$\dot{a}$ - *Surface velocity recesion,* $\frac{da}{dt}$

B - *Preexponential factor of reaction rate.*

c_c - *Solid specific heat.*

c_p - *Gas specific heat.*

D - *Mass diffusion coefficient.*

E - *Activation energy of reaction rate.*

e - *Specific internal energy, or basis of Naperian logarithms.*

h - *Specific enthalpy, sensible o thermal.*

h^t - *Specific thermal enthalpy,* $\int_{To}^{T} c_p dT$

$\hat{h}$ - *Defined function,* $h^t + q_o y_o$.

$\tilde{h}$ - *Defined function,* $\tilde{h} = \hat{h}/c_{p\infty} T_\infty$

k - *Conductivity.*

Le - *Lewis number,* α/D.

M - *Molecular weight.*

$\dot{m}$ - *Mass burning flow per unit length.*

p - *Pressure.*

q_{ig} - *Ignition system heat flux.*

q_o - *Heat of reaction per unit of oxidizer mass.*

q_R - *Radiation heat flux.*

q_v - *Specific heat of vaporization.*

R - *Universal constant for perfect gas.*

r, θ, z - *Radial coordinates.*

T - *Temperature.*

$\tilde{T}$ - *Nondimensional temperature,* T/T_∞.

t - *time.*

ϑ - *Volume.*

$\vec{v}$ - *Velocity vector*

v - *Radial velocity component.*

$\tilde{V}$ - *Nondimensional radial velocity,* $\frac{a_o}{\alpha_\infty} v$.

W - *Mass rate produced per unit volume.*

Y - *Mass fraction.*

$\tilde{Y}$ - *Mass fraction function,* $Y_o/\nu_o - Y_F$.

Greak symbols

α - *Thermal diffusion coefficient.*

ε - *Radiation emission coefficient.*

ξ - *Nondimensional radial coordinate,* r/a_o.

μ - *Nondimensional mass burning flow,* $\dot{m}/(2\pi\rho_\infty\alpha_\infty)$; *also* $(\tilde{\rho}\tilde{v}\tilde{\xi})_{\xi=\xi_s}$.

ν_o - *Oxygen to fuel mass stoichiometry ratio.*

ν' - *Stoichiometric coefficient.*

ρ - *Density.*

$\tilde{\rho}$ - *Nondimensional density,* ρ/ρ_∞.

τ - *Nondimensional time,* $\dfrac{\alpha_\infty}{a_o^2}\,t$.

σ - *Stefan-Boltzman constant, or surface.*

Subscripts

a - *Air.*

c - *Condensed (solid), or characteristic.*

F - *Fuel.*

f - *Flame.*

g - *gas phase.*

i - *Generic Specie.*

o - *Oxidizer or initial.*

s - *Interface or solid surface.*

∞ - *Far downstream.*

Supercripts

$^\circ$ - *Value at time* $t-\Delta t$.

5. WP4 - NUMERICAL STUDY ON QUIESCENT COMBUSTION

5.1. INTRODUCTION

The quiescent combustion process over PMMA rods, in microgravity conditions, was proposed in previous studies as a candidate for experimentation in a sounding rocket module.

The study that follows deals about the numerical simulation of this non stationary process, a scheme of which is shown in figure 5.1. The main objectives are to get a full knowledge of the process, and the acquisition of information and data needed for the geometric design of the module combustion chamber, and to select the operating variables.

This study was iniciated in a previous ESA contract[1], using a simplified model, where the effects of radiation, chemical kinetics or products dissociation were neglected. The model here developed includes all these effects. Inclusion of chemical kinetics as well as radiation are necessary to analyse the ignition problem, while dissociation becames very important when the chamber is operated at high oxygen concentration.

By other way, it has been developed a numerical program whose application makes possible to determine the process time evolution, from ignition to the rod consumption. This includes the computation of fluid variables and species profiles, and also of the burning mass, flame position and temperature, rod radius, and thermal front position.

Finally, the ignition problem has been analyzed and also the effects of rod surface radiation and of oxygen mass fraction content in the atmosphere.

5.2. MODEL ADOPTED

5.2.1. Assumptions

- We consider the combustion of an infinitely long rod, without forced or free-convective effects *(g=0)*. So that the gas flow will be radial, function of r and t (see fig.5.1).

- The viscous effects are negligible.

- Solid suface radiation follows the Stefan Boltzmann equation, that is $q_R=\varepsilon_S \sigma T_S^4$. But gas radiation is negligible.

- Gas phase chemical reaction is described by the reaction:

$$PMMA + \nu'_O O_2 \longrightarrow \text{COMBUSTION PRODUCTS}$$

and the reaction rate is modeled by an Arrhenius law, so that according Ref 9: $W_O=-Y_F Y_O p^{1.2} B_g e^{-Eg/RT}$. Also we will assume partial equilibrium for the products, so that the heat of reaction can be easily calculated and the effects of dissociation are incorporated.

- Solid reactions are confined at the surface and gasification is modeled by a surface pyrolysis model of Arrhenius type: $\dot{m}=B_s e^{-Es/RTs}$

- Perfect gas, with $M \simeq M_a$, but conductivity varies according to: $k/k_\infty = \left(T/T_\infty\right)^{.75}$.

- Changes of pressure and of some solid physical properties are negligible, so that we will suppose: $p(r,t)=p_\infty$, c_c=const., k_c=const.

- As other approximation we will assume that the gas kinetic energy is negligible and that the Lewis number is unity.

5.2.2. Governing equations

Using the stablished assumptions and carrying out a development similar to that of SVAB-ZELDOVICH, the conservation equations for the gas phase, in integral form, can be write as follows:

$$\frac{d}{dt}\int_{\vartheta(t)} \rho\varphi d\vartheta + \int_{\sigma(t)} \rho[(\vec{V} - \vec{V}_\sigma)\varphi - \alpha\nabla\varphi]\,\vec{n}\,d\sigma = \int_{\vartheta(t)} F d\vartheta \qquad (5.1)$$

where:

$$\varphi = \begin{bmatrix} 1 \\ Y_o \\ Y_F \\ h^t \end{bmatrix} \qquad F = \begin{bmatrix} 0 \\ W_o \\ W_F \\ -W_o q_o \end{bmatrix}$$

Combining the equations to eliminate the source term, excepting that of oxidizer conservation equation, we obtain:

$$\frac{d}{dt}\int_{\vartheta(t)} \rho\hat{\varphi} + \int_{\sigma(t)} \rho[(\vec{V} - \vec{V}_\sigma)\hat{\varphi} - \alpha\nabla\hat{\varphi}]\,\vec{n}\,d\sigma = \int_{\vartheta(t)} \hat{F} d\vartheta \qquad (5.2)$$

where

$$\hat{\varphi} = \begin{bmatrix} 1 \\ Y_o \\ Y_o/\nu_o - Y_F \\ h^t + q_o^\circ Y_o \end{bmatrix} = \begin{bmatrix} 1 \\ Y_o \\ \tilde{Y} \\ \hat{h} \end{bmatrix} \qquad \hat{F} = \begin{bmatrix} 0 \\ W_o \\ 0 \\ 0 \end{bmatrix}$$

The variables to be considered are ρV, Y_o, $\tilde{Y}$, $\hat{h}$. Temperature is obtained from the relation defining $\hat{h}$, while the density can be obtained from the ideal gas equation of state $\rho = p_\infty / RT$.

For the solid phase, the mass and energy conservation equations, give:

$$\frac{da}{dt} = - \frac{\dot{m}}{2\pi a \rho_c} \qquad (5.3)$$

$$\frac{d}{dt} \int_{\vartheta(t)} \rho_c T_c \, d\vartheta - \int_{\sigma} \rho_c [\vec{V}_\sigma T_c - \alpha_c \nabla T_c] \cdot \vec{n} \, d\sigma = 0 \qquad (5.4)$$

that are necessary to calculate the temperature into the solid and the rod radius.

5.2.3. Initial and boundary conditions.

Initial Conditions:

$a = a_o$

$V(r,0) = 0$; $Y_o = (r,0) = Y_{o\infty}$; $\tilde{Y}(r,0) = \tilde{Y}_{o\infty}$; $\hat{h}\,(r,0) = \hat{h}_\infty$, for $r \geq a_o$

$T_c(r,0) = T_\infty$, for $r < a_o$

Boundary Conditions:

$Y_o = Y_{o\infty}$; $\tilde{Y} = \tilde{Y}_{o\infty}$; $\hat{h} = \hat{h}_\infty$, for $r \to \infty$.

$\rho(V-\dot{a}) = \frac{\dot{m}}{2\pi a}$; $[(V-\dot{a})Y_o - D\nabla Y_o] = 0$; $\rho[(V-\dot{a})\tilde{Y} - D\nabla\tilde{Y}] = - \frac{\dot{m}}{2\pi a}$, at $r = a$

$$\left[\rho(V-\dot{a})\hat{h} - \rho\alpha\nabla\hat{h}\right]_{a+} + \left[\rho_c \dot{a} h_c + \rho_c \alpha_c \nabla h_c\right]_{a-} = q_{ig} + \dot{a}\,\rho_c q_v - q_R, \text{ at } r = a$$

$\nabla T_c = 0$, at $r = 0$

5.3. COMPUTATIONAL SOLUTION METHOD

5.3.1. Preliminary Comments

In order to solve the previous system of equations, it is used

the finite volume methods in the form fully implicit. This discretization method is studied extensively by Patankar[2]

The method of finite volume provides a convenient and natural procedure to make up the finite difference scheme. In addition, the Principles of Fluid Mechanics are preserved.

In this problem, a wide range of time scales are involved, such as, characteristic time of chemical reaction, convective and diffusion time delay, etc. This means, that the system of equations has stiff caracter and it is necesary to employ one implicit method of solution, seeing that, the explicit methods are strong limited for stability reason[7,8].

5.3.2. Grid Characteristics

The grid on which the equations are discretized is shown, esquematically, in the Fig.5.3, Fig.5.4a and 5.4b. In these figures the main grid and the staggered grid are shown. The staggered grid is only used to discretize the continuity equation.

With the objetive to obtain the best accuracy, stability and computing time, the grid has some special characteristics:

a) Adaptability:

In the aim to include the recession of the rod radius (can be reduce at half), the gridpoint on the surface moves with it. Therefore, it is necessary to make a special processing of the finite volume surrounding the superficial point. And it is also necessary to create and to remove adjacent gridpoints. The variables are polinomically interpolated in the new gridpoints.

b) Multispacing:

With the objective to obtain a level of homogeneous accuracy over

all numerical field (solid & gas), with a minimum amount of memory and computational time, the separation between grid point are not equal in all the grid. The spacing is different for solid and gas phases. Besides, for the gas field, the grid spacing changes smoothly from fine near the surface to wide downstream, where the changes of fluid variables are low.

c) Staggered grid:

With the use of a staggered grid some difficulties can be resolved[2], and a good representation is obtained. Only the velocity is calculated for the points that lie on the faces of the main control volumes (Fig.5.4a) by using the integral formulation on the staggered volume (Fig.5. 4b).

5.3.3. Discretization

If the equation of continuity is applied to the control volume of Fig.5.4b, we obtain:

$$(\rho rv)_i = (\rho rv)_{i-1} + \frac{\rho_j - \rho_j^\circ}{\Delta t} r_j \Delta r_j \qquad (5.5)$$

From the rest of equations of conservation, using the control volume of Fig.5.4b (main grid), we can write in generic form[1]:

$$\frac{\rho_j \hat{\varphi}_j - \rho_j^\circ \hat{\varphi}_j^\circ}{\Delta t} r_j \Delta r_j + \hat{J}_i - \hat{J}_{i-1} = \hat{F}_j r_j \Delta r_j \qquad (5.6)$$

where

$$\hat{J}_i = \left(\rho rv \, \hat{\varphi} - \rho \frac{k}{c_p} r \frac{\partial \hat{\varphi}}{\partial r} \right)_i \qquad (5.7)$$

[1] Remember that here $\hat{\varphi}$ denotes $, Y_o$, $\tilde{Y}$ or $\hat{h}$, for more details see references 1 and 2.

and rearranging terms:

$$a_j \tilde{\varphi}_j = a_{j-1} \tilde{\varphi}_{j-1} + a_{j+1} \tilde{\varphi}_{j+1} + b$$

where

$$\tilde{\varphi} = \begin{Bmatrix} \tilde{Y} \\ Y_o \\ T/T_\infty + q_o \dfrac{Y_o}{c_p T_\infty} \end{Bmatrix} \qquad (5.8)$$

with

$$a_{j+1} = \left(\frac{\tilde{k}\xi}{\Delta\xi}\right)_i A(|P_i|)$$

$$a_{j-1} = \left(\frac{\tilde{k}\xi}{\Delta\xi}\right)_{i-1} A(|P_{i-1}|) + (\tilde{\rho}\tilde{v}\xi)_{i-1}$$

$$a_j = a_{j+1} + a_{j-1} + \tilde{\rho}^\circ_j (\xi\Delta\xi)_j / \Delta\tau$$

$$b = (\tilde{\rho}^\circ \tilde{\varphi}^\circ \xi\Delta\xi)_j / \Delta\tau + \tilde{F}_j \xi_j \Delta\xi_j$$

(note that the last term is not linealized, for simplicity purposes).

$$P = \rho V \Delta r / \rho D$$

$$A(|P|) = \max [0, (1-0.1|P|)^5]$$

$$\tilde{F}_j = \frac{\hat{F}_j}{(a_o^2/\alpha_\infty)} ; \qquad \tilde{v} = \frac{v}{(\alpha_\infty/a_o)}; \qquad \tilde{k} = \frac{k/k_\infty}{c_p/C_{p_\infty}}$$

5.3.4. Source Term Linealization

To obtain high efficiency performing each iteration and to make large convergence radius, it is necessary to linealize the chemical

source term, which appears in the oxidant conservation equation, that is:

$$W_o = -p^{1.2} B_g \, Y_F Y_o e^{-E_g/RT} \qquad (5.9)$$

After several tentative proofs, the best result is obtained as follows:

Replacing $Y_F = \frac{Y_o}{\nu_o} - \tilde{Y}$ in *(5.9)*, gives:

$$W_o = -p^{1.2} B_g \left(\frac{Y_o}{\nu_o} - \tilde{Y} \right) Y_o e^{-E_g/RT} \qquad (5.10)$$

Expanding W_o in series, we can write:

$$W_o^p \simeq W_o^{p-1} + \left(\frac{\partial W_o}{\partial Y_o} \right)^{p-1} \left(y_o^p - \dot{Y}_o^{p-1} \right)$$

where p denotes each iteration, and finally:

$$W_o^p = -p^{1.2} B_g e^{-E_g/RT^{p-1}} \left[\left(\frac{2Y_o^{p-1}}{\nu_o} - \tilde{Y}^p \right) Y_o^p - \frac{(Y_o^{p-1})^2}{\nu_o} \right]$$

The coefficient of Y_o is obtained as a combination of the value of the last iteration $2Y_o^{p-1}/\nu_o$ and of the present iteration for mass function $-\tilde{Y}^p$.

5.3.5. Solution Procedure

The problem resulting from the discretized equations is highly nonlineal. So, it is necessary to use a iterative method of solution which general scheme can be seen in the Fig.5.5.

The main details of the process are the following:

- In each iteration, the initial solution is the one refered to the previous time step.

- To see if the aproximation is valid, the value of each variable at the surface, where the changes are greater, is checked.

- The species concentration values, in each iteration, are checked, with the objetive to restrict the aparition of unrealistic negative values. This negative values are eliminated and the program flux is changed, to get up a good coupling between variables. This problem appears frecuently under fast chemical condition where the flame front changes the sense of movement.

5.4. APPLICATIONS, RESULTS AND ANALYSIS

The numerical program developed has been used to simulate the quiescent combustion process around PMMA rods, ignited by a superficial heat source such an electric heating wire.

The main objectives are to get a full knowledge of the process, to analyze some effects (chemical kinetics, ignition system, radiation and atmosphere oxygen mass fraction) and to get useful data to be used for the sounding rocket module design.

Rod geometry, initial conditions, material properties, operating condition or physical properties used for this study, are shown in Tables 5.1, 5.2 and 5.3.

In the following, we will describe the results of each objective in detail.

5.4.1. Results and analysis of the process. Chemical kinetics influence.

Time evolution for some variables of interest to know the process, are depicted in figures 5.6 to 5.9.

Figure 5.6 shows that there is an initial starting phase, ($0 \leq \tau \sim 25$) with high properties fluctuations, followed by a transition phase ($25 \sim \tau \sim 200$) where variables vary monotically towards a quasi-steady value.

During the starting phase, the burning mass increases towards a maximum and then decreases. This happens just at the instant that the ignition system is switched off. If the starting fails, the burning mass diminishes continuously till extintion occurs; while when the starting is successful, the burning mass decreases towards a minimum (that is the end of this phase) and then begins to increase during the transition phase.

Part of the period between the ignition "switch on" and ignition "switch off" is very complex and of greatest interest, that is because this period of time has been analized in more depth.

Figures 5.10 and 5.11, show the time history of the most significative variables to the understanding of the process, during the period $0<\tau<4$. While in figures 5.9 and 5.10, are depicted the temperature profiles and the oxygen and fuel concentration profiles, at different instants of this period for which there are some interesting event. The details of these events and also the fundamental characteristics of the process are described in figure 5.14.

5.4.2. Perfomances analysis of the ignitor.

To obtain the requirements and performances of ignitor, the starting process has been simulated, modeling the ignitor as a heat

source of constant flux, but with diferent ignition times (τ = 6.4, 7.2 and 8), that is, with variable ignition energy.

The more interesting results are shown in figures 5.15 to 5.22. It can be seen that the existence of a minimum ignition energy for the sucessful starting of the process appears clearly. As well, the burning mass peak produced, increases as the ignition energy is increased. The influence of the ignition energy on the quasi stationary phase is negligible. In effect, no variation of burning mass and flame temperature is observed and there is little increase for the advance of the flame or thermal front.

5.4.3. Effect of radiation and oxygen mass fraction

To analyze the influence of heat radiation from the rod surface, we have computed two limiting cases, that is without radiation (ε = 0), and blackbody radiation (ε = 1). The more significative results are shown in figures 5.23 to 5.26. We can see that starting is more difficult with radiation if the starting phase is observed. For quasi-stationary phase, it is shown that radiation produces a decrease in surface temperature and flame temperature (200 K). This leads to a significant reduction in burning mass (35%) and also in the advance of the flame or of the thermal front.

In the same way, to analyze the effect of oxygen mass fraction content in the atmosphere, we have considered the case of standard atmosphere ($Y_{0\infty}$=.23) and that of pure oxygen ($Y_{0\infty}$=1). The more relevant results are shown in figures 5.27 to 5.32. Rod surface temperature increases as oxygen mass fraction increases, and also flame temperature (ΔT_f~ 620 $^{\circ}$K). This leads to an increase of burning mass greater than 300% in pure oxygen, being the fuel depleted in half a time. The final advance of the flame or of the thermal front diminishes because this great time reduction.

REFERENCES

1. Sánchez Tarifa, C. et al., *"Heterogenous Combustion Processes Under Microgravity Conditions"*, ESA.-C.R. N° 6934/86/F/FL. 1988.

2. Patankar, S.V., *"Numerical Heat Transfer and Fluid Flow"*, Hemisphere Publishing Corporation, 1980.

3. Peyret, R. and Taylor, T.D. *"Computational Methods for Fluid Flow"*, Springer-Verlag, N.Y. Inc., 1.983.

4. Blasi, C.D., Crecitelli, S., Russo, G. and Fernández-Pello, A.C. *"Predictions of the Dependence on the Opposed Flow Characteristics of the Flame Spread Rate over Think Solid Fuel"*.Document. 1987.

5. Lengelle, G., AIAA Journal Vol. 8, N° 11. 1970.

6. Chapman, A.J. *"Transmision del Calor"*, Ed. Interciencia, Madrid, 1965.

7. Anderson, D.A., Tannehill, J.C. and Pletcher, R.H., *"Computational Fluid Mechanics and Heat Transfer"*. Mc Graw-Hill, New York, 1984.

8. Oran, E.S. and Boris, J.P., *"Numerical Simulation of Reactive Flow"*, Elsevier, New York, 1987.

9. Fernández-Pello, A. and Williams, F.A. *"A Theory of Laminar Flame Spread Over Flat Surfeces of Solid Combustibles"*, Combustion and Flame 28, 251-277 (1977).

10. Williams, F.A. *"Combustion Theory"*, The Benjamin/Cummings, Second Editions, 1985.

11. Fernández-Pello, A.C. Ray, S.R. and Glassman, I. *Flame Spread in an opposed Forced Flow: The Effect of Ambient Oxygen Concetration"*. Eigteenth Symp. Comb. 1981.

TABLE 5.1: BASIC IMPUT DATA

ENVIROMENTAL CONDITIONS:

Temperature	288°K
Pressure	101325 N/m^2
Mass fraction of oxygen	0.23 to 1.00

GEOMETRICAL DESCRIPTIONS:

Rod Radius (PMMA)	2 mm.
Supporting wire radius (typical steel)	1 mm.

TABLE 5.2: GAS AND SOLID PROPERTY VALUES

NAME	VALUE	UNITS
	Gas Phase	
Thermal Conductivity	0.02524	J/(m°Ks)
Specific Heat	1125	J/(Kg°K)
	Solid Phase	
PMMA:		
Density	1200	Kg/m^3
Thermal Conductivity	0.225	J/(m°Ks)
Specific Heat	1875	J/(Kg°K)
Supporting Wire (typical steel):		
Density	7801	Kg/m^3
Thermal Conductivity	43	J/(m°Ks)
Specific Heat	472	J/(Kg°K)

TABLE 5.3: GAS AND SOLID PROPERTY VALUES

NAME	SYMBOL	VALUE	UNITS
Preexponential factor (gas-phase reaction)[9]	B_g	$5.6 \cdot 10^{17}$	$g/cm^3 s\ atm^{1.2}$
Activation energy (gas-phase reaction)[9]	E_g	$42 \cdot 10^3$	cal/mol
Preexponential factor (surface pyrolysis)[4,5]	B_s	10^6	m/s
Activation energy (surface pyrolysis)[4,5]	E_s	125.52	KJ/mol
Efective heat of vaporization[11]	q_v	380	cal/gr
Heat of reaction[11]	q_F	$2.5952 \cdot 10^7$	J/Kg(PMMA)
Oxyen to fuel mass stoichiometry ratio	ν	1.92	

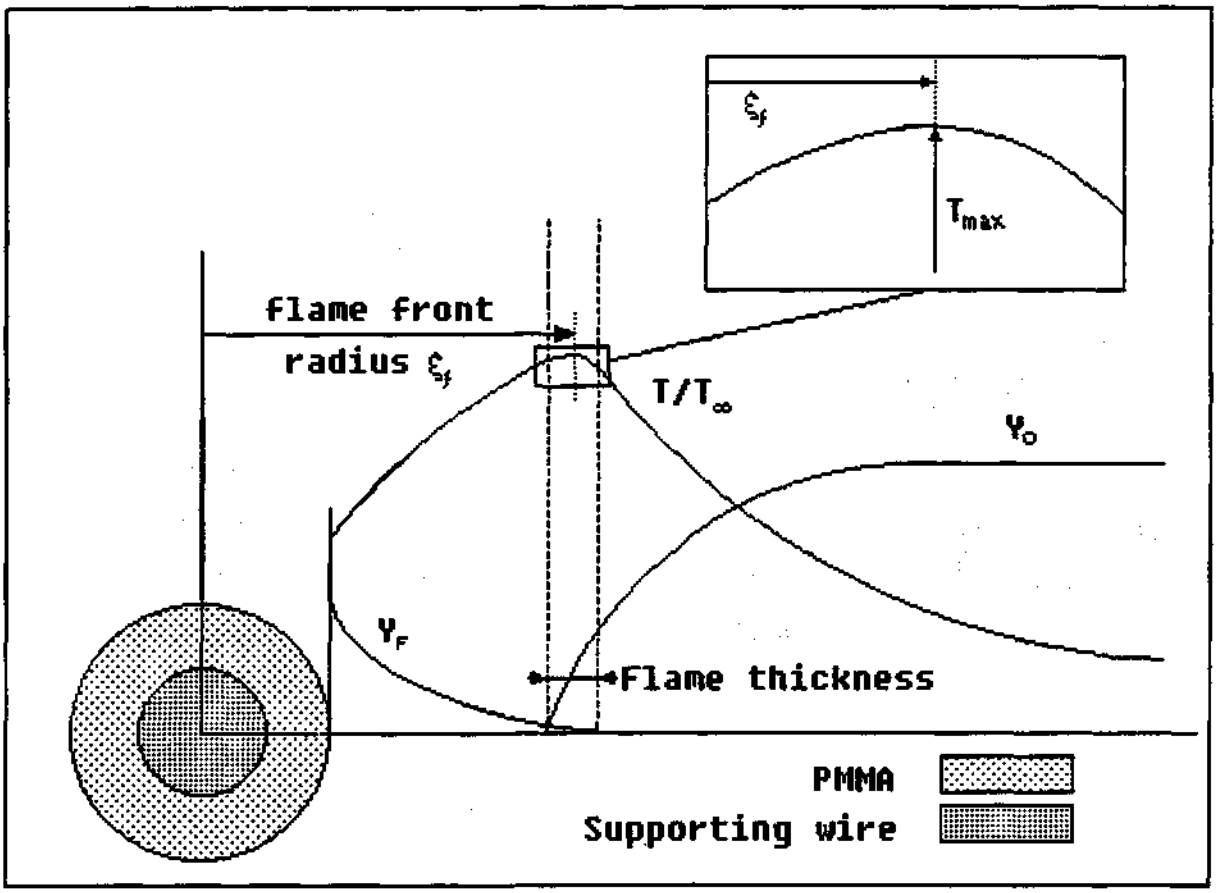

Fig. 5.1.- Scheme of quiescent combustion

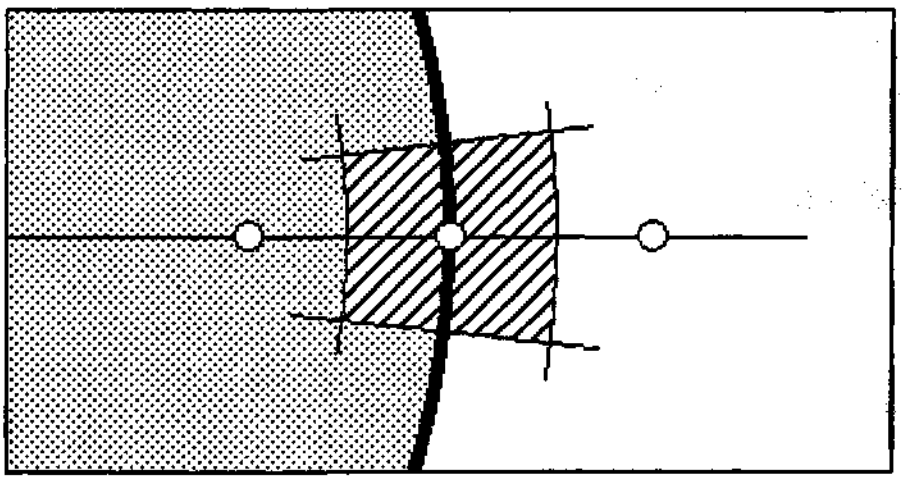

Fig. 5.2.- Surface volume control

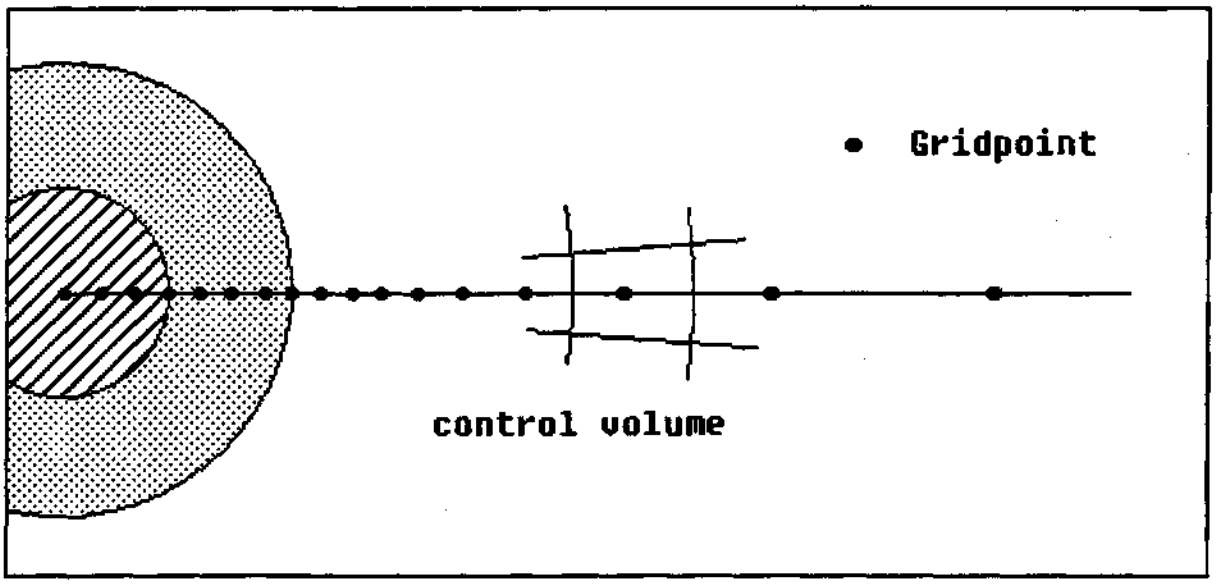

Fig. 5.3.- Schene of computational domain

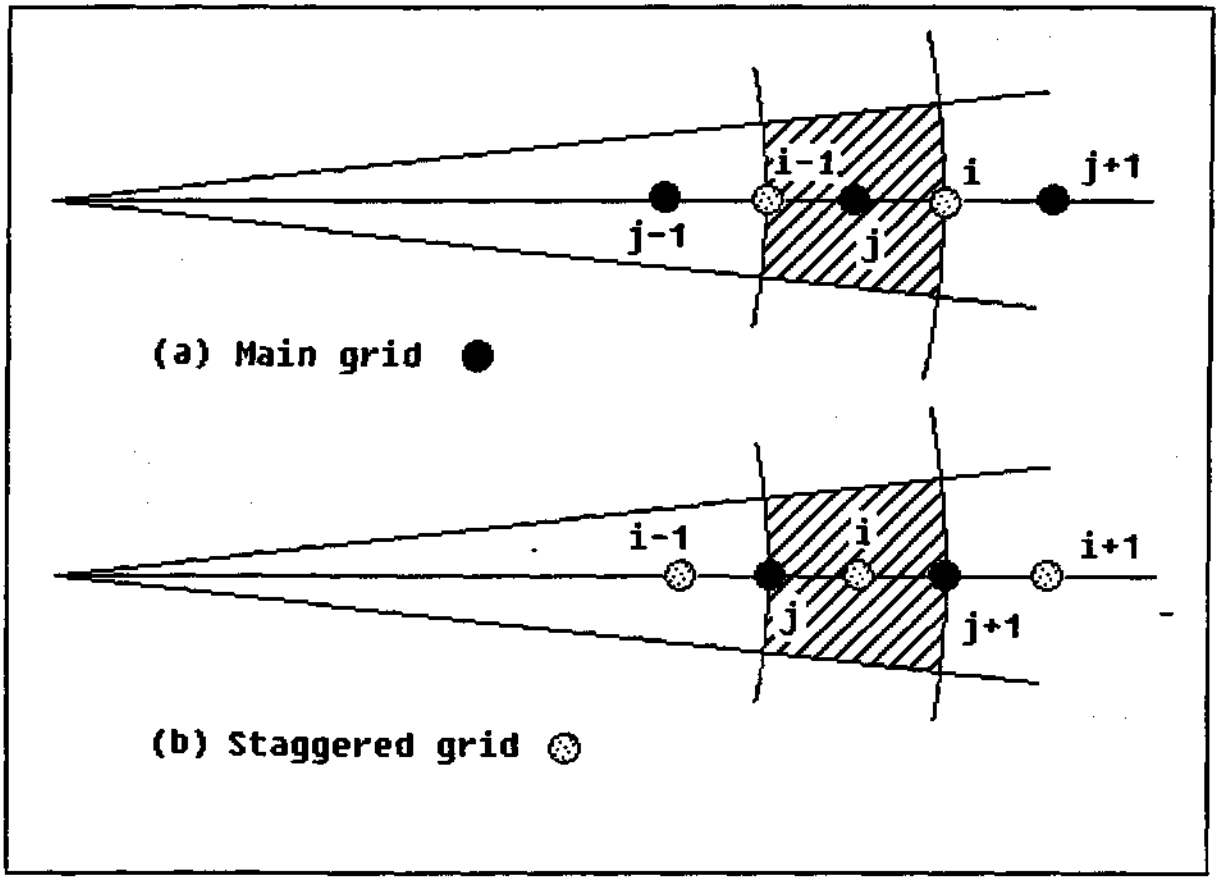

Fig. 5.4.- Control volumes

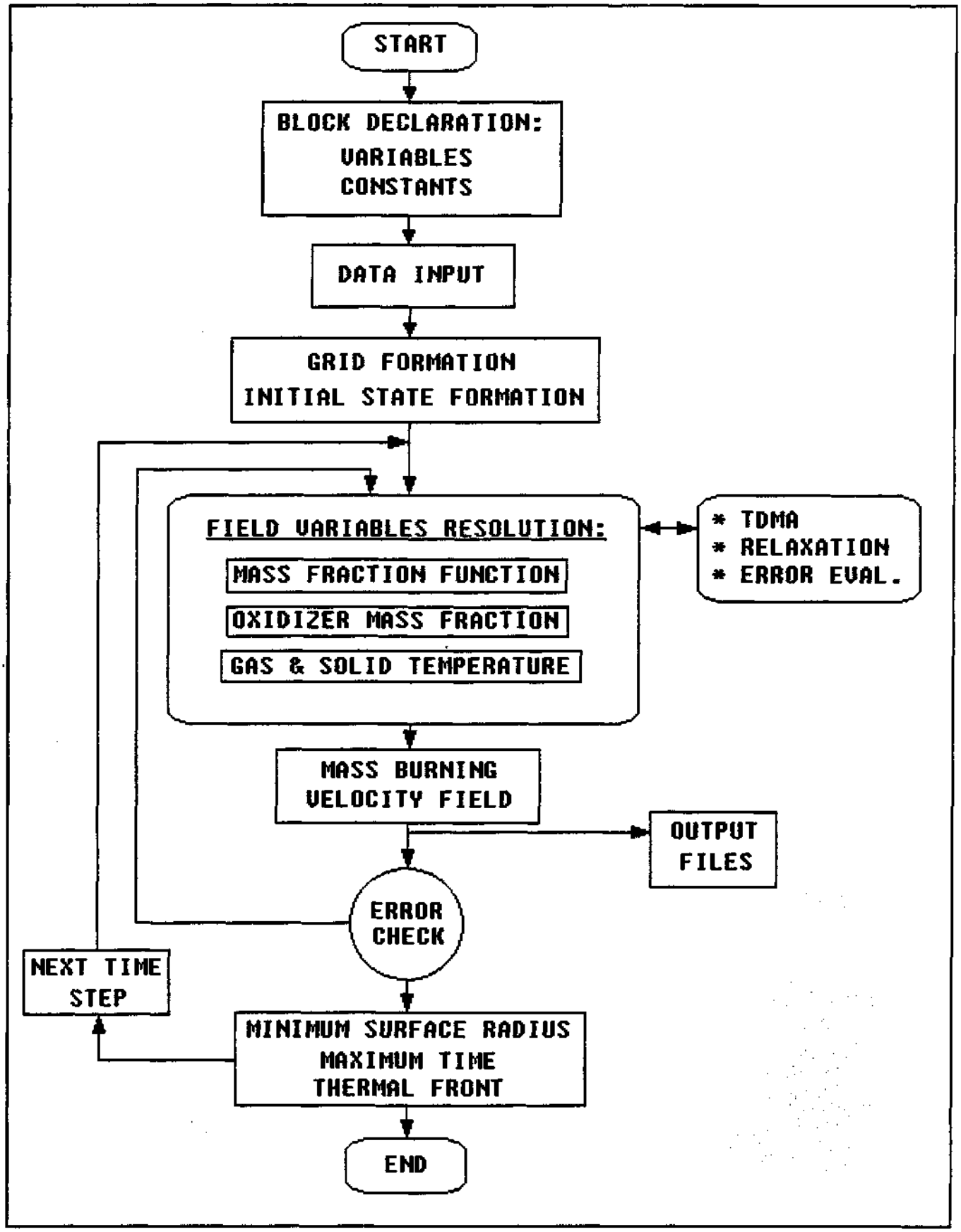

Fig. 5.5.- Computer program blocks diagram

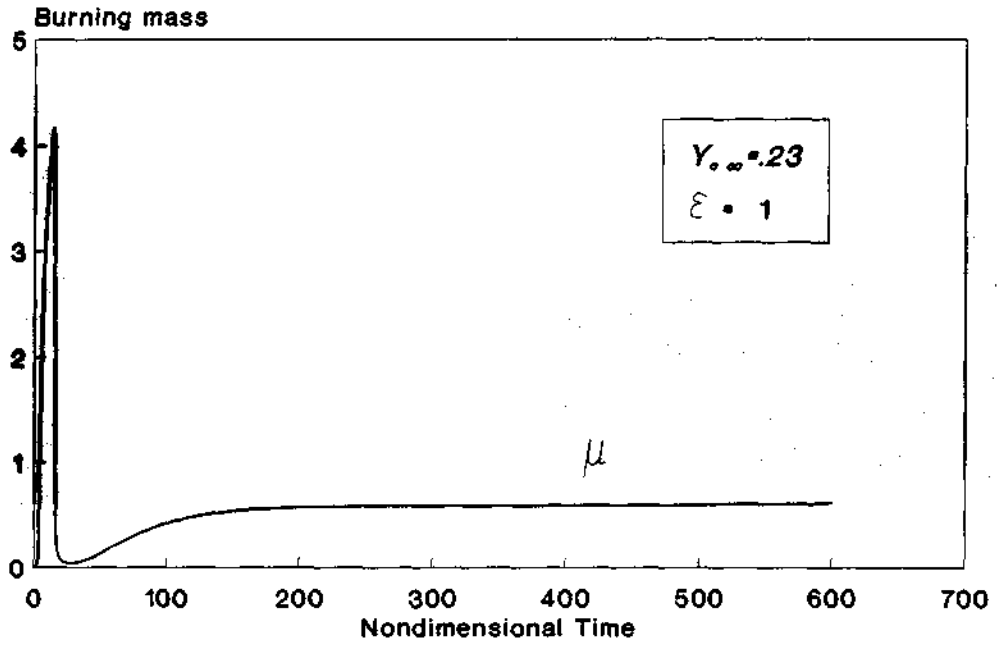

Fig. 5.6.- Tipical Time Evolution

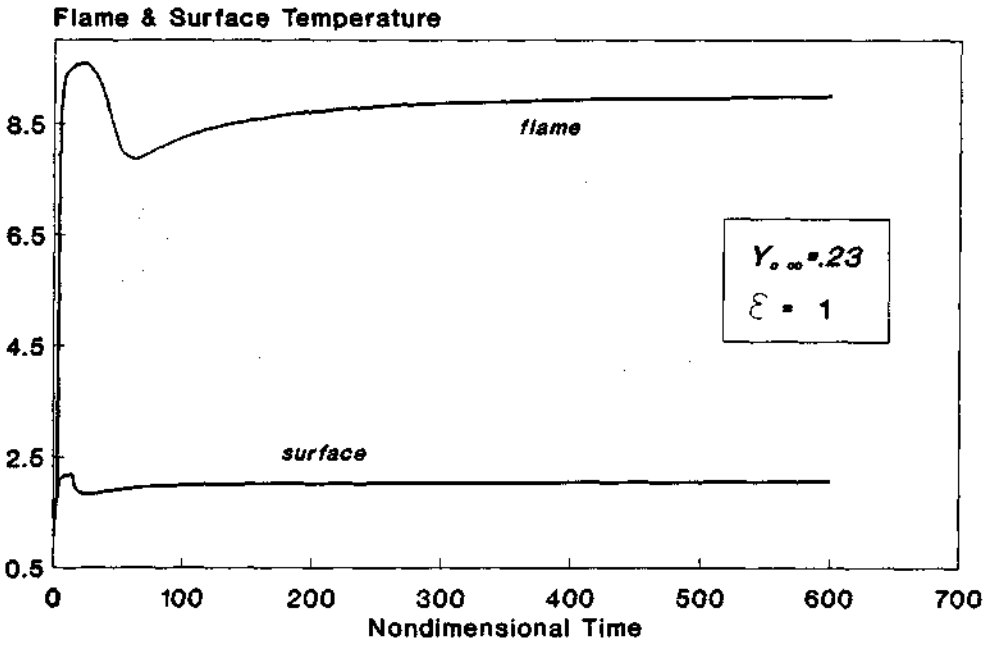

Fig. 5.7.- Tipical Time Evolution

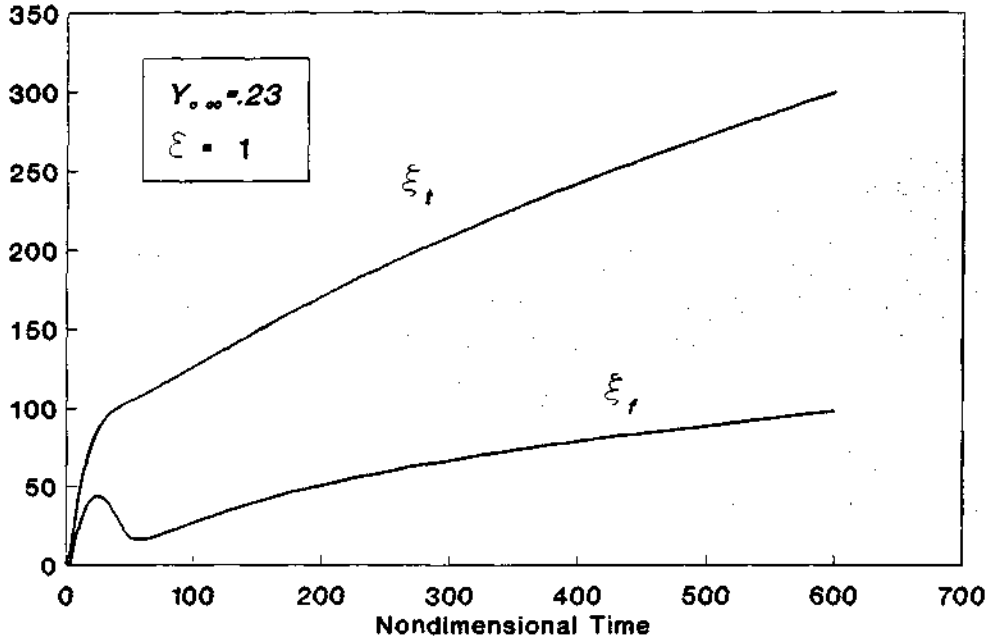

Fig. 5.8.- Tipical Time Evolution

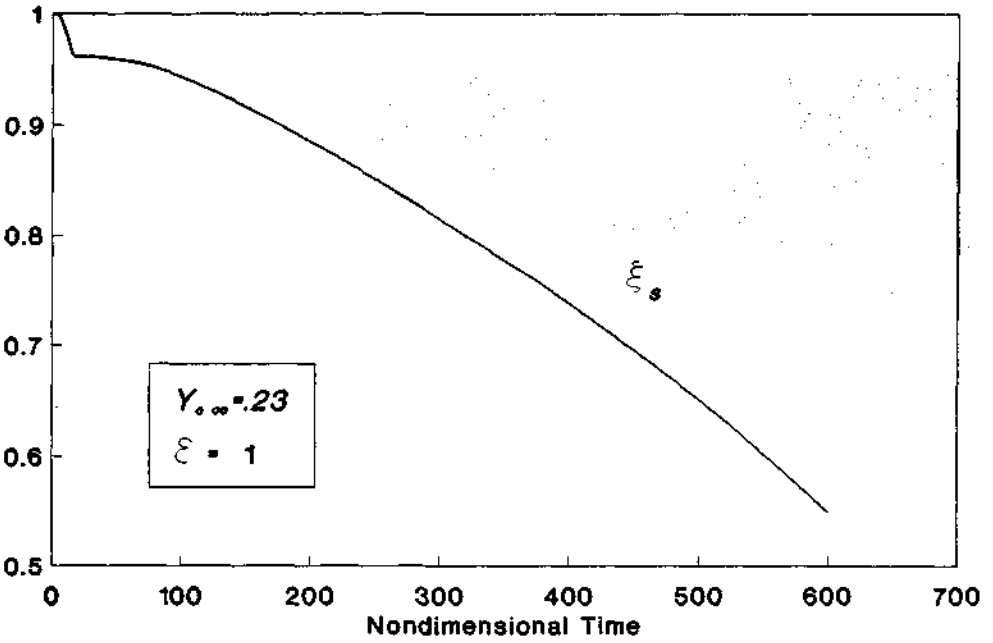

Fig. 5.9.- Tipical Time Evolution

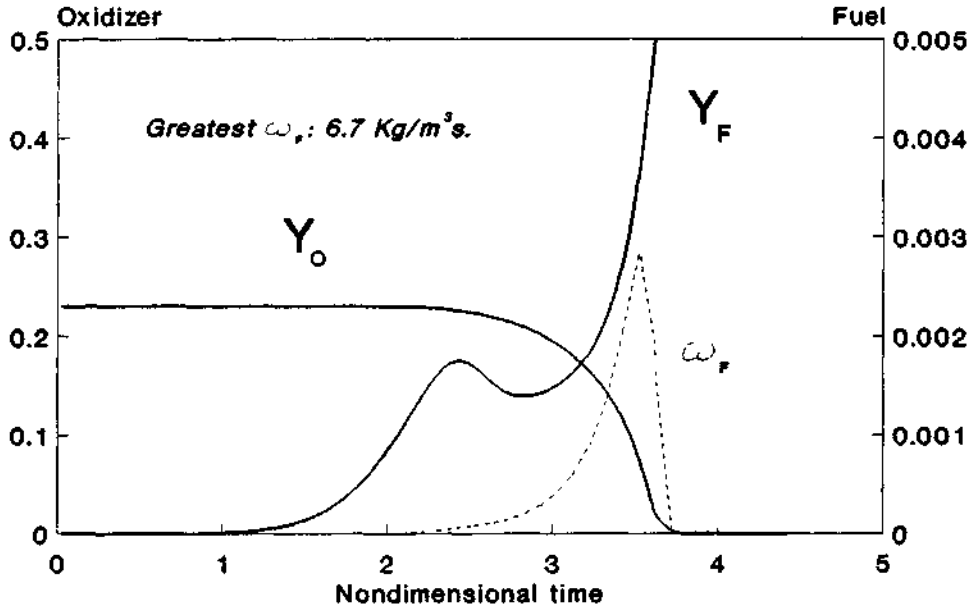

Fig. 5.10.- Time evolution of variables at the surface.

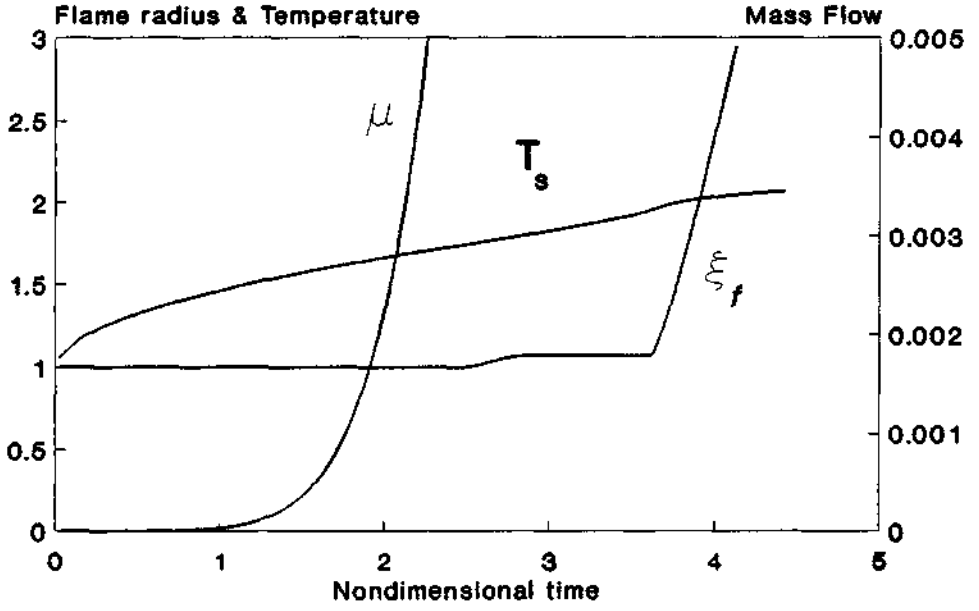

Fig. 5.11.- Time evolution of variables at the surface.

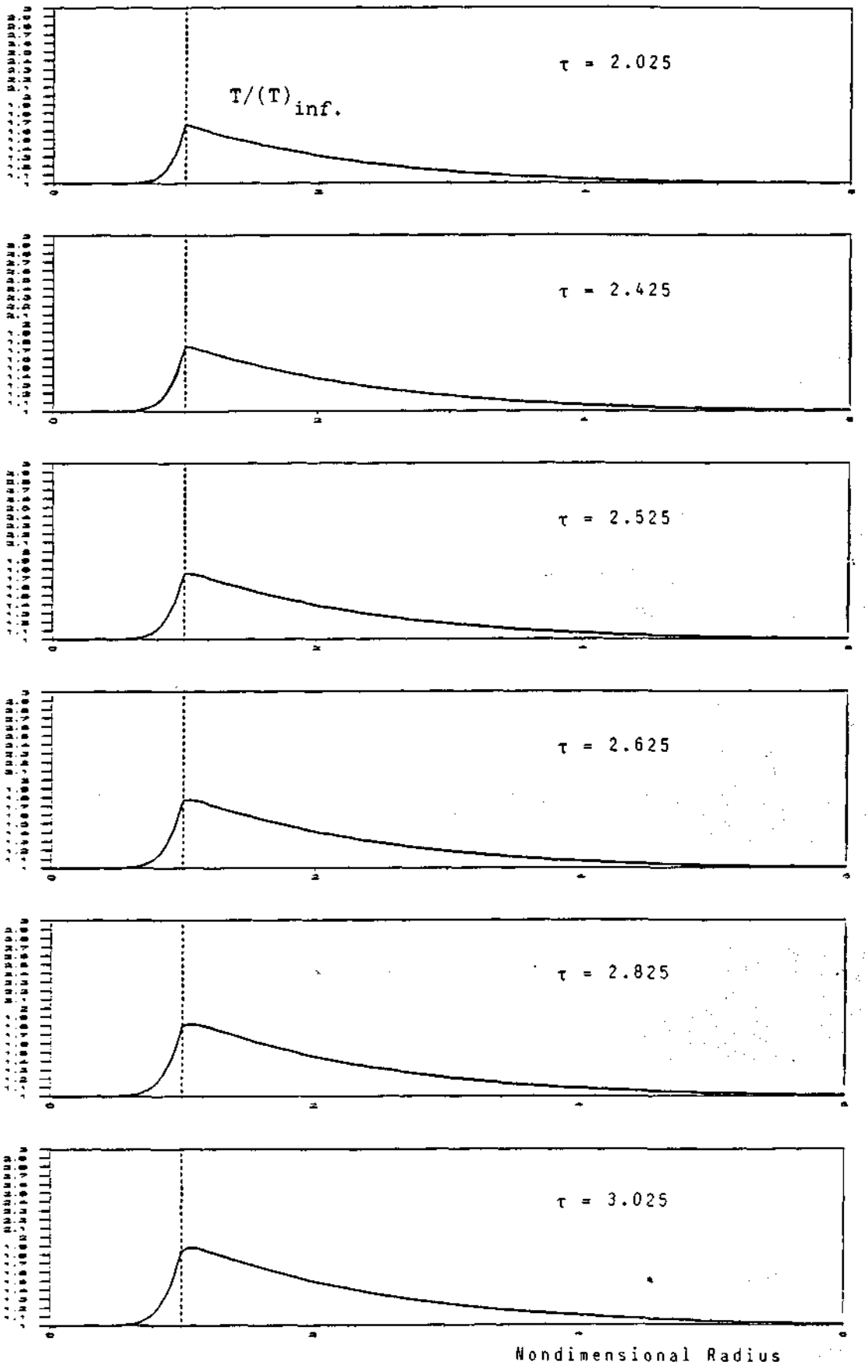

Fig. 5.12.- Computed temperature profiles.

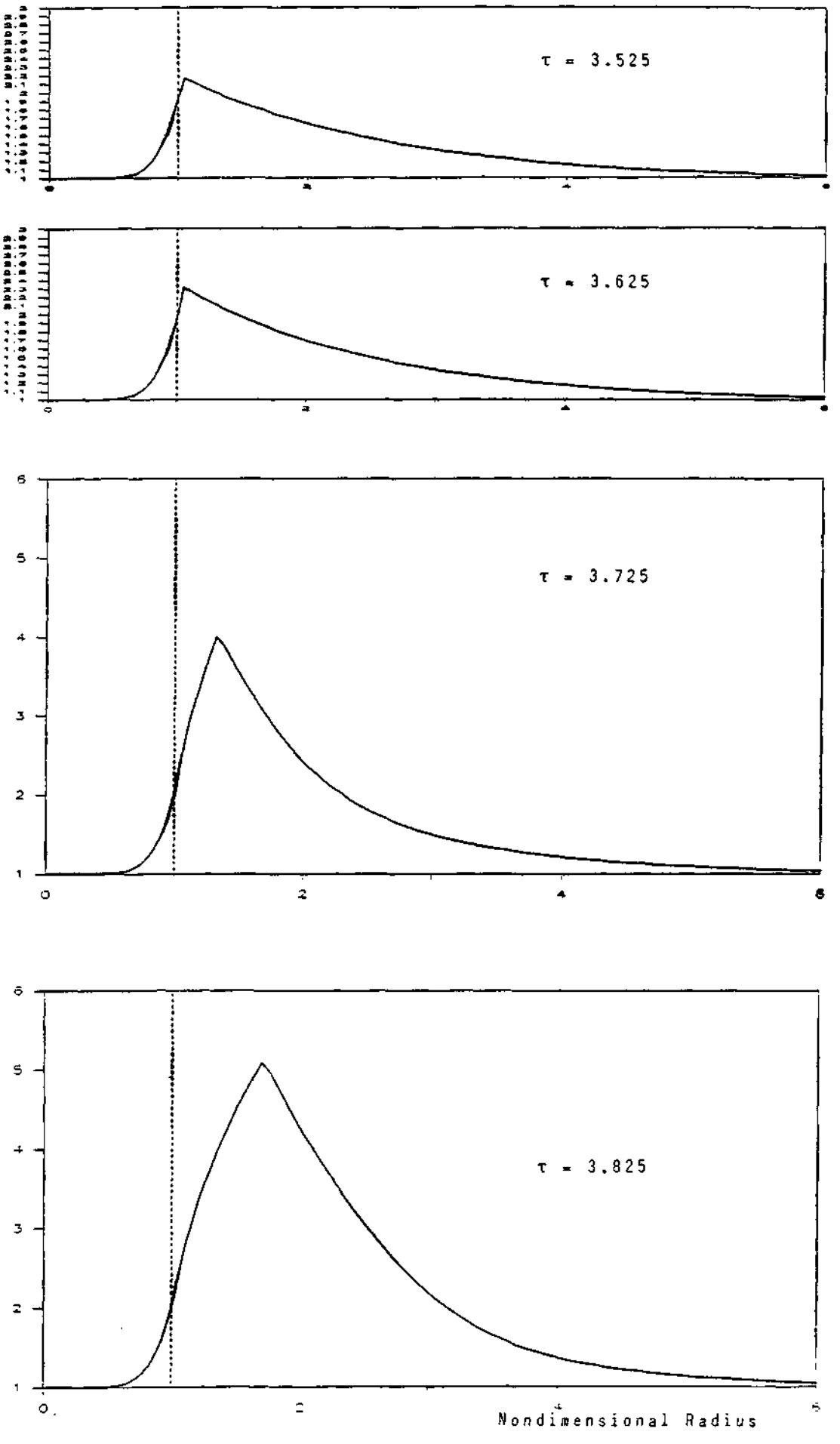

Fig. 5.12.- (Continued) Computed temperature profiles.

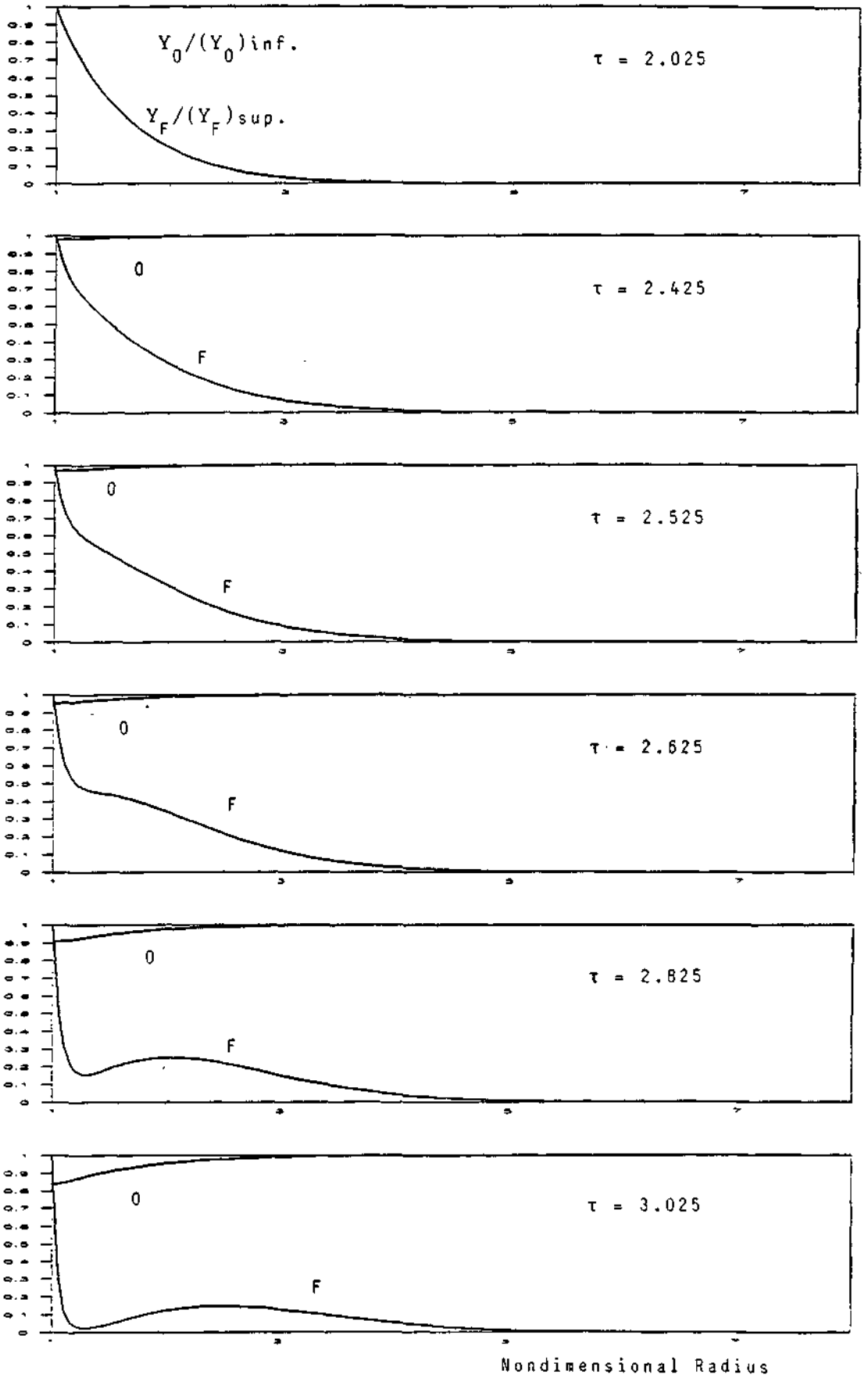

Fig. 5.13.- Computed oxygen and fuel mass fraction profiles.

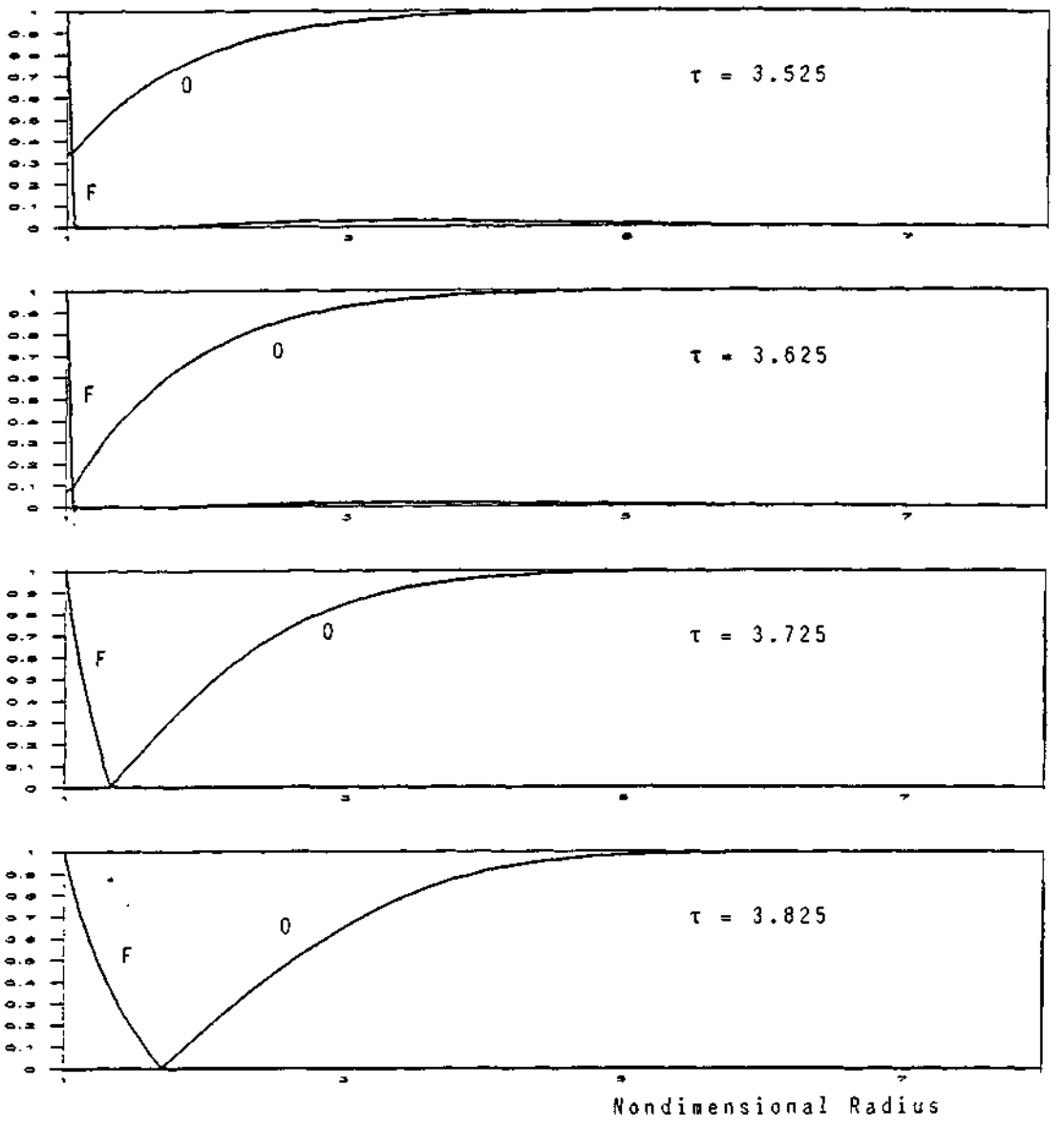

Fig. 5.13.- (Continued) Computed oxigen and fuel mass fraction profiles.

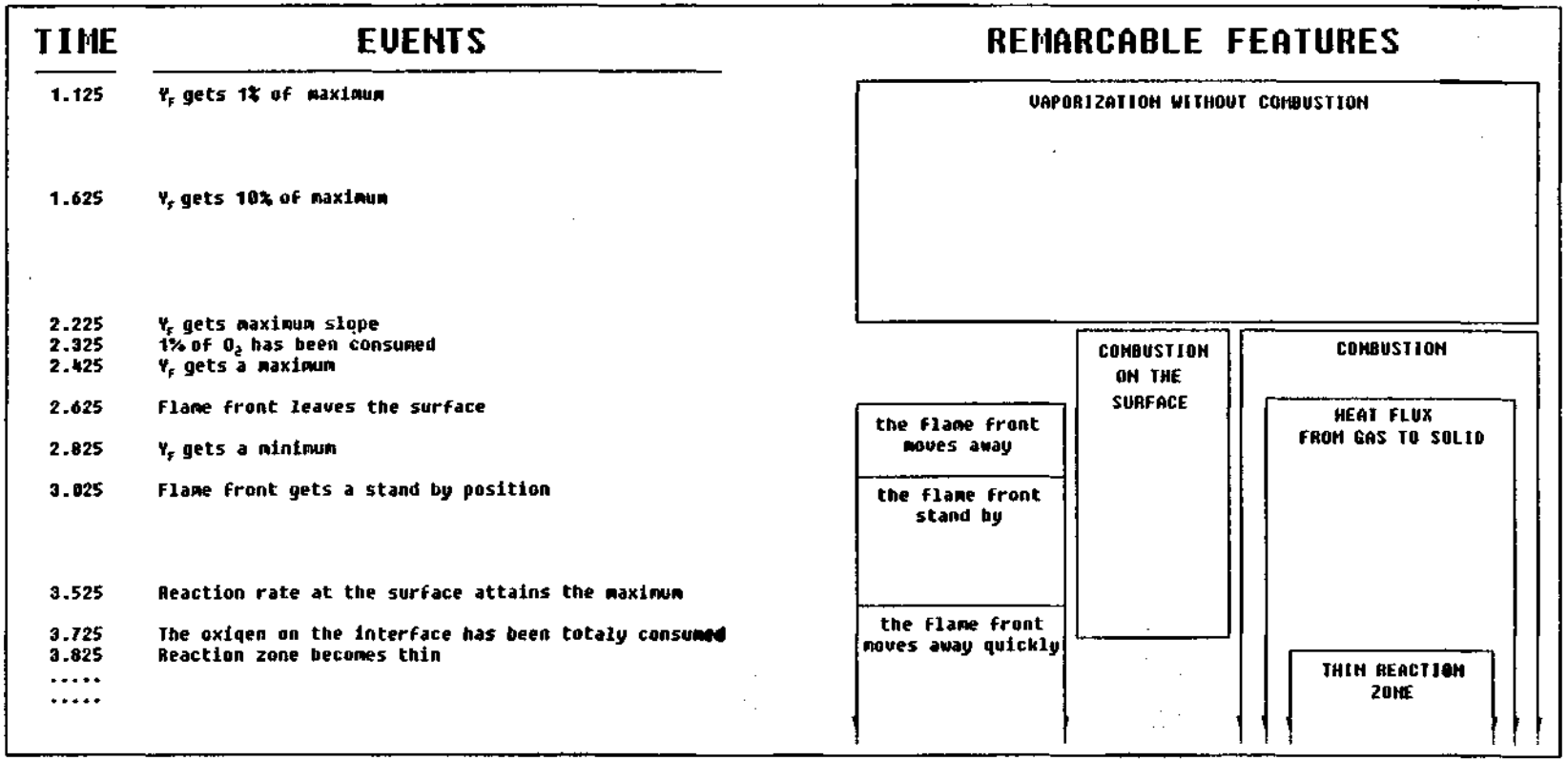
TIME
EVENTS
REMARCABLE FEATURES
1.125
Y_F gets 1% of maximum
1.625
Y_F gets 10% of maximum
2.225
Y_F gets maximum slope
2.325
1% of O_2 has been consumed
2.425
Y_F gets a maximum
2.625
Flame front leaves the surface
2.825
Y_F gets a minimum
3.025
Flame front gets a stand by position
3.525
Reaction rate at the surface attains the maximum
3.725
The oxigen on the interface has been totaly consumed
3.825
Reaction zone becomes thin
.....
.....
VAPORIZATION WITHOUT COMBUSTION
COMBUSTION ON THE SURFACE
COMBUSTION
HEAT FLUX FROM GAS TO SOLID
THIN REACTION ZONE
the flame front moves away
the flame front stand by
the flame front moves away quickly

Figure 5.14

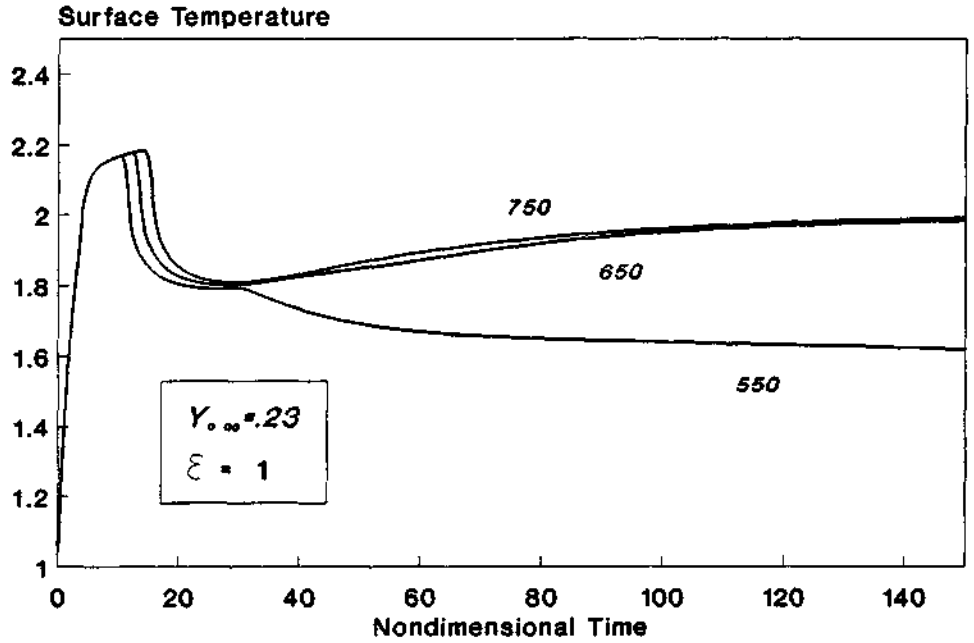

Fig. 5.15.- Effect of ignition energy.

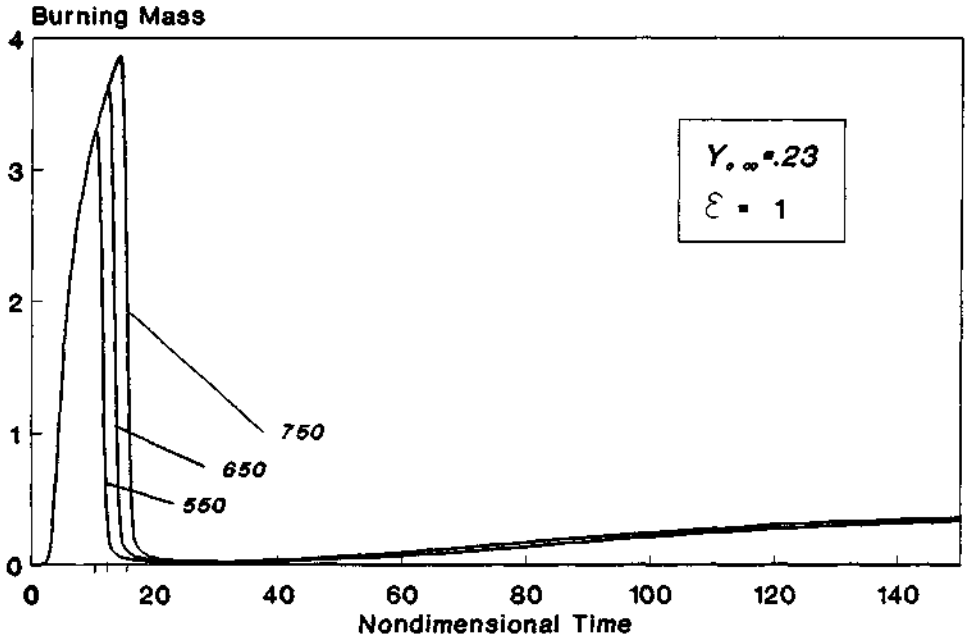

Fig. 5.16.- Effect of ignition energy.

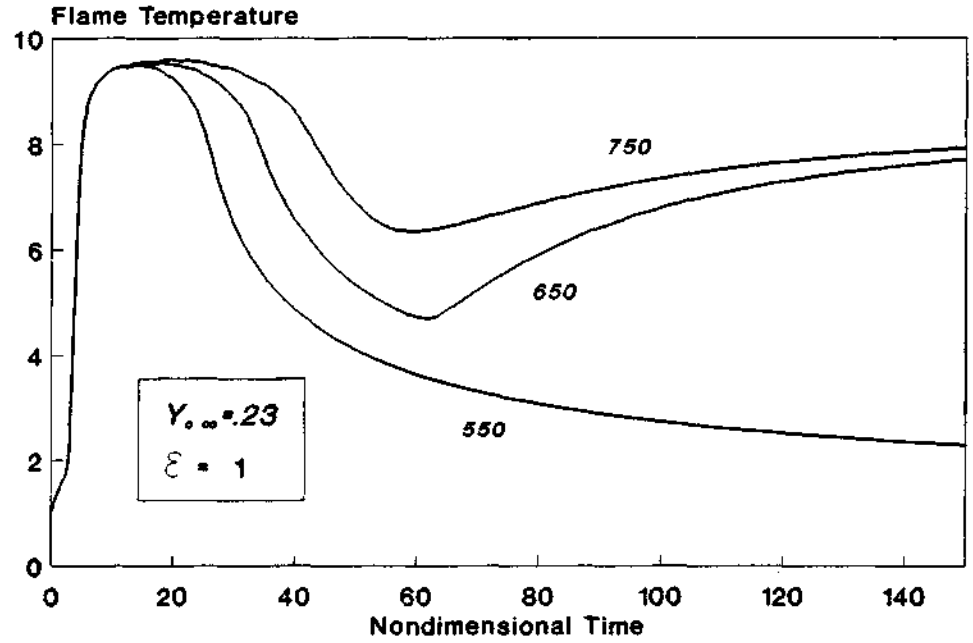

Fig. 5.17.- Effect of ignition energy.

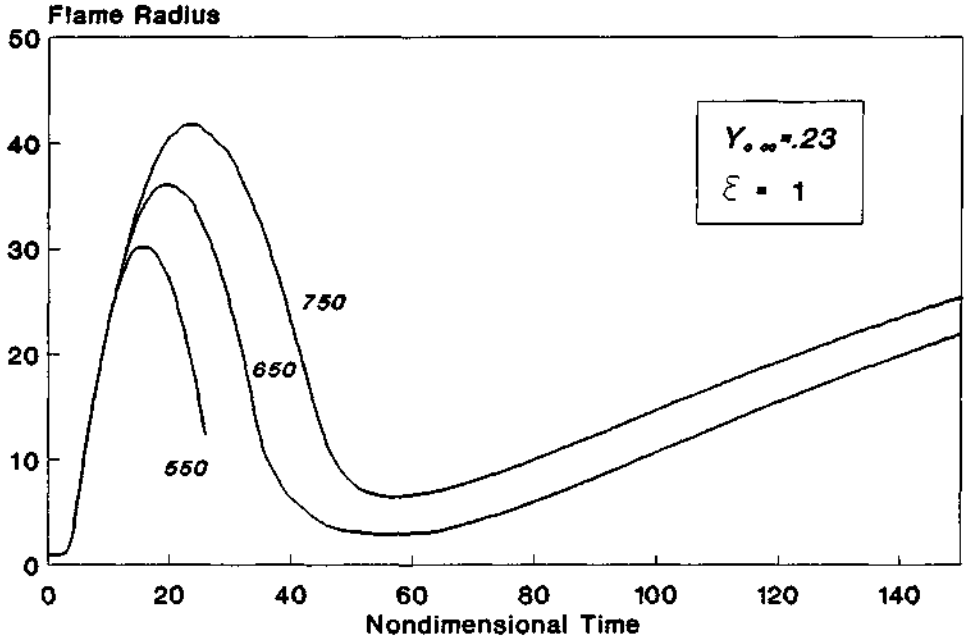

Fig. 5.18.- Effect of ignition energy.

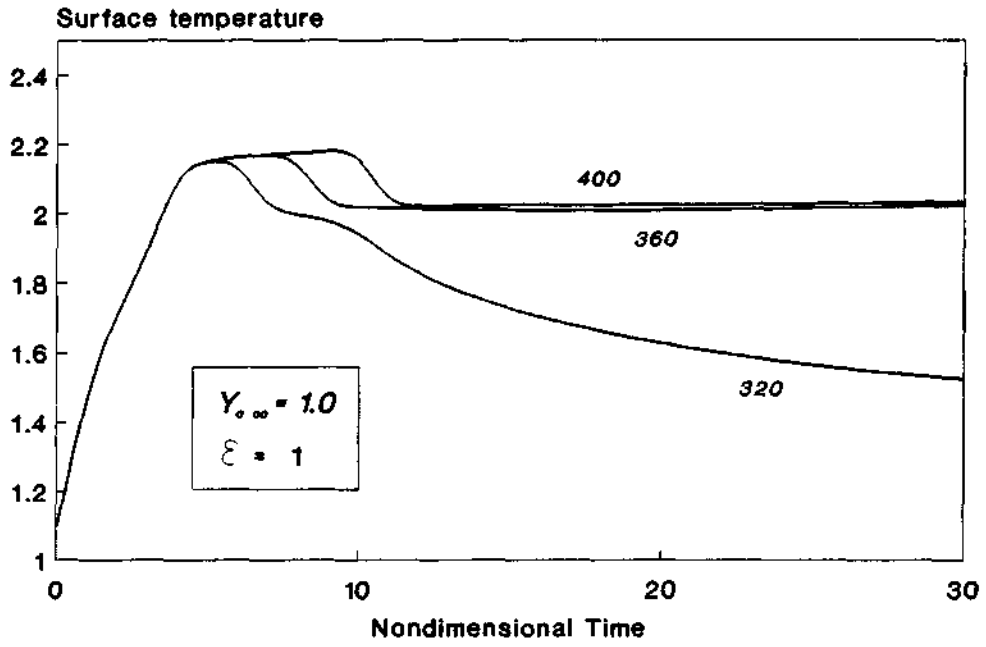

Fig. 5.19.- Effect of ignition energy.

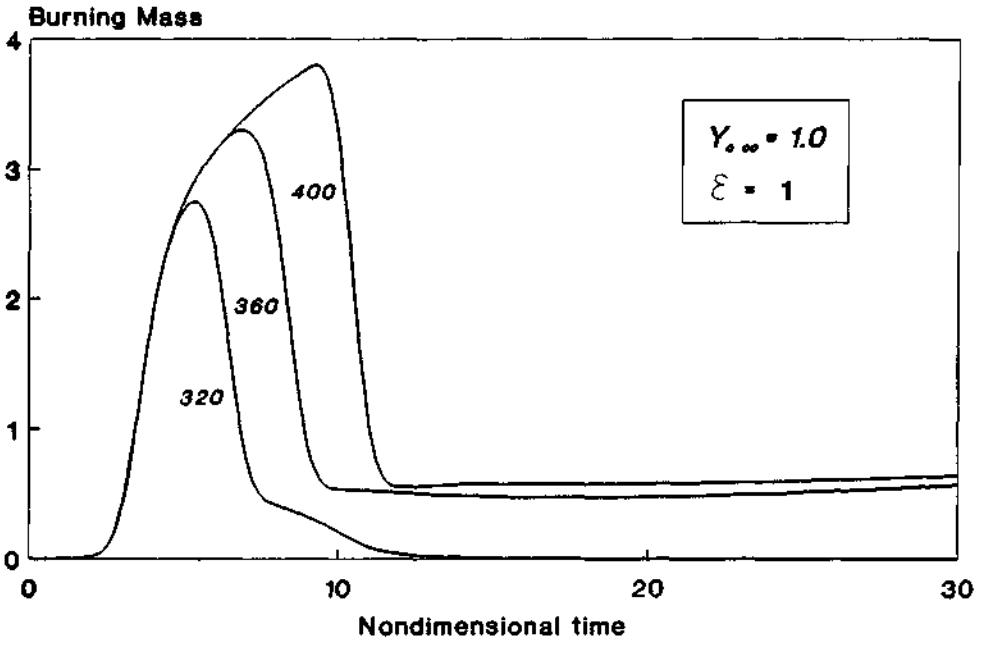

Fig. 5.20.- Effect of ignition energy.

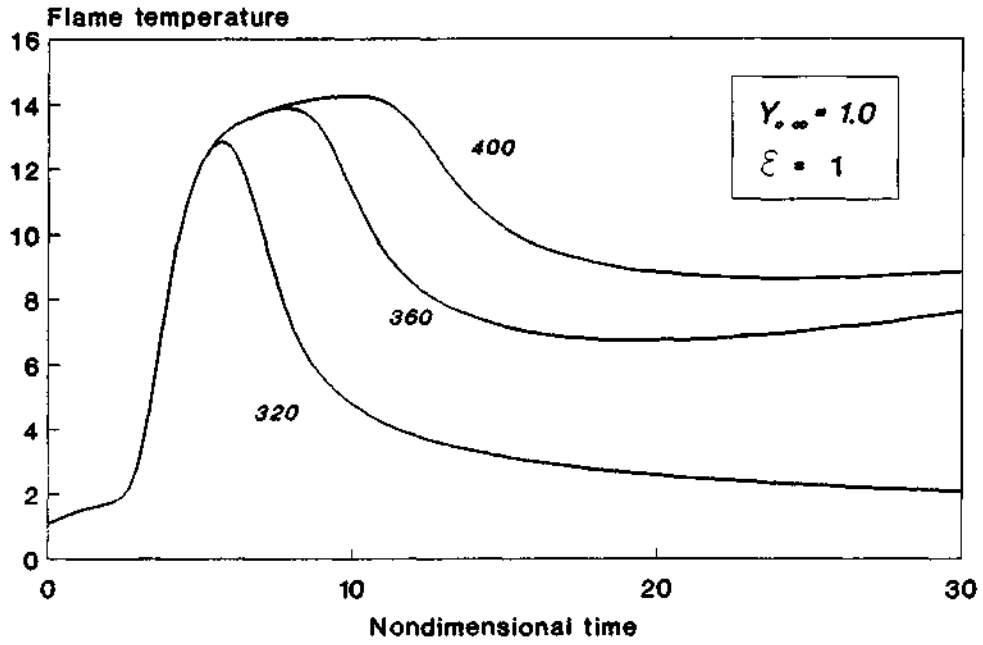

Fig. 5.21.- Effect of ignition energy.

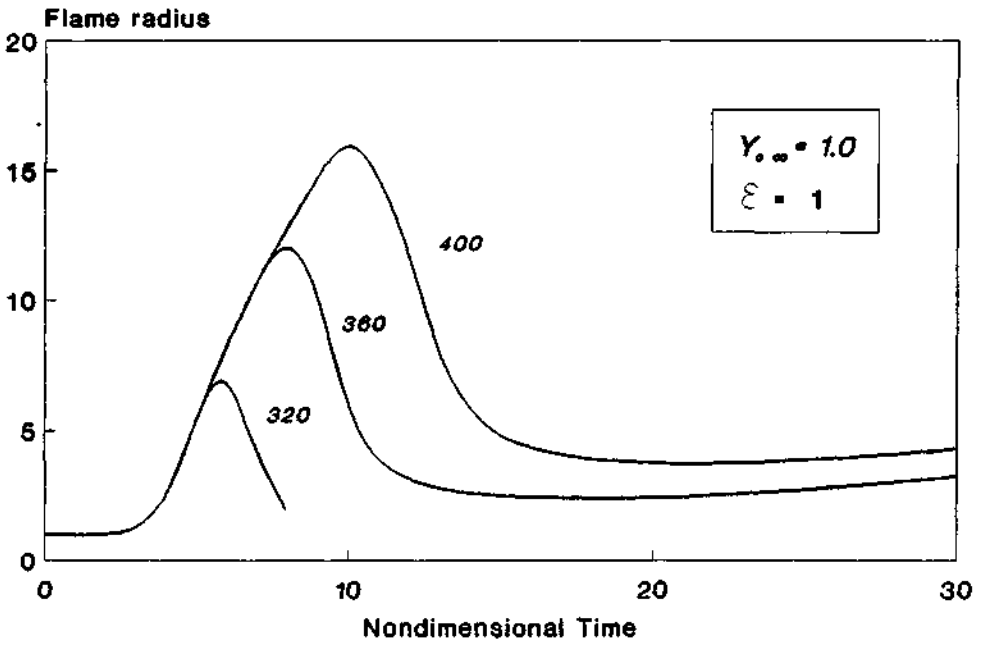

Fig. 5.22.- Effect of ignition energy.

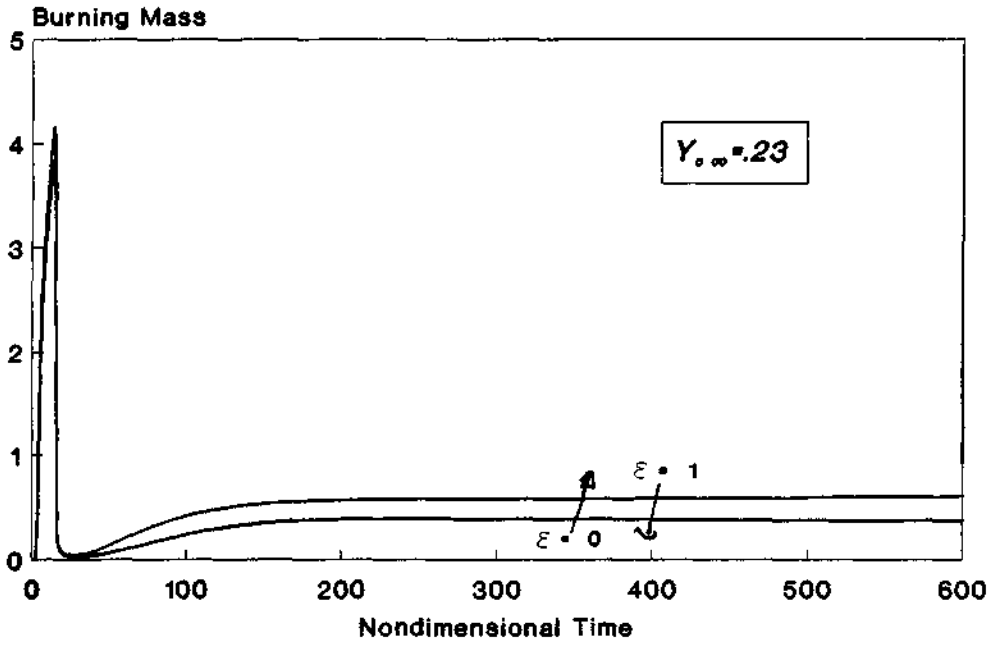

Fig. 5.23.- Effect of radiant coeff.

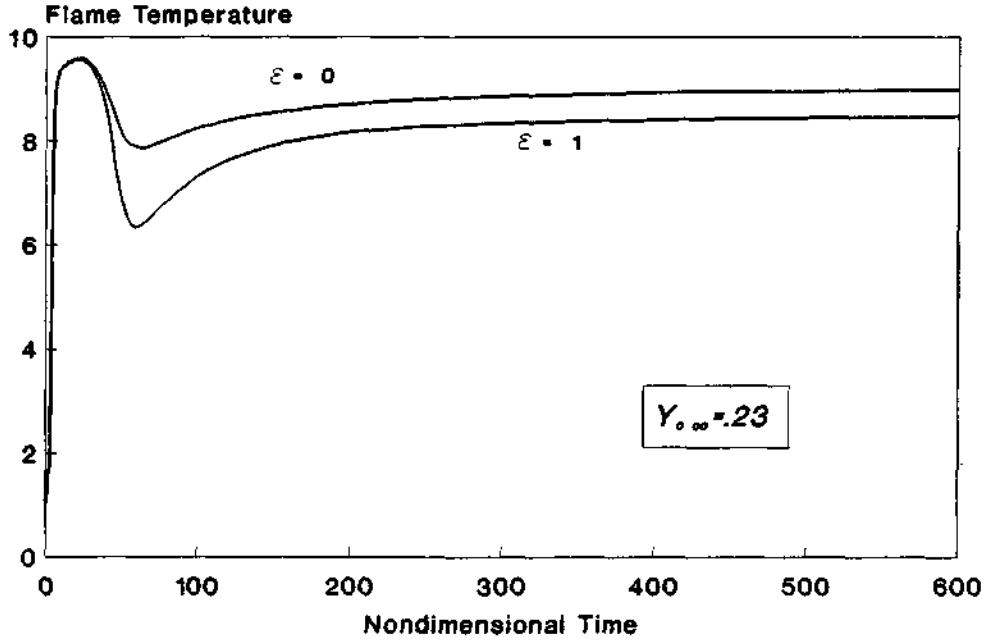

Fig. 5.24.- Effect of radiant coeff.

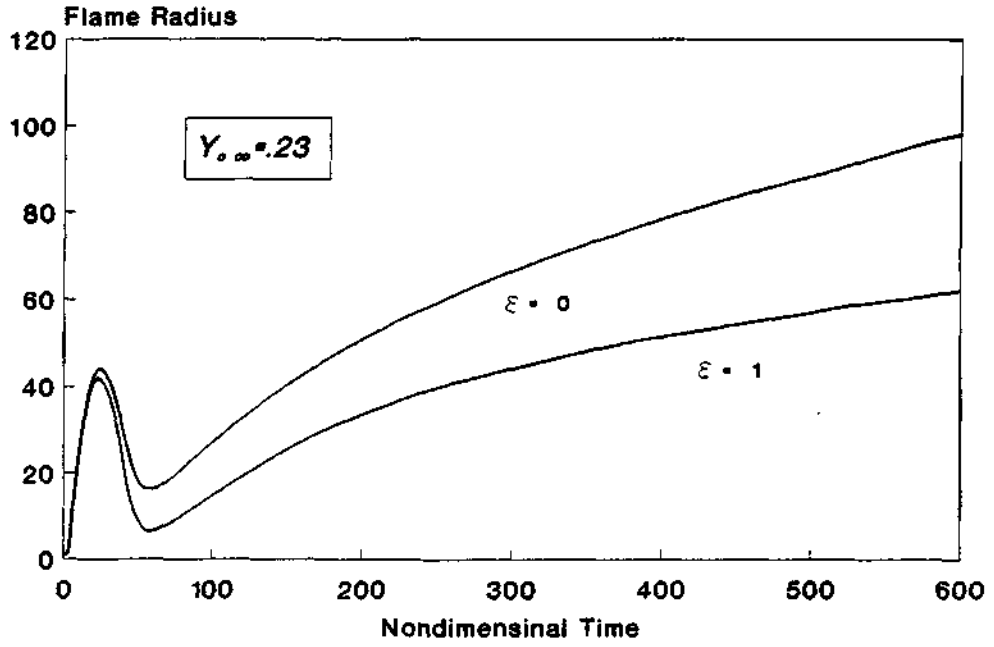

Fig. 5.25.- Effect of radiant coeff.

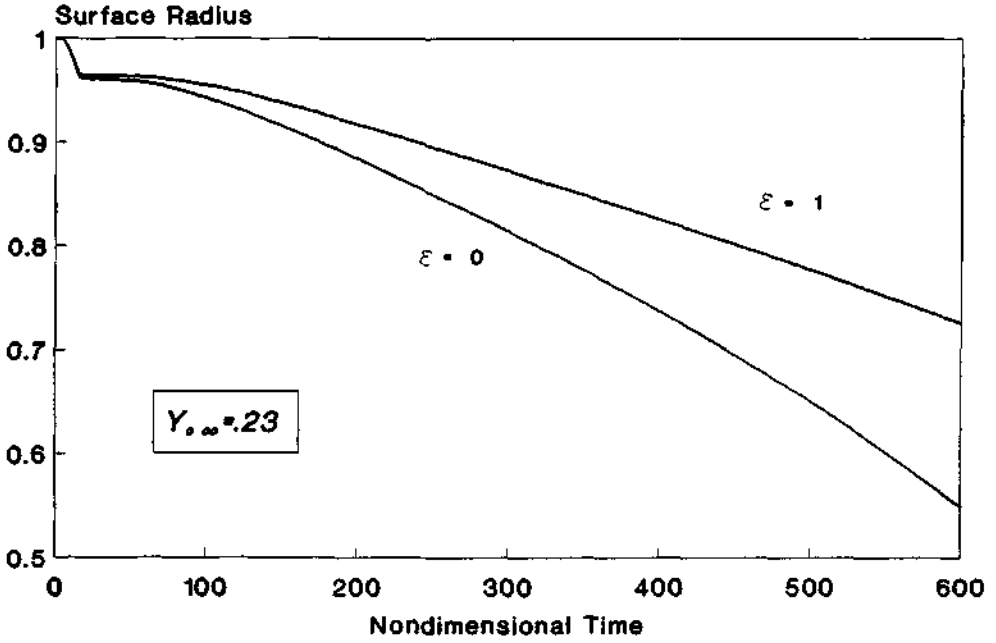

Fig. 5.26.- Effect of radiant coeff.

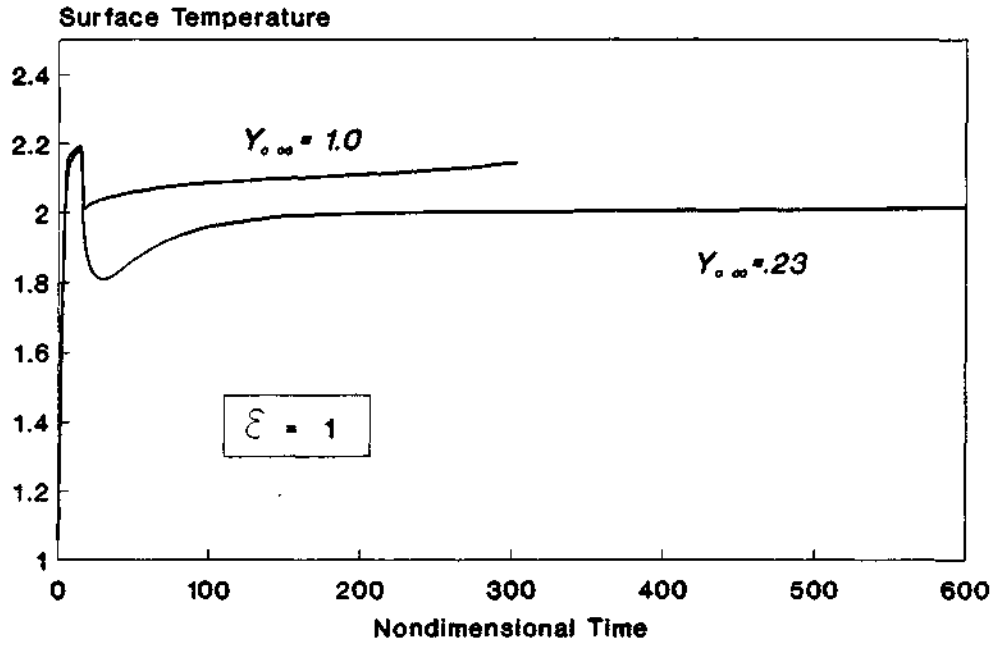

Fig.5.27.-Effect of oxygen mass fraction

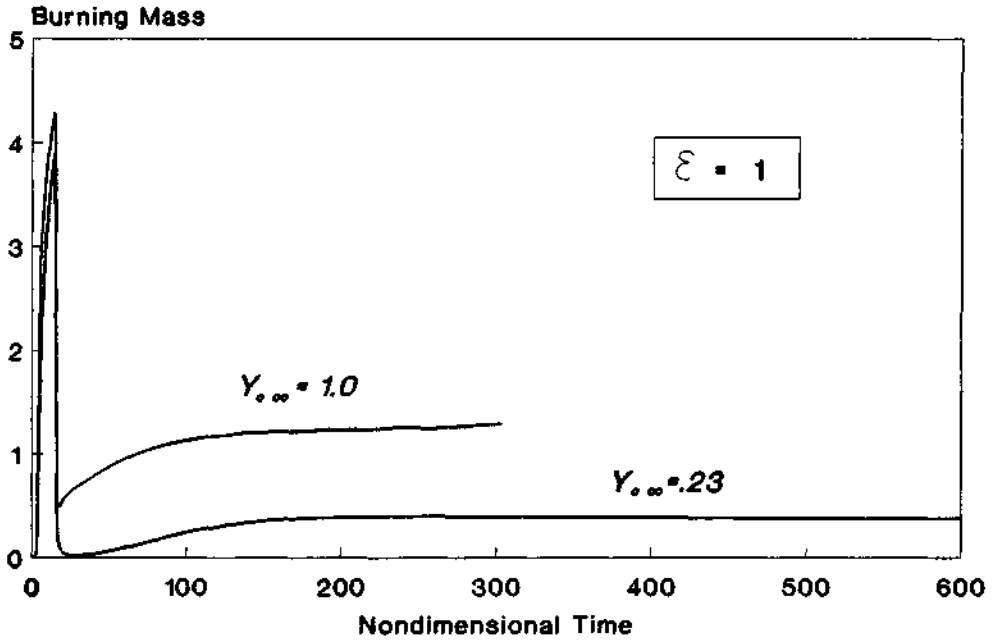

Fig 5.28.-Effect of oxygen mass fraction

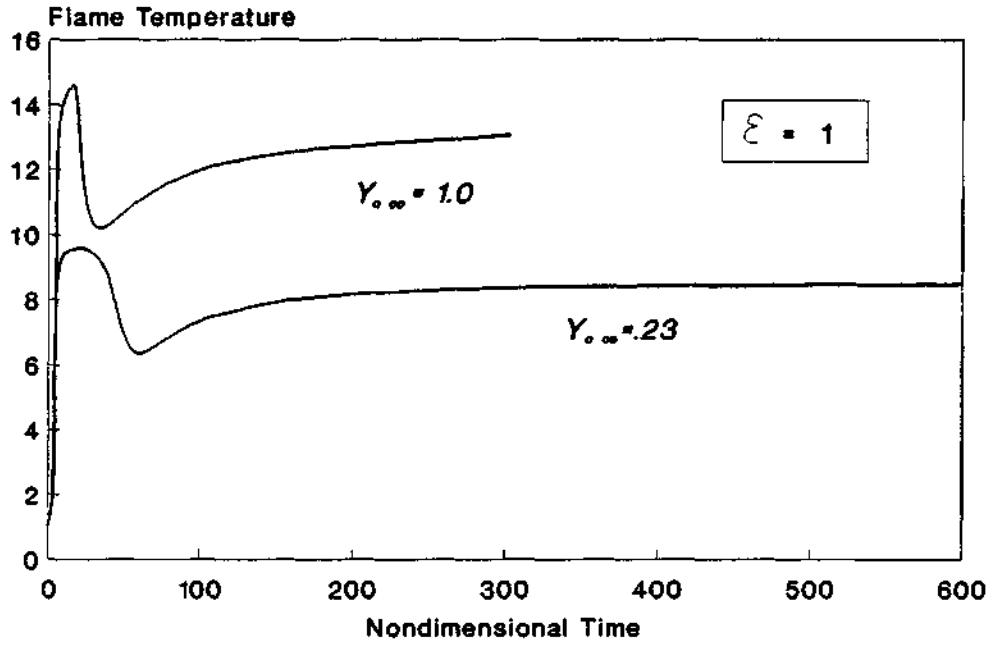

Fig 5.29.-Effect of oxygen mass fraction

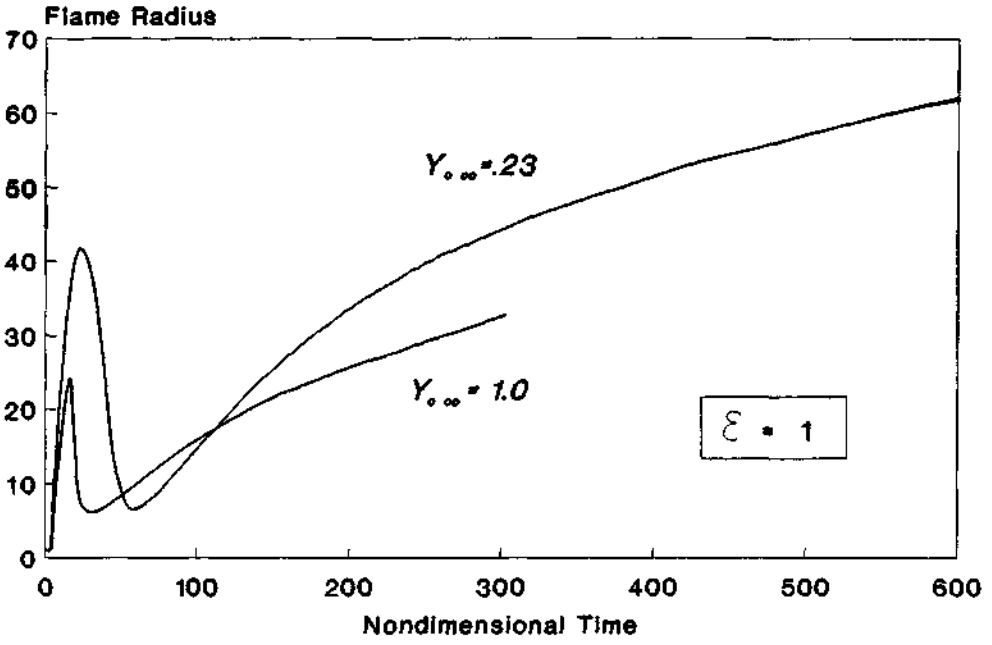

Fig.5.30.-Effect of oxygen mass fraction

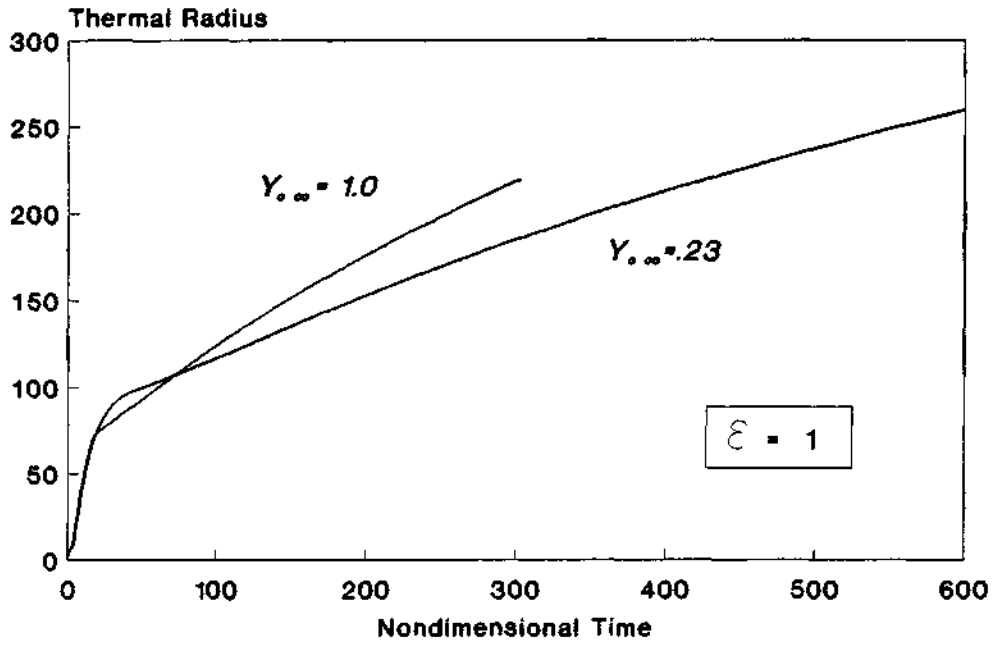

Fig.5.31.-Effect of oxygen mass fraction

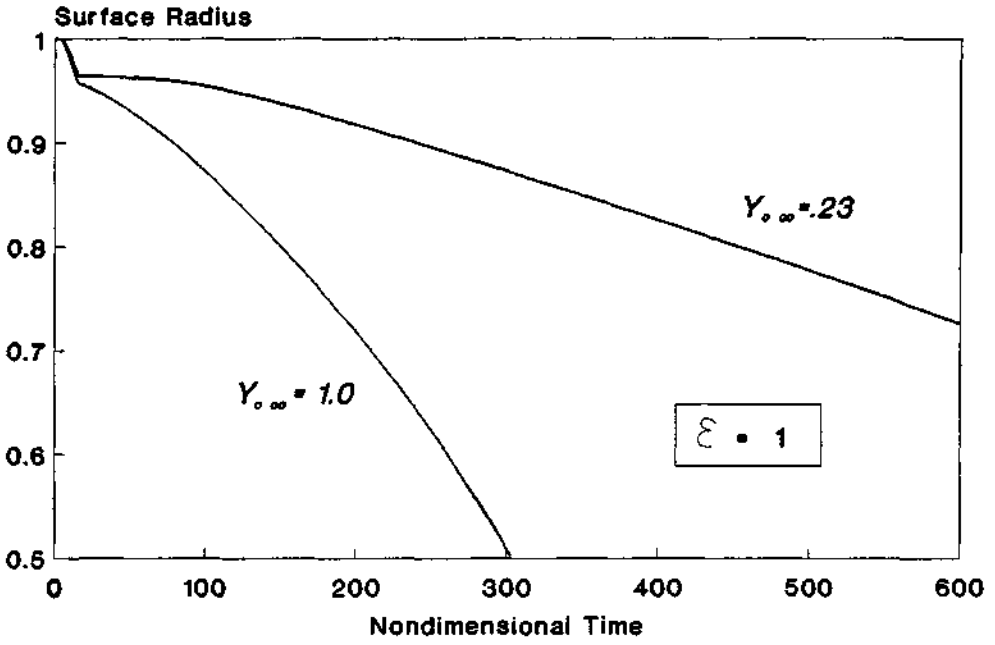

Fig.5.32.-Effect of oxygen mass fraction

6. WP5. PROPOSED EXPERIMENT

6. WP5. PROPOSED EXPERIMENT

The following experiment is proposed for consideration:

"FLAME SPREADING WITH FORCED CONVECTION ALONG THE SURFACE OF A SOLID FUEL AT REDUCED GRAVITY"

DETAILS OF THE EXPERIMENT

Forced convection effects would be experimented at low Reynolds Number by means of a sequence of tests, starting without convection and reaching flow velocities up to values of the order of 10 *cm/s*.

Within these values it is expected that it will be covered the transition region in which the law of variation of the spread velocity as function of the flow velocity changes.

The solid fuel would be PMMA in form of a cylindrical rod or a rectangular slab.

In the first set of experiments the convective flow would have a velocity opposite to the direction of the flame spread. Experiments with the convective flow in the same and in a transversal direction to that of the flame spread would also be of high interest.

JUSTIFICATION

Forced convection effects at low flow velocity on flame spread processes along the surface of solid fuels is a problem of current high interest.

These effects cannot be experimentally studied on the ground at 1g, because free convection effects would be predominant or at least they would perturb significantly the process, depending on the relative values

of the Grashof and Reynolds Numbers.

On the other hand, in the event of a fire in a spacecraft or space laboratory, it would take place in all probability in an atmosphere of low gas currents, orginated by the air-oxygen conditioning equipment or even by the motion of people.

There is some experimental evidence on this subject obtained in free fall towers, which has been obtained with very thin sheets of solid materials, and restricted to the very short time available in this towers.

There are no experimental results whatever on the flame spreading process when the fuel is thick (one or more *mm*), which is the really important case in prractice and in which the flame spreading mechanism follows different laws.

SEQUENCE OF EX EXPERIMENTS

It will be assumed, in principle, that forced convection is generated by the motion of the sample within an oxygen atmosphere at rest.

The useful length of the chamber for the motion of the sample is assumed to be of the order of 120-130 *cm*.

The following sequence of four experiments might be performed during the 360 seconds available at reduced gravity in each launching:

EXPERIMENT	ELAPSED TIME (sec)
1. Ignition. Flame spreading along about half the length of the sample in a still atmosphere.	20-30
2. Motion of the same sample along the chamber at low speed *(~20 mm/s)*	20-30

EXPERIMENT	ELAPSED TIME (sec)
3. Emptying and filling the chamber with oxygen. Replacing the sample.	20-25
4. Time required to reduce the fluctuation velocities of the oxygen down to values of ≤ *2mm/s*.	~120
5. Ignition of a new sample and flame spread moving the sample at about *40-50 mm/s*.	20-25
6. Emptying and filling the chamber. Replacing the sample.	20-25
7. Time required to reduce the fluctuation velocities down to values of the order of *4 mm/s*.	~75
8. Ignition of a new sample, and flame spread at a sample motion velocity of about *80-100 mm/s*.	12-16
9. Emptying the chamber and end of the experiment.	~10 (extinction time)
Total maximum elapsed time	356 seconds

REMARKS

- The values of the velocities and times are only tentative. Their final values would be selected after numerical and experimental evaluations.

- A quiescent combustion of the rod or slab might be tested after the first sequence of flame spreading at zero convective flow. The following sequences would be slightily modified.

- There will be no special problems to carry out these experiments with the sample at rest and moving the oxygen with the convective system previously studied in this Report. Possibly, more experiments might be carried out in each launching.

  In this case means would have to be provided to extinguish the flame after each experiment before changing the sample. This might be carried out by circulating through the chamber an inert gas (CO_2 or N_2) during a few seconds. This inert gas would be contained in an additional small bottle. Alternatively, a mechanical extinction device of the flame might be designed.

- A sounding rocket module gives the ideal conditions to carry out the proposed experiment. However, it is important to point out that these flame spreading experiments with forced convection might be performed in parabolic aircraft flights, with the typical well known limitations for testing in theses flights.

  Actually, the refilling process would be easier, since it would be carried out after each parabolic flight, with ample time to reduce the fluctuation velocities of the oxygen down to the required level. It looks feasible to experiment in one campaign the three forced convection modes (velocities in opposite, equal or transversal direction).

  However, there exist the possible important problem of the variation of gravity during each parabolic flight. They might introduce disturbances in the spreading processes, specially in the range of very low convective velocities.